UNIVERSITÀ DEGLI STUDI DI PADOVA

DIPARTIMENTO DI SCIENZE BIOMEDICHE

CORSO DI DOTTORATO DI RICERCA IN SCIENZE BIOMEDICHE
CICLO 31°

THE ROLE OF MCU IN VERTEBRATE DEVELOPMENT AND PHYSIOLOGY USING ZEBRAFISH (DANIO RERIO) AS A MODEL ORGANISM

TESI REDATTA CON IL CONTRIBUTO FINANZIARIO DELLA FONDAZIONE CARIPARO

COORDINATORE: CH.MO PROF. PAOLO BERNARDI

SUPERVISORE: CH.MO PROF. ROSARIO RIZZUTO

CO-SUPERVISORE: DOTT.SSA GIORGIA PALLAFACCHINA

DOTTORANDA: ELISA LIDRON

Science *means constantly walking a tightrope between blind* ***faith*** *and* ***curiosity****; between* ***expertise*** *and* ***creativity****; between* ***bias*** *and* ***openness****; between* ***experience*** *and* ***epiphany****; between* ***ambition*** *and* ***passion****; and between* ***arrogance*** *and* ***conviction*** *- in short, between an* ***old today*** *and a* ***new tomorrow****.*

Heinrich Rohrer

TABLE OF CONTENTS

LIST OF FIGURES

LIST OF ABBREVIATIONS

ACH: acetylcholine

ACHR: acetylcholine receptor

ADP: Adenosine diphosphate

ATP: Adenosine triphosphate

BP: base pairs

BSA: bovine serum albumine

Ca^{2+}: Calcium Ion

CRISPR: Clustered Regularly Interspaced Short Palindromic Repeats

DN: dominant negative

DNA: desoxyribonucleic acid

DPF: days post fertilization

EMRE: Essential Mcu REgulator

ER: endoplasmic reticulum

FCCP: Carbonyl cyanide 4-(trifluoromethoxy)phenylhydrazone

GFP: green fluorescent protein

HPF: hours post fertilization

IMM: inner mitochondrial membrane

KO: knockout

MCU: Mitochondrial Calcium Uniporter

MICU: Mitochondrial Calcium Uptake

MO: Morpholino

NMJ: neuromuscular junction

OCR: oxygen consumption rate

O/N: over night

OMM: outer mitochondrial membrane

PBS: Phosphate buffered saline

PBT: Phosphate buffered saline + Tween 20

PDH: pyruvate dehydrogenase

PVDF: Polyvinylidene difluoride

PBTx: Phosphate buffered saline + Tryton-X100

PTU: 1-phenyl 2-thiourea

RNA: Ribonucleic acid

SR: sarcoplasmic reticulum

RT: room temperature

RyR: ryanodine receptor

SDS-PAGE: sodium dodecyl sulfate polyacrylamide gel electrophoresis

sgRNA: single guide RNA

TCA tricarboxylic acid cycle

TBE: Tris/Borate/EDTA

TBS: Tris buffered saline

Tg: transgenic line

WB: western Blot

WT: Wild Type

SUMMARY

Mitochondria play a fundamental role in regulating cellular Ca^{2+} dynamics. Their strategic localization ensures the efficient coupling between Ca^{2+} release from the stores and Ca^{2+} uptake into the organelle, which guarantees a tight control of cell death/cell survival pathways, energy production and metabolism. Since the identification of the mitochondrial calcium uniporter (MCU), the biochemical and molecular characterization of the mitochondrial Ca^{2+} contribution to cell homeostasis made a great step forward. The variability of the $MCU^{-/-}$ mouse phenotype, firstly described as unexpectedly mild in 2013, but dependent on the genetic background, underlies a role of MCU during embryogenesis. Our work aims to explore the role of mitochondrial Ca^{2+} uptake in the regulation of vertebrate development using the zebrafish (*Danio rerio*) as a model organism. We undertook a reverse genetic approach to target Mcu, which we initially downregulated by injecting morpholino antisense oligonucleotides (MOs) in fertilized zebrafish eggs to block its expression in developing embryos. *Mcu* morphants develop with no major abnormalities nor alterations in mitochondria morphology, despite displaying a hardly detectable Mcu protein expression level and blunted mitochondrial Ca^{2+} uptake. However, they show a slight reduction in body size and the analysis of their locomotor activity revealed an impaired touch-evoked escape response compared to control embryos. In addition, analysis of skeletal muscle in *mcu*MO-injected and control fish at 48 hpf evidenced defects in tissue architecture, fiber organization, and myofibrillar structure, which was confirmed at the ultrastructural level by transmission electron microscopy at 5 dpf, evidencing enlarged sarcoplasmic reticulum vesicles which interrupt the

ordered myofibrillar array, abnormal triads and reduction of mitochondria cristae in *mcu* morphants.

As skeletal muscle differentiation and motor neuron pathfinding are intimately connected processes during zebrafish embryogenesis and muscle pioneer adaxial cells are required for driving early motor neuron axon growth, we analyzed their distribution in 30 hpf *mcu*MO-injected and control embryos. We found a remarkable mislocalization and a reduction in the number of adaxial cells in *mcu* morphants versus controls. Moreover, the analysis of the motor neuron population evidenced a reduction of the number of also these cells and of their axon branching in developing *mcu* morphants. Thus, the deficit in adaxial cells may be responsible for the defective skeletal muscle-motor neuron developmental axis observed in Mcu-deficient embryos.

We also analyzed *mcu* morphant metabolism by SeaHorse, reporting a significantly lower basal and maximal respiration, which was accompanied by an increased sensitivity to oxidative stress compared to control animals.

To pursue the characterization of Mcu contribution to later stages of zebrafish development and to adulthood, we engaged in the generation of stable *mcu* mutant fish by CRISPR-Cas9 technology.

Two mutant lines mcu^{del14} and mcu^{ins20} were obtained and are currently under characterization. Preliminary results already showed that *mcu* mutant zebrafish phenotype is very similar to that of *mcu*MO-downregulated animals.

Notably, mutant fish reach adulthood, are fertile and do not show major morphological abnormalities. However, subtle but significant alterations are observed in different tissues.

In conclusion, our work highlights the fundamental contribution of Mcu and mitochondrial Ca^{2+} uptake to vertebrate development, in particular, to the differentiation of skeletal muscle tissue and motor neuron network and to global fish metabolism. The characterization of *mcu* mutant fish will help to further elucidate the involvement of mitochondrial Ca^{2+} uptake in vertebrate organogenesis, physiology and, importantly, in pathology.

RIASSUNTO

I mitocondri svolgono un ruolo fondamentale nel controllo dei segnali Ca^{2+} cellulari. Essi infatti accumulano Ca^{2+} in seguito al suo rilascio dai depositi, prevenendone l'eccessivo accumulo nel citosol. Il Ca^{2+} che entra nell'organello svolge un ruolo chiave nel regolare il metabolismo, stimolare la respirazione e quindi la produzione di ATP, nonché controllare l'attivazione delle vie di sopravvivenza e morte cellulare. L'identificazione del gene per l'uniporto mitocondriale del calcio (MCU) ha permesso la caratterizzazione molecolare del ruolo del Ca^{2+} mitocondriale nell'omeostasi cellulare e tessutale. Il primo modello di topo $MCU^{-/-}$ descritto nel 2013 dimostrava un fenotipo relativamente lieve, ma la sua severità dipende grandemente dal genotipo considerato, il che suggerisce un ruolo di MCU durante l'embriogenesi.

Questo lavoro di tesi si è focalizzato sulla caratterizzazione del ruolo di MCU durante lo sviluppo dei vertebrati, impiegando lo zebrafish (*Danio rerio)* come animale modello. Utilizzando un approccio di genetica inversa, l'espressione di Mcu è stata silenziata mediante l'iniezione di oligonucleotidi morfolino antisenso specifici per *mcu* (*mcu*MO) in uova di zebrafish fecondate.

Gli embrioni morfanti *mcu* non dimostrano evidenti alterazioni morfologiche e i loro mitocondri appaiono normali, nonostante l'espressione di Mcu sia minima e i transienti di Ca^{2+} mitocondriali risultino drammaticamente ridotti. I morfanti *mcu* presentano solo ridotte dimensioni e una significativa diminuzione dell'attività locomotoria, probabilmente legata ad alterazioni del tessuto muscolare scheletrico. Gli embrioni silenziati per mcu, infatti, presentano anomalie nella morfologia e distribuzione dei diversi tipi di fibra muscolare, perdita dell'organizzazione miofibrillare sarcomerica dovuta ad un

compartimento sarcoplasmatico allargato, e cambiamenti ultrastrutturali nelle cristae mitocondriali negli embrioni silenziati per *mcu* rispetto ai controlli.

Inoltre, l'analisi della popolazione motoneuronale nei morfanti *mcu* a 48 hpf ha evidenziato una riduzione del numero di motoneuroni e una diminuita ramificazione dei loro assoni.

Dato che muscolo scheletrico e componente motoneuronale hanno uno sviluppo strettamente interconnesso durante l'embriogenesi e una popolazione di cellule muscolari, chiamate "adaxial", è fondamentale per il corretto orientamento degli assoni dei motoneuroni, abbiamo analizzato la loro distribuzione in embrioni morfanti e relativi controlli. Gli embrioni morfanti dimostrano un ridotto numero e una mislocalizzazione di queste cellule "adaxial", il che potrebbe essere la causa dei difetti riscontrati nell'asse neuro-muscolare osservato in presenza del silenziamento di *mcu*.

Inoltre, l'analisi del metabolismo di embrioni a 4 giorni di sviluppo ha dimostrato che i morfanti *mcu* hanno una respirazione, sia basale che massima, significativamente più bassa dei controlli e sono più sensibili allo stress ossidativo.

Per poter studiare il ruolo di Mcu a stadi di sviluppo successivi e nell'adulto, abbiamo generato delle linee mutanti di zebrafish (*mcu*^{del14} *e mcu*^{ins20}*)* in cui l'espressione di Mcu è stabilmente abrogata, tramite la tecnologia CRISPR/Cas9. La loro caratterizzazione è attualmente in corso ma analisi preliminari confermano il fenotipo osservato nei pesci morfanti *mcu*. I pesci mutanti infatti raggiungono l'età adulta e sono fertili, ma mostrano riduzioni delle dimensioni corporee e alterazioni metaboliche. I nostri risultati evidenziano il contributo fondamentale di Mcu e dell'accumulo mitocondriale di Ca^{2+} nello sviluppo dei vertebrati e, in particolare, nella regolazione del metabolismo e del differenziamento muscolare e motoneuronale durante lo sviluppo. La caratterizzazione dei mutanti *mcu*$^{-/-}$ aiuterà a chiarire ulteriormente il coinvolgimento del Ca^{2+} mitocondriale nella funzionalità di organi e tessuti in condizioni fisiologiche e, possibilmente, patologiche.

1. INTRODUCTION

1.1. MITOCHONDRIA: THE GENERAL FRAMEWORK

Mitochondria play a critical role in the metabolism of eukaryotic cells. They are responsible for most of the energy production that derives from the breakdown of carbohydrates and fatty acids, which is converted to ATP by the process of oxidative phosphorylation. Mitochondria are unique among the cytoplasmic organelles as they contain their own DNA, thus the assembly of the organelle involves proteins encoded by their own genome, as well as proteins encoded by the nuclear genome. Mitochondria are delimitated by two structurally and functionally different membranes: the outer mitochondrial membrane (OMM), permeable to ions and metabolites up to 5 KDa and the highly selective inner mitochondrial membrane (IMM), characterized by invaginations called *cristae* which enclose the mitochondrial matrix. The space between the two membranes is called intermembrane space (IMS). The *cristae* define internal compartments formed by profound invaginations which originate from narrow tubular structures called *cristae junctions* (Mannella, 2006), thus creating a micro-environment where the mitochondrial Electron Transport Chain (mETC) complexes are hosted. The mETC is formed by complex I, composed by NADH dehydrogenase, complex II, composed by succinate dehydrogenase, complex III, composed by ubiquinol cytochrome c reductase, complex IV composed by cytochrome c oxidase, and finally there is the complex F_1F_o-ATP synthase (Cooper, 2000).

The most important task of mitochondria is the oxidative phosphorylation, finally leading to ATP production. In the 60's, Peter Mitchell clarified the

process by which electron transfer is coupled to ATP synthesis in the process of oxidative phosphorylation, and he proposed, for the first time, an indirect mechanism named “chemiosmotic theory”. He suggested that the flow of electrons through the respiratory electron-transfer chain complexes drives protons across the IMM, thus creating an electrochemical proton gradient across the membrane. The synthesis of ATP is driven by a reverse flow of protons down the gradient through the F_1F_o ATP synthase, a big protein complex that uses the energy generated by proton flow down electrochemical gradient to produce ATP. This electrochemical gradient across the IMM is reflected in a huge membrane potential difference ($\Delta\Psi m$) of -180 mV (negative inside) (Mitchell, 1961, 1966).

Mitochondria are not only the primary energy-generating system in most eukaryotic cells, they even form a dynamic, interconnected network, intimately integrated with other cellular compartments. They participate in the maintenance of cell homeostasis, playing a role in many processes from Ca^{2+} signaling, to lipid metabolism, Reactive Oxygen Species (ROS) production and cell death regulation. Importantly, mitochondrial functions can influence the whole organism's physiology, regulating communication between cells and tissues. For all these reasons, mitochondrial dysfunction has emerged in the last years having a central role in a number of diseases, including neurodegenerative and metabolic disorders (Nunnari and Suomalainen, 2012).

1.2. ROLE OF MITOCHONDRIA IN Ca^{2+} HOMEOSTASIS

Mitochondria were the first organelles to be associated to Ca^{2+} handling. Almost 60 years ago, it was described for the first time that energized mitochondria could accumulate large amount of Ca^{2+} (DELUCA and ENGSTROM, 1961; VASINGTON and MURPHY, 1962). In the following years, when the scientific community accepted the chemiosmotic theory proposed by Mitchell, the properties of mitochondrial Ca^{2+} transport became clear. The negative membrane potential generated by the translocation of protons across

the IMM or by the reverse action of the ATP synthase, allows mitochondria to rapidly accumulate Ca^{2+} inside the matrix, thanks to a channel called the mitochondrial Ca^{2+} uniporter (MCU). Ca^{2+} accumulation does not reach electrochemical equilibrium with the membrane potential thanks to the existence of Ca^{2+} efflux mechanisms. The two main players involved in mitochondrial Ca^{2+} efflux are the Na^{+}/Ca^{2+} (NCLX) and H^{+}/Ca^{2+} (mHCX) exchangers (Bernardi, 1999). However, not all the proteins involved in the Ca^{2+} efflux have been discovered yet, moreover, the complete block of mitochondrial Ca^{2+} efflux is not possible using the available drugs.

The molecular identification of the H^{+}/Ca^{2+} exchanger is still debated (Nowikovsky et al., 2012). Recent works by Clapham and coworkers proposes Letm1 as a possible candidate (Jiang et al., 2009; Tsai et al., 2014), however another work suggest that Letm1 is a part of the K^{+}/H^{+} antiporter (Dimmer et al., 2008; McQuibban et al., 2010). Regarding the NCLX, in 2010 Sekler's group discovered the molecular identity of the NCLX, demonstrating that it is expressed only in the internal membranes and is highly enriched in the mitochondrial fraction (Palty et al., 2010). Now we know that NCLX regulates automaticity in cardiomyocytes (Takeuchi et al., 2013), oxidative metabolism in pancreatic β cells (Nita et al., 2014, 2015) and Ca^{2+} signaling in astrocytes (Parnis et al., 2013). The main routes of Ca^{2+} entrance and extrusion in the mitochondria are depicted in Figure 1. In the 80's, accurate measurements of cytosolic $[Ca^{2+}]$ with fluorescent indicators revealed that the low affinity of MCU would not allow substantial Ca^{2+} uptake into the organelle. Thus, in the exploding field of Ca^{2+} signaling, mitochondria were not considered as major players in such a complex scenario. Only with the advent of genetically encoded Ca^{2+} probes targeted to mitochondria, the role of this organelle in Ca^{2+} homeostasis returned finally central (Rizzuto et al., 1992). Indeed, these probes allowed to measure mitochondrial $[Ca^{2+}]$ transients during cell stimulation: only in this way it was possible to appreciate that the speed and the amplitude of mitochondrial Ca^{2+} accumulation greatly exceed the values that were previously predicted in isolated mitochondria (Rizzuto et al., 1993).

In detail, in living and intact Hela cells a transient increase of cytosolic [Ca^{2+}] to 1-3μM, induced by stimulation, is always associated with a parallel increase in [Ca^{2+}] in the mitochondrial matrix, reaching high concentrations up to 60-80 μM. It was thus clear that mitochondria play an active and important role in Ca^{2+} signaling.

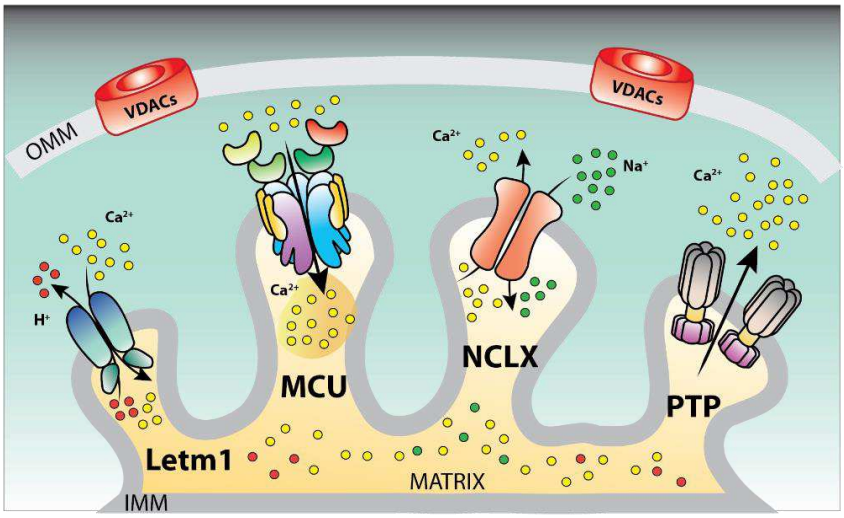

Figure 1. Schematic view of mitochondrial channels involved in mitochondrial Ca^{2+} transport, influx and efflux. (kindly provided by Sofia Zanin, PhD).

However, this finding raised an apparent contradiction between the prompt accumulation of Ca^{2+} and the low affinity of the MCU. This apparent discrepancy was solved by the discovery that mitochondria are strategically located in close proximity to ER- Ca^{2+} channels, where it has been observed that mitochondria form synaptic-like junction with ER membranes, thus generating a dedicated signaling unit between the two organelles (Csordás et al., 2010; Mannella et al., 1998; Rizzuto et al., 1992, 1993; Szalai et al., 2000). Therefore, mitochondria are able to sense microdomains of high [Ca^{2+}] (Giacomello et al., 2010), which are sufficient to ensure rapid Ca^{2+} entry through MCU and they also act as a safety lock that prevent mitochondrial Ca^{2+} overload (Rizzuto and Pozzan, 2006).

This is possible thanks to specialized structures, named mitochondria associated membranes (MAMs), that allow the just-apposition of mitochondria to Ca^{2+} release sites in the ER (Hayashi et al., 2009). These structures, have

been observed for the first time in the 90's, and the area of the contact sites has been estimated to be the 5-20% of the total mitochondrial surface (Mannella et al., 1998; Rizzuto et al., 1998).

1.3. MITOCHONDRIAL Ca^{2+} REGULATION OF CELLULAR METABOLISM AND CELL SURVIVAL

During the 70's it has been discovered that Ca^{2+} directly regulates three key enzymes of the tricarboxylic acid (TCA) cycle: pyruvate dehydrogenase (PDH), isocitrate dehydrogenase and α-ketoglutarate dehydrogenase. It has been demonstrated that a Ca^{2+}-dependent phosphatase can directly modulate the pyruvate dehydrogenase activity (Denton et al., 1972), while the direct binding of Ca^{2+} to isocitrate dehydrogenase and α-ketoglutarate dehydrogenase has an important regulatory role (McCormack et al., 1990; Rutter and Denton, 1988). The reactions catalyzed by these enzymes are rate limiting steps of the TCA cycle, and for this reason the positive modulation of Ca^{2+} can reflect a substantial increase in the activity of these enzymes and a consequent increased feeding of mETC by NADH and $FADH_2$.

In addition, these three dehydrogenases are also regulated by intrinsic factors such as the ADP/ATP ratio, the NAD^+/NADH ratio and pH, which all together contribute to their regulation (Denton, 2009). In conclusion, cytosolic Ca^{2+} mobilization and the consequent mitochondrial Ca^{2+} uptake stimulates the TCA cycle, thus increasing NADH availability and electron flow through the respiratory chain ultimately leading to ATP production.

Mitochondrial Ca^{2+} uptake is well-known to be involved in the induction of cell death pathways, both necrosis and apoptosis. The cell itself decides to activate apoptosis or succumb to necrosis, depending on the intracellular ATP concentration (Gramaglia et al., 2004). Regarding necrosis, bioenergetics crisis due to ATP depletion causes a dramatic increase in cytosolic [Ca^{2+}], deriving from the impairment of the ATP-dependent Ca^{2+} transporters (such as PMCA, SERCA and Na^+/Ca^{2+} exchangers). This dramatic increase is paralleled by an

increase in mitochondrial Ca^{2+} accumulation, finally leading to swelling of mitochondria and necrosis of the cell. This occurs for example in neurons, when in response to Ca^{2+} overload is activated the necrotic pathway, and this phenomenon is called neuronal excitotoxicity. Activation of NMDRs (N-methyl-D-aspartate receptors) (Nicholls, 2009; Pivovarova and Andrews, 2010) lead to direct Ca^{2+} entrance into the cell, voltage-gated Ca^{2+} channels open thanks to the depolarization event causing a super-physiological increase in cytosolic [Ca^{2+}], which in the end activates calpain (Khorchid and Ikura, 2002; Momeni, 2011). Calpain activation leads to degradation of membranes, cytoplasmic and nuclear substrates, causing the breakdown of cellular architecture. In addition, the major plasma membrane Ca^{2+} extruding system, the Na^{+}/Ca^{2+} exchanger (NCX), is cleaved and this causes an extensive accumulation of Ca^{2+} for several hours after the toxic signal. In the meantime, mitochondria accumulate Ca^{2+} to buffer the cytosolic Ca^{2+} rise, and are finally overloaded with Ca^{2+}, the membrane potential totally collapses leading to necrotic cell death (Bano et al., 2005).

Mitochondria Ca^{2+} overload is also an important trigger of apoptosis. Indeed, Ca^{2+} can directly and positively stimulate mitochondrial permeability transition pore (PTP) opening (Rasola and Bernardi, 2011). The PTP opening has a key role in the intrinsic pathway of apoptosis: its opening induces *cristae* remodelling and subsequent release in the cytosol of mitochondrial-residing pro-apoptotic factors, such as cytochrome c (Scorrano et al., 2002). These events are a key step in the induction of caspase-dependent or -independent apoptosis. Normally, physiological [Ca^{2+}] oscillations do not induce PTP opening, but become effective with the synergistic action of pro-apoptotic challenges (Giorgi et al., 2012). It has been demonstrated that the anti-apoptotic oncogene BCL-2 affects intracellular Ca^{2+} homeostasis by increasing Ca^{2+} leak from the ER and by regulating the release kinetics upon cell stimulation (Foyouzi-Youssefi et al., 2000; Pinton et al., 2000, 2001). By contrast, pro-apoptotic proteins trigger the opposite effect (Scorrano et al., 2003). For example, in cells lacking the pro-apoptotic protein BAK, Ca^{2+} release

from ER is reduced and this correlates with a reduction in cell proliferation (Jones et al., 2007).

1.4. THE MOLECULAR IDENTITY OF THE MITOCHONDRIAL CALCIUM UNIPORTER

The first evidence that mitochondria are able to uptake Ca^{2+} occurred during the 60's, but the molecular identity of the mitochondrial Ca^{2+} uniporter was discovered only 50 years later. It was even suggested that mitochondria-localized RyR1 could be the mitochondrial Ca^{2+} channel in the rat heart (Beutner et al., 2001; Ryu et al., 2011), however the tissue distribution and the electrophysiological properties of the RyR1 excluded it as a candidate. UCP2 and UCP3 were chosen as essential components of the MCU machinery (Trenker et al., 2007), although, more recent studies report them having an indirect effect on ATP production (Brookes et al., 2008; De Marchi et al., 2011).

In 2009, Letm1 has been identified as a putative H^+/Ca^{2+} antiporter by Clapham and coworkers using a siRNA genomic screening in Drosophila (Jiang et al., 2009). Despite that, the role of Letm1 is still debated (Nowikovsky et al., 2012), indeed the same protein was identified as being the mitochondrial K^+/H^+ exchanger (Dimmer et al., 2008). In any case, its properties do not reflect the ones of the MCU.

The turning point was the publication of the MitoCarta by Mootha's group, which consists in an inventory of human and mouse genes encoding proteins with mitochondrial localization (Pagliarini et al., 2008). In 2010, from the MitoCarta database the same group identified MICU1 (Mitochondrial Ca^{2+} Uptake 1), and they demonstrated that the silencing of the protein drastically reduced mitochondrial Ca^{2+} uptake in HeLa cells (Perocchi et al., 2010). Anyway MICU1 presents two EF-hand Ca^{2+}-binding domain and just a single putative transmembrane domain, and this last feature excluded the possibility of being the channel itself.

In order to find the perfect candidate the MitoCarta gene data set was examined taking into account several criteria: i) the protein should have a broad expression profile in all tissues, ii) have at least two predicted transmembrane domains, iii) be absent in *S. cerevisiae*, which lacks Ruthenium Red-sensitive mitochondrial Ca^{2+} uptake and last iv) the candidate should be present in organisms displaying mitochondrial Ca^{2+} uptake.

In 2011, our and Mootha's laboratory, independently and using different approaches, identified an uncharacterized protein, encoded by the *ccdc109a* gene, which owned all the requirements present in the above list, to be the Rethenium Red-sensitive Ca^{2+} channel of the inner mitochondrial membrane, named Mitochondrial Calcium Uniporter (MCU) (Figure 2) (De Stefani et al., 2011; Baughman et al., 2011). In line with the evidence of the pleiotropic role that mitochondrial Ca^{2+} signals play within the cell, it was clear that MCU could not work alone.

1.5. CORE COMPONENTS OF THE MEMBRANE PORE

Up to now, we know that the pore forming subunit is composed of three different proteins: MCU, MCUb and EMRE (see Figure 2). MCU appears to be the only obligatory component, because all organisms that displays mitochondrial Ca^{2+} uptake capacity express this protein.

MCU. The MCU gene is well conserved in all eukaryotes except for yeasts (Bick et al., 2012; Cheng and Perocchi, 2015). MCU is a 40kDa protein that presents two transmembrane domains and two coiled-coil domains separated by a short loop enriched in acidic residues. It can oligomerize, but the exact stoichiometry of the functional channel is still debated, even if very recently it has been reported to form tetrameric structures (dimer of dimers) (Baradaran et al., 2018; Fan et al., 2018; Lee et al., 2016b; Nguyen et al., 2018). MCU silencing leads to abolishment of mitochondrial Ca^{2+} uptake, while its

overexpression triggers a significant increase of mitochondrial transients, as recorded by patch clamp technique in mitoplasts (De Stefani et al., 2011; Chaudhuri et al., 2013).

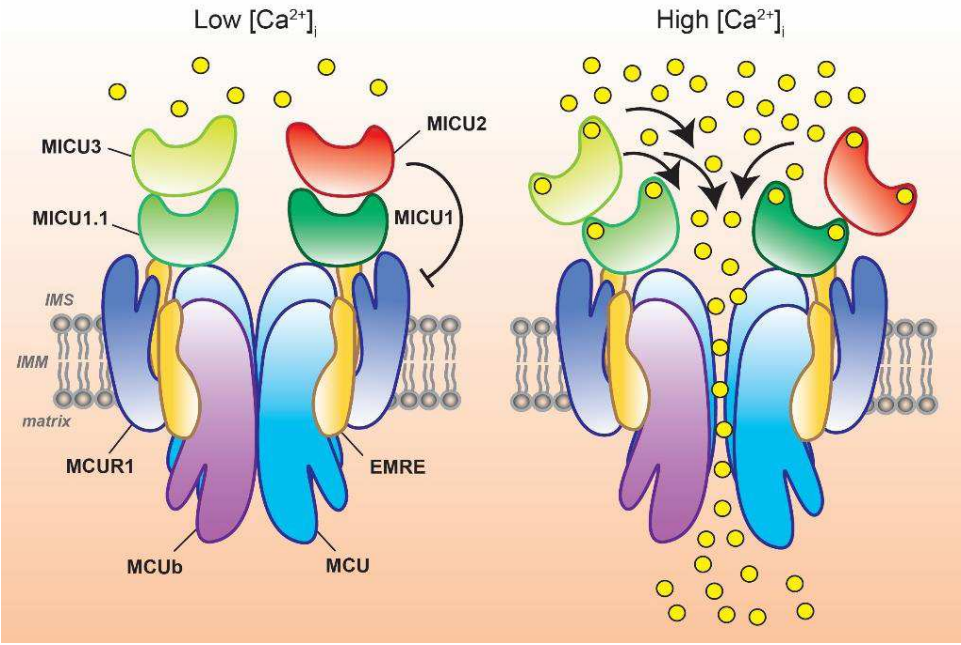

Figure 2. The mitochondrial calcium uniporter (MCU) complex. Schematic representation of the MCU-mediated Ca^{2+} entry into mitochondria. Mitochondrial Ca^{2+} uptake is controlled by a multiprotein complex consisting of MCU, MCUb and EMRE (the pore-forming subunits) and the MICU proteins, MICU1, MICU1.1, MICU2 and MICU3. At low cyt[Ca^{2+}] (left) MICU protein heterodimers ensure the MCU gatekeeper activity. At high cyt[Ca^{2+}] (right) MICU proteins act as positive regulators allowing efficient mitochondrial Ca^{2+} uptake. IMS = intermembrane space, IMM = inner mitochondrial membrane. (kindly provided by Sofia Zanin, PhD).

Importantly, recombinant MCU is sufficient *per se* to form a Ca^{2+}-selective channel in planar lipid bilayer (De Stefani et al., 2011a). In addition, channel activity is inhibited by Ruthenium Red and gadolinium (Kirichok et al., 2004). In the last years, the role of MCU as an essential component for mitochondria Ca^{2+} uptake has been confirmed in different systems. MCU ablation abolished mitochondrial Ca^{2+} transients in cardiomyocytes (Kwong et al., 2015), pancreatic β cells (Alam et al., 2012; Tarasov et al., 2012a), neurons (Qiu et al., 2013), skeletal muscle fibers (Mammucari et al., 2015) and breast cancer cells (Tosatto et al., 2016). Finally, isolated mitochondria derived from MCU knockout mice completely lack mitochondrial Ca^{2+} uptake, thus demonstrating the requirement of the MCU gene (Pan et al., 2013).

MCUb. After the molecular identification of the uniporter, a gene closely related to MCU, *ccdc109b*, started to be investigated and now it is known as MCUb. The protein shares 50% similarity to MCU, it is conserved in most vertebrates and, as MCU, possesses two coiled-coil domains and two transmembrane domains separated by a loop that is slightly different from the one of MCU, namely a crucial amino acid substitution (E256V) which removes a critical negative charge (Raffaello et al., 2013).

MCU is able to form hetero-oligomers with MCUb, and this strongly affects Ca^{2+} permeation through the channel. In detail, MCUb overexpression decreases mitochondrial Ca^{2+} transients, both in HeLa cells and in planar lipid bilayer experiments. In addition, MCUb silencing triggers a significant increase in mitochondrial Ca^{2+} uptake (Raffaello et al., 2013).

MCU activity is highly variable between tissues (Fieni et al., 2012), and for this reason they have different MCU/MCUb ratio, according to their needs. Most importantly, the correlation between MCU/MCUb expression ratio and the recorded mitochondrial Ca^{2+} current is apparent. For example, MCU/MCUb ratio in heart is low, whereas in skeletal muscle is high (Raffaello et al., 2013). It is plausible that this ratio contributes to set the mitochondrial Ca^{2+} uptake capacity of different tissue.

EMRE. The Essential MCU Regulator (known as EMRE) is a 10 kDa protein, widely expressed among mammalian tissues, with one single predicted transmembrane domain and a highly acidic C terminus. Mootha's group proposed that this protein is required for the binding of MICU1/MICU2 dimer to the MCU complex. However, EMRE homologs are not present in fungi or in plants, in which MCU and MICU1 are highly conserved (Sancak et al., 2013). Its downregulation or knockout abolishes mitochondrial Ca^{2+} uptake, even when MCU is overexpressed (Sancak et al., 2013). These data have been confirmed by Miller and coworkers recently (Tsai et al., 2016), thus suggesting a fundamental role of EMRE in the efficient assembly of the MCU complex. It

should be noted that in yeast EMRE is required for the formation of a functional channel together with the mammalian MCU, but not with the MCU derived from fungi (Kovács-Bogdán et al., 2014). For this reason the molecular mechanism and regulatory function of EMRE is still under debate. In 2016, Foskett and coworkers demonstrated that MCU channel activity is regulated by matrix Ca^{2+} concentration through EMRE, which acts as a Ca^{2+} sensor. In addition, MCU regulation by EMRE requires the localization of MICU1 and MICU2 in the IMS and cytosolic Ca^{2+} (Vais et al., 2016).

1.6. THE MICU FAMILY

A fundamental property of the mitochondrial Ca^{2+} uptake machinery is the sigmoidal response to $[Ca^{2+}]$: a very low rate at resting levels and a very large Ca^{2+} carrying capacity at higher concentrations that ensures prompt responses to stimuli. The sigmoidal response could be due either to the channel itself, or to the activity of channel regulators. The former hypothesis was excluded, because MCU exposes in the IMS only a small loop. The latter has been investigated by many groups, and the findings are reported hereafter.

MICU1. In 2010, as already above-mentioned, Mootha's group identified MICU1 and proposed that this protein is required for mitochondrial Ca^{2+} uptake (Perocchi et al., 2010). MICU1 has only one predicted transmembrane domain and functional and structural data suggest that it is located in the IMS, together with other members of the family (Hung et al., 2014; Martell et al., 2012). It has been shown that mitochondria of MICU1 silenced cells are constitutively overloaded with Ca^{2+}, thus suggesting a gatekeeping role of this protein (Mallilankaraman et al., 2012a). This was even confirmed by Hajnoczky and coworkers immediately after and in addition, they demonstrated that, in the absence of MICU1, mitochondrial Ca^{2+} uptake is less efficient at high Ca^{2+} concentrations (Csordás et al., 2013).

MICU2. Formerly known as MICU2 (EFHA1) is an isoform of MICU1. Our laboratory described that MICU2 forms obligate heterodimers with MICU1 that interact with MCU in the loop facing the IMS. In addition, we demonstrated that MICU2 has a gatekeeping function at low Ca^{2+}concentrations. Indeed, its overexpression is able to decrease mitochondrial Ca^{2+} uptake upon stimulation in HeLa cells (Patron et al., 2014). As already reported by Hajnoczky and coworkers, we confirmed that the stability of MICU2 is dependent on the presence of MICU1. Indeed, MICU1 silenced cells have a drastic reduction also in MICU2 protein level (Patron et al., 2014). According to this model, at low [Ca^{2+}] prevails the inhibitory effect of MICU2, that ensures minimal Ca^{2+} accumulation thus preventing the deleterious effects of mitochondrial Ca^{2+} overload in the matrix. As soon as cytosolic [Ca^{2+}] increases, the cation binding to the EF-hand domains inhibits MICU2 and activates MICU1 guaranteeing the prompt initiation of rapid mitochondrial Ca^{2+} accumulation, finally leading to the stimulation of aerobic metabolism.

MICU3. Referred to as MICU3 (EFHA2), and it has probably a minor role in this process, since it appears to be predominantly expresses in the CNS (central nervous system) (Plovanich et al., 2013). Our laboratory recently showed that MICU3 can dimerize with MICU1, but not MICU2, enhancing mitochondrial Ca^{2+} uptake. Silencing of MICU3 in primary cortical neurons impairs Ca^{2+} signals during synaptic activity, thus suggesting a specific role for this protein in the regulating of neuronal function (Patron et al., 2018).

1.7. OTHER PUTATIVE MCU REGULATORS

In 2012, Madesh and coworkers performed a direct human RNAi screen in HEK293T cells of 45 mitochondrial membrane proteins predicted to be part of the IMM (Mallilankaraman et al., 2012b). They identified two different proteins, SLC25A23 and MCUR1 (formerly known as CCDC90A).

MCUR1. The latter is a 40 kDa protein of the IMM with one predicted transmembrane domain, one coiled-coil region and the N terminus facing the IMS. They demonstrated that MCUR1 silenced cells displayed a decrease in agonist-induced mitochondrial Ca^{2+} uptake but also caused a decrease of basal mitochondrial [Ca^{2+}] (Mallilankaraman et al., 2012b). Recently, Shoubridge's group demonstrated that the silencing of MCUR1 causes a drop of mitochondrial membrane potential that correlates with a decrease of complex IV assembly and activity (Paupe et al., 2015).

SLC25A23 belongs to a family of solute carriers that transport Mg–ATP/P_i across the IMM (Hoffman et al., 2014). Apparently, it participates in mitochondrial Ca^{2+} uptake probably due to its interaction with MCU and MICU1. The effect of this EF-hand containing mitochondrial protein is likely to depend on the local [Ca^{2+}]. Indeed, mutation of these Ca^{2+}-binding sites exhibited a dominant-negative effect, reducing mitochondrial Ca^{2+} transients (Hoffman et al., 2014). It was proposed that SLC25A23 could act by sequestering MICU1 in order to increase the MCU-mediated Ca^{2+} uptake. Further work is needed to clarify this mechanism.

1.8. THE ROLE OF MITOCHONDRIAL Ca^{2+} UPTAKE IN ORGANISM PATHOPHYSIOLOGY

The first MCU knockout mouse model. The first *in vivo* study surprised most of the scientists in the field: in 2013, Finkel and coworkers generated a total MCU knockout mouse (MCU^{KO}), using gene trap technique, characterized by a very mild phenotype (Pan et al., 2013). Animals devoid of MCU present normal features and no histological abnormalities. No differences in cardiac physiology have been appreciated, either in basal conditions or after increase workload and, most importantly, the response to Ischemia/Reperfusion (I/R) injury of MCU depleted mice does not differ from controls (Holmström et al., 2015). The only evident defect was an impairment of skeletal muscle

performance. The lack of a major phenotype in this model is an unresolved problem, considering that deletion of MCU caused dramatic effects in other organisms (see below).

It should be noted that Finkel and coworkers obtained viable mice only in an outbred strain (C57/BL6 and CD1 backgrounds) and that birth ratio of the homozygous MCU^{KO} mice was lower than expected, confirming a role of mitochondrial Ca^{2+} uptake during embryonic development. Few years after the generation of the MCU^{KO} model, it became clear that the ablation of MCU in a pure background leads to embryonic lethality, and this has been confirmed in two independent mouse models (Dickinson et al., 2016; Luongo et al., 2015). It is still unclear how these MCU^{KO} animals could developed without evident problems, an explanation could be the existence of compensatory mechanisms, however the nature of this compensation is still unknown. After this model, the majority of the *in vivo* studies focused on MCU modulation in striated muscles, in particular on cardiac muscles.

Selective knockout of MCU in the heart. The first heart-specific mouse model generated was a transgenic mouse expressing a dominant-negative MCU isoform (DN-MCU), in the same mixed C57BL/6xCD1 background of the constitutive MCU^{KO} model (Wu et al., 2015). This mouse model clearly shows that MCU is dispensable for normal heart beat, however, under stress conditions, MCU-dependent increase of ATP production is necessary to sustain sarco/endoplasmic reticulum Ca^{2+} ATPase (SERCA) activity and to maintain the proper Ca^{2+} load of the sarcoplasmic reticulum in sinus atrial node (SAN) cells (Wu et al., 2015). Hearts overexpressing DN-MCU exhibit impaired performance at increasing workload. Importantly, similarly to the MCU^{KO} mouse, MCU inhibition does not protect the heart from I/R injury. This finding has been recently challenged by the generation of a new mouse model, where MCU gene deletion was induced in adult mice (tamoxifen treatment led to an 80% decrease of MCU protein level), and the cardiac function was then

evaluated (Kwong et al., 2015; Luongo et al., 2015). In this model, MCU ablation strongly protects from I/R injury (Kwong et al., 2015; Luongo et al., 2015), completely the opposite result of what has been obtained in MCU^{KO} and DN-MCU mouse model (Pan et al., 2013; Wu et al., 2015).

These studies confirm the presence of an impairment in the fight-or-flight response triggered by β-adrenergic stimulation, as reported by Anderson and coworkers (Wu et al., 2015). Cardiomyocytes derived from these mice present normal oxygen consumption rate (OCR) in basal conditions, but a decreased OCR was detected after increased workload (Kwong et al., 2015; Luongo et al., 2015). Finally, in all the above-mentioned models has been reported a decrease in the PDH activity (Pan et al., 2013; Wu et al., 2015; Kwong et al., 2015; Luongo et al., 2015).

Selective knockdown and knockout of MCU in skeletal muscle. In literature, it is well established that mitochondrial Ca^{2+} uptake plays a role in all tissues, and in particular in those that relies on an oxidative metabolism. The role of mitochondrial Ca^{2+} uptake in skeletal muscle has been studied first in our lab by positive and negative modulation of MCU at the protein level. To avoid compensatory effects, adeno-associated viruses (AAV) have been used to overexpress or silence MCU after birth. Briefly, our colleagues demonstrated that modulation of mitochondrial Ca^{2+} accumulation contributes to skeletal muscle trophism in adult mice. Indeed, MCU overexpression triggers muscle hypertrophy, whilst its downregulation leads to atrophy. Moreover, MCU overexpression protects from denervation-induced muscle atrophy caused by sciatic nerve excision. These effects on muscle trophism are independent from the control of aerobic metabolism: i) PDH activity, although defective in MCU silenced muscles was unaffected in MCU overexpressing muscle, ii) hypertrophy was comparable in both oxidative and glycolytic muscles and, iii) analyses of aerobic metabolism revealed no major alterations. Instead, MCU-dependent mitochondrial Ca^{2+}

uptake modulates PGC-1α4 and IGF1-AKT/P, two major hypertrophic pathways of skeletal muscle.

These results demonstrate the existence of a Ca^{2+}-dependent mitochondria-to-nucleus signaling axis that links organelle physiology to the control of muscle mass (Mammucari et al., 2015). Moreover, our colleagues decided to investigate more in detail the metabolic changes occurring upon MCU silencing. For this purpose they generated a skeletal muscle specific knockout ($skMCU^{-/-}$). They demonstrated that the impairment in muscle performance of $skMCU^{-/-}$ mice is majorly due to reduced glucose oxidation, which results from PDH activity inhibition and thus reduction in the TCA cycle activity. This metabolic change leads to fiber type remodelling towards faster myosin heavy chains (MyHCs). Metabolic flexibility allows the shift toward increased FA oxidation to compensate for the impairment in carbohydrates utilization to sustain muscle activity (Gherardi et al., 2018). This metabolic rewiring contributes to explain the mild phenotype of MCU-deficient mouse models, and, despite metabolic adaptation, the loss of MCU specifically in skeletal muscle tissue still has a negative impact on muscle strength and performance, thus highlighting once again the physio-pathological relevance of a functional mitochondrial Ca^{2+} uptake machinery.

MICU1 modulation in human patients. In 2014 a loss-of-function mutation of MICU1 was identified in patients (Logan et al., 2014). Homozygous individuals carrying the mutation are characterized by early-onset of proximal muscle weakness, moderately or grossly elevated creatine kinase levels in blood serum (usually sign of muscle damage), learning difficulties, and a progressive movement impairment. Fibroblasts derived from these patients display an impairment of MCU gating accompanied by mitochondrial fragmentation and decreased oxidative metabolism. In 2016 another work described two cousins with a deletion of entire exon 1 in MICU1 gene, characterized by muscle fatigue, lethargy and weakness, despite having

normal muscle biopsy (Lewis-Smith et al., 2016). The fibroblasts of these two patients displayed normal mETC enzymatic activities, albeit functional studies revealed defects in mitochondrial Ca^{2+} uptake. Although in both cases the pathogenesis is still unclear, these findings underline the importance of mitochondrial Ca^{2+} transport in pathophysiology.

MICU1 modulation in animal models Up to now, two different MICU1 knockout mouse models have been generated (Antony et al., 2016; Liu et al., 2016). Hajnoczky and coworkers generated a MICU1 knockout, of which animals died perinatally, demonstrating that MICU1 is essential for adaptation to postnatal life. The other one is a hepatocyte-specific MICU1 deletion ($MICU1^{hepko}$). In liver regeneration experiments, $MICU1^{hepko}$ displayed an impaired pro-inflammatory response and subsequent failure in liver regeneration, leading to extensive necrosis due to Ca^{2+} overload followed by accelerated PTP opening (Antony et al., 2016). Soon after, Finkel's group generated MICU1 knockout mice using the CRISPR/Cas9 system. MICU1 deletion resulted in significant, but not complete, perinatal mortality. Few animals survived, maybe due to adaptation of other MCU complex component (Liu et al., 2016). Taken together, these data demonstrate that even alterations in MICU1 activity play a critical role in physiological and pathological conditions, due to the fundamental control of cellular Ca^{2+} homeostasis exerted by mitochondria.

Other animal models. Genetical manipulation of MCU has been performed even in lower organisms. *Trypanosome brucei* (a parasite), upon MCU ablation, has an impaired energy production with an increase in the autophagy process (Huang et al., 2013a), leading to impaired growth capacity *in vitro* and reduced infectivity *in vivo*. In *Caenorabditis elegans* (worms), the deletion of MCU leads to viable individuals, even though ROS production is impaired (Xu and Chisholm, 2014).

MCU inhibition in mushroom body neurons, a brain region critical for olfactory memory formation, during pupation in *Drosophila melanogaster* (fruit fly*)*, triggers memory impairment (Drago and Davis, 2016). In *Danio rerio* (zebrafish), mitochondrial Ca^{2+} uptake has been reported to drive gastrulation (Prudent et al., 2013).

1.9. THE ZEBRAFISH MODEL ORGANISM

Danio rerio (also known as zebrafish) is a tropical freshwater teleost that belongs to the *Cyprinidae* family. Its natural habitat are rivers of South Asia, namely northern India, as well as northern Pakistan, Bhutan, and Nepal (Dahm and Geisler, 2006). They are characterized by a distinctive color pattern based on alternating dark and light horizontal stripes, and have been named zebrafish for this reason. Even though it is the main color pattern, there can even be other types of pigmentation: leopard *Danio*, which has a spotted pigmentation, and the albino, which does not have pigmented cells. Female and male are easily recognized because of their clear sexual dimorphism: males present a fusiform body shape and gold-reddish fins and abdomen, whilst females have a rounded body shape, due to the presence of the ovary, and a light-silver coloured abdomen (Nasiadka and Clark, 2012). Its natural diet consists primarily of zooplankton and insects. In the last decades, it has been widely used in research thanks to its several advantages: first, it is a small (3-4 cm in length), thus it can be kept easily and cost-effectively in the laboratory, second, females can spawn every week and a single clutch may contain hundreds of eggs, moreover they breed all year round. The external fertilization and the transparency of the embryos make them suitable for microinjection, drug treatments and *in vivo* imaging. The increasing number of available transgenic lines together with embryo optical clarity allow tracking of fluorescently tagged transgenes and monitoring of reporter genes activities.

The zebrafish embryo has a very rapid development: the first division occurs after 45 minutes from the fertilization (at 28,5°C), gastrulation occurs within 10 hours post fertilization (hpf) and by 24 hpf the body axes have already been established, allowing the distinction of eyes, somites, the vascular system and the developing nervous system.

Drug administration in zebrafish is simple: small molecular compounds can be dissolved in fish water and diffuse into the embryos, allowing easy treatment in the first developmental stages. After 5-6 days post fertilization (dpf), organogenesis is completed (see Figure 3) and embryos have become swimming larvae that display food-seeking behavior. At 30 dpf the sexual determination takes place whereas at 3-4 months they reach sexual maturity (Dahm and Geisler, 2006; Kimmel et al., 1995; Vacaru et al., 2014).

Its genome is composed by 25 chromosomes, more than 26000 codifying genes, is completely sequenced, and can be easily found in many databases. Genes and molecular mechanism defining embryonic development are highly conserved in this model (70 to 80% of genic positions). In addition, 80% of genes known to be associated with human diseases have a zebrafish counterpart (Howe et al., 2013). These data together with the highly sequence homology make the zebrafish a good model organism for genetic studies and for the investigation of human diseases as well. A significant difference between human and zebrafish genomes, however, derives from a whole-genome duplication event, the teleost genome duplication (TGD): this duplication event, occurred in teleost and not in humans, was followed by a functional specialization of some of the duplicated genes and the loss of other genes, respectively (Postlethwait et al., 2004, 2000; Taylor et al., 2003).

Nowadays it has become a popular model organism used to study the genetics underlying development (Vacaru et al., 2014), it a commonly used disease model (Goessling et al., 2007; Lin, 2012; Zang et al., 2018) and it is used for drug screening (Goldsmith, 2004) and toxicology studies.

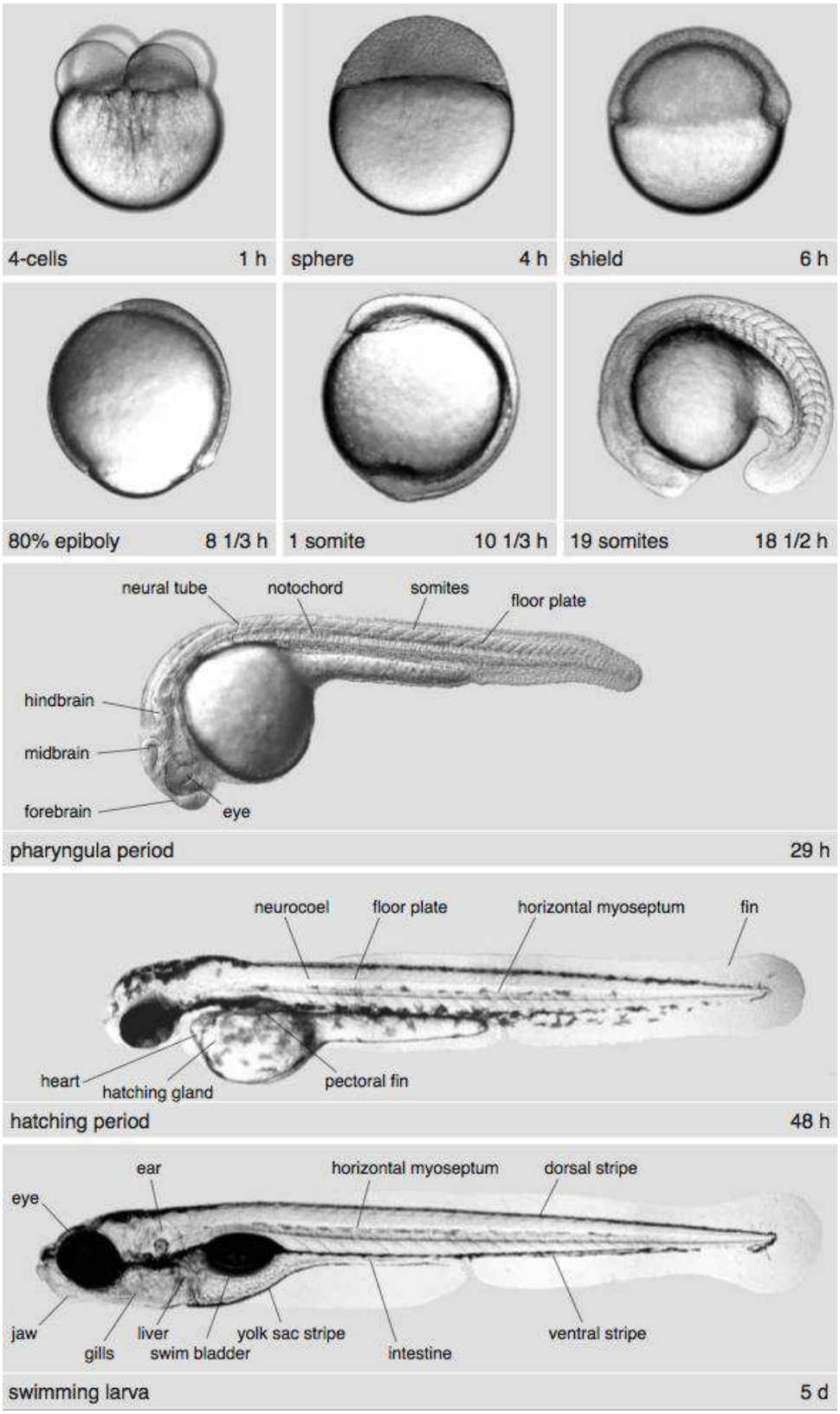

Figure 3. Relevant stages in zebrafish development from 0 hpf to 5 dpf.
(from *Haffter et al., Development 1996*)

1.10. Ca^{2+} SIGNALING IN THE DEVELOPING ZEBRAFISH EMBRYO

In 1999, Lee and coworkers demonstrated that a Ca^{2+} wave propagates across fertilized zebrafish eggs (Lee et al., 1999). Localized Ca^{2+} transients have also been shown to accompany cytokinesis during the early cell division cycles in zebrafish embryos and Chang and Meng demonstrated that intracellular free Ca^{2+} is required for triggering cytokinesis (Chang and Meng, 1995). Furthermore, they showed that most of the cytokinesis-associated Ca^{2+} is released from internal stores, most likely being an ER-IP3Rs dependent release. When zebrafish development progresses from the blastula to gastrula periods, there is a concomitant progression from intracellular/short-range intercellular Ca^{2+} signaling events to large-scale Ca^{2+} signalling events (that occur during gastrulation). In addition, from 75% epiboly to bud stage (i.e. 8 hpf to 10 hpf), the elevated level of Ca^{2+} in the dorsal margin increases further and propagates as a wave in an anterior direction along the forming trunk. Then, a series of Ca^{2+} transients are generated from an "hot spot", and each transient is followed by a pan-embryonic Ca^{2+} wave. Gilland and colleagues also reported that these pan-embryonic waves arise until the end of epiboly, after which the wave frequency increases during early somitogenesis (Gilland et al., 1999). Embryos treated with thapsigargin, a sarco/endoplasmic reticulum Ca^{2+}-ATPase inhibitor, displayed subsequent abnormal patterning, and the developmental abnormalities were different depending on the time point of Ca^{2+} transients blocking. All this data taken together underline the importance of Ca^{2+} signaling during embryogenesis, starting from the earliest time points, and can be easily imagined that a disruption or alteration in mitochondrial Ca^{2+} uptake would certainly alter such a finely orchestrated developmental patterning. Many studies during the last decades underlined the importance of intracellular Ca^{2+} signaling toolkit, but not much is known, up to now, about mitochondrial Ca^{2+} accumulation contribution to the developmental process. In 2013, Prudent and coworkers reported that mitochondrial Ca^{2+} uptake drives gastrulation in zebrafish, and to study the

mechanism they downregulated Mcu in zebrafish to abolish mitochondrial Ca^{2+} transients. This point will be further discussed, but it has to be noted that it was not reported the evidence of effective Mcu downregulation at such early stages (Prudent et al., 2013). To date, the contribution of mitochondrial Ca^{2+} uptake to the developmental process is still largely unknown.

1.11. ZEBRAFISH SKELETAL MUSCLE, AN OVERVIEW

In vertebrates, skeletal muscle contains two different type of fibers, which display specific physiological and biochemical properties that allows their functional diversification (Schiaffino and Reggiani, 2011). Slow-twitch fibers (Type I) are oxidative fibers, they contain a large number of mitochondria and ATP is generated by oxidative metabolism, thus providing a high resistance level and allowing the maintenance of contractile activity for long period (Jackson and Ingham, 2013a). These fibers are tipically red, thanks to the high levels of myoglobin and the high vascularization. Fast-twitch fibers (Type I) are, instead, glycolytic fibers and contain a low number of mitochondria. In these fibers, ATP is generated by anaerobic metabolic processes, and their contractile activity is lower than that of slow fibers (Jackson and Ingham, 2013a). The difference in the contractile activity is due to the different myosin isoforms present in the thick filament. Zebrafish is a great model organism to study muscle development: a large proportion of the body is constituted by muscle (around 80% in embryos and larvae) and the fiber-type differentiation that occurs in the embryonic development is maintained throughout fish life. Fast muscle fibers are multinucleated and located in the internal part of the myotome, deep into the somite, whilst slow muscle contains mononucleated fibers, located at the edges of the myotome, forming a subcutaneous layer (Devoto et al., 1996; Jackson and Ingham, 2013a; Ochi and Westerfield, 2007). The zebrafish myotome contains also muscle pioneer cells, that are slow muscle precursors located along the mid-line of the developing somite, adjacent to the notochord and the medial fast fibers (Ochi and Westerfield, 2007). Muscle activity starts at different developmental time points and

involves different fiber types. Slow fibers are responsible for the first spontaneous contractions that appear in embryos from 18 to 30 hpf (Brustein et al., 2003; Naganawa and Hirata, 2011a). The touch-evoked escape response instead, is due to fast-twitch fibers that start contracting after hatching 44 to 52 hpf (Naganawa and Hirata, 2011a). Zebrafish myogenesis is regulated by myogenic regulatory factors (MRFs), members of the basic helix-loop-helix (*bhlh*) transcription factor family (Coutelle et al., 2001). In particular, the first genes to be expressed are *myod1* and *myf5*. In zebrafish, the myogenic process starts before somite segmentation, and it is promoted by Hedgehog signalling which induces presomitic mesodermal cells to differentiate into adaxial cells (Coutelle et al., 2001; Devoto et al., 1996; Feng et al., 2006; Wolff et al., 2003). These cells are slow muscle precursors, as well as muscle pioneer cells (Devoto et al., 1996), and are initially aligned medially next to the notochord (see Figure 5), they migrate radially to reach the lateral surface of the somite, and they form the superficial layer of slow twich mononucleated fibers (Honjo and Eisen, 2005). A small portion of adaxial cells maintains the original localization and express Engrailed (Eng), later during development they differentiate into muscle pioneer cells, which form the horizontal myoseptum (Ochi and Westerfield, 2007). Finally, differentiated slow fibers express the transcription factor Prox1 (Glasgow and Tomarev, 1998) and the slow isoform of the MyHC. Fast twitch multinucleated fibers arise from the differentiation of a second

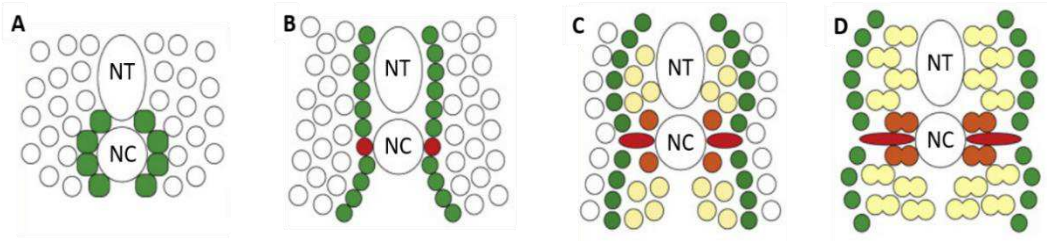

Figure 4. Different cell sub-populations within the zebrafish myotome. A) Adaxial cells (green) are initially located close to the notochord, B) as they begin to migrate dorsally and ventrally, the one that remain closest to the notochord express Engrailed (Eng) proteins (red). Eng expressing adaxial cells will differentiate into mononucleated Muscle Pioneer cells. C) Following lateral migration of adaxial cells, fast-twitch myoblasts (yellow) juxtaposed to the notochord D) also activate Eng expression (orange) and differentiate into multinucleated Medial Fast Fibers. NC=notochord, NT=neural tube. Adapted from Jackson and Ingham, Mechanisms of Development 2013.

population of cells expressing MyoD and independently of Hedgehog signalling (Coutelle et al., 2001; Devoto et al., 1996), and the fast MyHC isoform.

1.12. MOTOR AXON PATHFINDING IN ZEBRAFISH

Zebrafish trunk motor neurons develop in two waves. In each hemisegment, three primary motor neurons can be easily identified, named CaP, MiP and RoP (for caudal, middle and rostral primary) (Hutson and Chien, 2002). All three primary motor neurons extend their axons within the spinal cord to a shared exit point, and then follow a shared "common pathway" until they reach the horizontal myoseptum (HMS), which is marked by a set of specialized muscle pioneer cells (see Figure 5). Here they pause before diverging to distinct targets. It has been previously reported that even the migration of pioneering primary motor axons into the periphery relies on extrinsic cues provided by a subset of five to six dorsal adaxial cells that delineates the initial part of the future motor nerve path (Zeller et al., 2002a; Zhang and Granato, 2000). As the first motor growth cones extend into the common path, adaxial cells initiate their radial migration to the surface of the myotome, where they differentiate into a single layer of slow-twitch muscle fibers (Devoto et al., 1996; Zeller and Granato, 1999). For this reason, it has been proposed a model in which adaxial cells deposit specific cues on the surface of the somite, prior to migration. Thus, as primary motor growth cones exit the spinal cord and encounter the medial surface of the somites, the cues left behind by the adaxial cells path lead axon innervation (Zeller and Granato, 1999). Although is evident the essential role of adaxial cells in motor axons migration, it is unclear whether this reflects a general principle of vertebrate motor axon path-finding, mainly because these particular type of cells, defined by their lineage and migratory behavior, have only been reported in fish (Devoto et al., 1996). Nevertheless, this does not preclude the existence of equivalent cell types in mammals, and in addition it raises the question of whether myotomal cells play an equally important role in motor axon migration of higher vertebrate embryos (Tannahill et al., 2000).

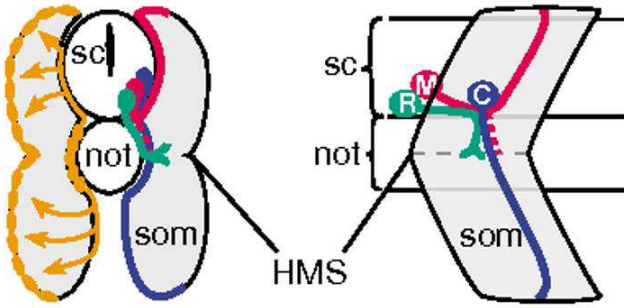

Figure 5. Schematic view of motor axon pathfinding. Transverse and lateral views showing wild-type projections of the three primary motor neurons, RoP (R; green), MiP (M; red) and CaP (C; blue), in each hemisegment (HMS). Axons from RoP, MiP and CaP project ventrally from the spinal cord (sc) along the common pathway to the HMS, and then diverge. RoP invades the myotome at the level of the HMS, whereas MiP retracts its common pathway projection and instead projects to dorsal myotome. CaP continues on and projects to ventral myotome. Adaxial cells (orange), have an essential role in guiding motor axons. These cells originate adjacent to the notochord (not), migrate laterally and eventually differentiate to form slow muscle fibers. Adapted from Hutson, Lara D. and Chi-Bin Chien, Current opinion in neurobiology 2002.

1.13. GENETICS TOOLS IN ZEBRAFISH

As reported before, genes and molecular mechanisms of embryonic development and physiology conserved in zebrafish are highly. A comparison with the human genome reveal that 70% of human genes have an orthologue in zebrafish(Howe et al., 2013). In addition, similarity in organ structure organization and organ physiology with mammals make zebrafish a good animal model for several human diseases, including muscular dystrophies (Berger and Currie, 2012), neurodegenerative disease (Babin et al., 2014), cancer (Goessling et al., 2007), diabetes (Zang et al., 2018) and cardiovascular diseases (Nguyen et al., 2008).

To obtain a genetic model in zebrafish there are two main approaches.

Forward genetics. It is based on the screening of mutants that show a phenotype, randomly generated with chemical compounds like N-ethyl-N-nitrosourea (ENU), retroviruses or transposons. This approach has been the most popular and widely used in the past 20 years, but it lacks specificity and the analysis to identify the mutated region is time- and money-consuming.

Furthermore, as the Teleost underwent genome duplication, many genes are present as paralogous genes and can exert a functional compensation between them, making the analysis of the phenotypes more difficult (Fuentes et al., 2018; Grunwald and Streisinger, 1992; Lawson and Wolfe, 2011; Nair and Pelegri, 2011).

Reverse genetics. This approach was adopted after the sequencing of the zebrafish genome. It is based on site-directed mutagenesis that may be obtained with different techniques (Skromne and Prince, 2008) and the subsequent analysis of the phenotypic consequences. In zebrafish, reverse genetics can be performed using gene knock-down and knock-out approaches (Huang et al., 2012; Shah et al., 2015, 2016). Knockdown agents are antisense short nucleotide strands that bind sense RNA to silence gene expression. There are three main types of knockdown agents (Summerton, 2007): i) phosphorothioate-linked DNAs (S-DNAs), where an enzyme is used to cut the RNA target sequence, but they have a very low percentage of success (only 20% of targets are successfully silenced), ii) siRNAs (short interfering RNAs), constituted by synthetic double-stranded RNA molecules of 20-25 base pairs (bp). These molecules lead to the degradation of mRNA after transcription, thus preventing translation according to the RNA interference (RNAi) pathway (Kelly and Hurlstone, 2011; Shinya et al., 2013), iii) Morpholinos (MOs) that make a steric obstruction inhibiting translation (atg-MO) or splicing (spl-MO) of the target gene. They are more stable and reproducible if used with the appropriate controls (Blum et al., 2015; Corey and Abrams, 2001a; Stainier et al., 2017; Summerton, 2017).
The reverse genetics approach can help solving the problem of redundancy in the zebrafish genome, as it is possible to target both paralogous genes (Rikin et al., 2010).

1.14. MORPHOLINO-MEDIATED GENE KNOCKDOWN

In zebrafish, the most common approach to gene knock down are antisense oligonucleotides called morpholino (MOs). They are synthetic molecules, typically of 20-to-25 bp, and they are produced by Gene Tools (http://www.gene-tools.com). This molecules are nucleic acid analogues, which target RNA sequences by complementary base-pairing. A morpholine-ring (6C) substitute the ribose (5C). Morpholino subunits are subsequently protected with a trityl group, to prevent degradation, and a phosphoroamidate linking agent substitutes the natural phosphate group (Summerton, 2007, 2017). These modifications lead to a strong resistance of these molecules to endonucleases and thus increasing the stability of these knockdown agents. There two types of morpholino: i) the translation blocking MOs (atg-MO), designed to be complementary to a region between the 5'-CAP and the first 25 nucleotides after the first methionine codon (ATG). Thanks to this feature, they prevent ribosomes from mRNA recognition, thus leading to the block protein translation, and ii) splice-blocking MOs (spl-MO), which are designed to be complementary to an acceptor-donor splicing site and, by sterically blocking the intron-exon or exon-intron boundaries, they interfere with pre-mRNA maturation (Figure 6). Translational-blocking MOs have one considerable advantage: they can block translation of maternal mRNAs present in the

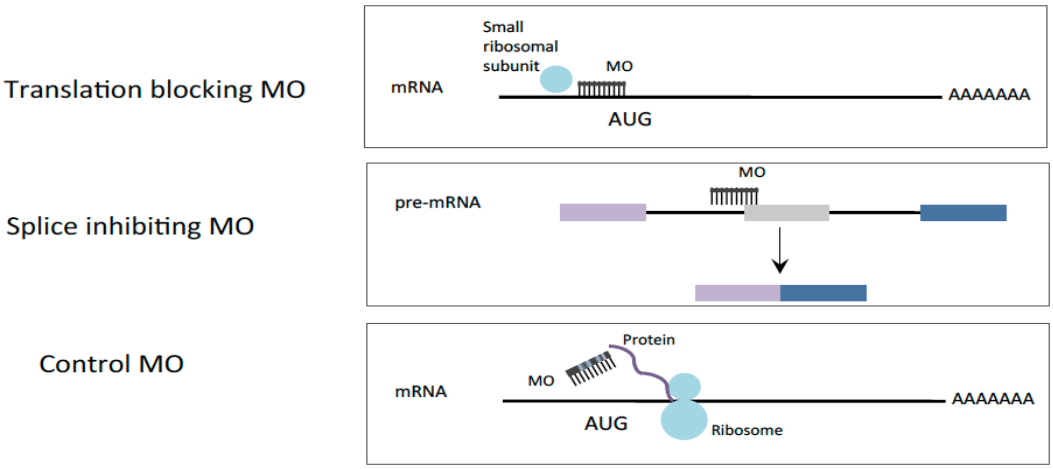

Figure 6. Schematic representation of morpholino mechanisms of action.
(Https://tatyscientificillustrations.com/)

embryos as these are mature mRNA, and this allows knockdown of maternally inherited transcripts since the zygotic period.

Nowadays, MO approach is still widely used in zebrafish to study gene function. MOs are microinjected in fertilized eggs at the stage of one/two cells. The resulting embryos showing a phenotype are called morphants (Nasevicius and Ekker, 2000). To verify the specificity of morphant phenotypes this experimental approach requires specific controls since MOs can be toxic and/or can produce off-target effects driven by their similarity to other sequences in the genome. Highly respected scientists extensively discussed the topic and listed a number of controls that are useful when adopting the MO-injection knockdown approach that have to be considered when analyzing and interpreting the MO results (Stainier et al., 2017). These guidelines can be applied when studying gene function using antisense reagents, and are extremely precious and useful for the scientific community.

1.15. CRISPR-CAS SYSTEM AND ITS UTILIZATION IN THE ZEBRAFISH MODEL

In the last years, a novel powerful gene targeting strategy revolutionized the generation of knockout in zebrafish (Auer et al., 2014; Li et al., 2016a; Ota et al., 2014; Varshney et al., 2015). This new tools have enormously increase genome editing possibilities not only in zebrafish, but also in many other animal models.

The CRISPR-Cas system is based on an adaptive immunity mechanism of archaea and bacteria. The Clustered Regularly Interspaced Shorts Palindromic Repeats (CRISPR) *loci* are organized in patterns composed of palindromic repeats alternated with the protospacer regions, containing fragments of foreign DNA. This locus is normally located near CRISPR-associated protein (Cas), which are endonucleases. The endonuclease cuts the DNA from invading viruses, or plasmids, into small fragments, which are inserted between the short repeats. If the same viruses invade the host a second time, the CRISPR

array are transcribed into crRNA (CRISPR RNA) to specifically guide the Cas proteins, finally leading to invasive DNA cleavage and degradation (Marraffini and Sontheimer, 2010; van der Oost et al., 2014). This process allows the formation of an adaptive sequence-specific immunity.

There are three main types of CRISPR-Cas systems: i) type I, that uses helicase-nuclease Cas proteins, ii) type II, that involves Cas9 endonuclease, and iii) type III, that involves a Cas10 protein (Makarova et al., 2011).

The system used in genetic engineering involves the type II nuclease Cas9, which need a particular sequence, a protospacer adjacent motif (PAM) near the protospacer, which is composed by 3 nucleotides downstream the target sequence: the presence of the PAM sequence is essential for DNA cleavage.

The Cas9 protein first interacts with a specific guide-RNA (sgRNA), formed by the crRNA trans-encoded CRISPR RNA (tracrRNA), and this is a fundamental step for the positioning of the nuclease, then another protein domain recognizes the PAM sequence and exerts the exonuclease activity (van der Oost et al., 2014). The most widely used Cas9 derives from *Streptococcus pyogenes*, and recognises the specific PAM sequence "NGG", from 5' to 3'. To

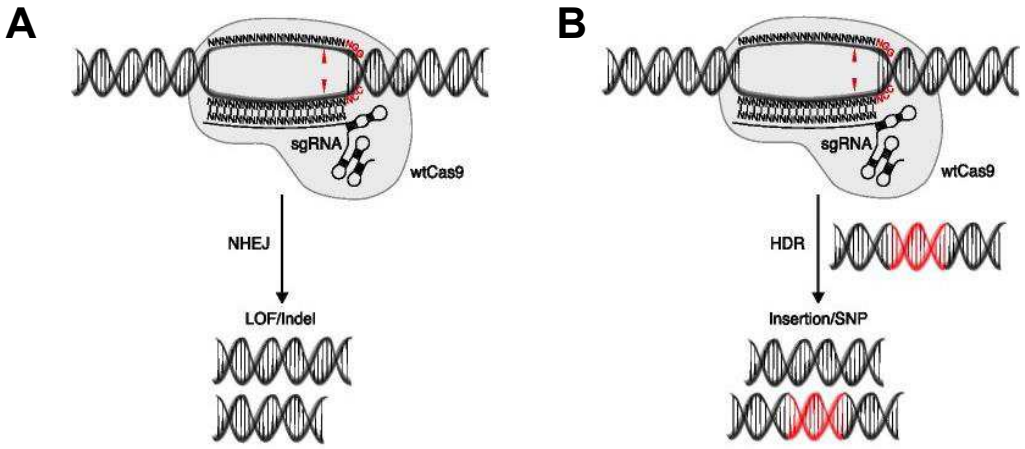

Figure 7. CRISPR/Cas9 mechanism of action. (A) Knockout approaches generate null alleles by means of indel mutations incurred by erroneous repair of DNA double-strand breaks by non-homologous end joining (NHEJ). (B) To introduce defined mutations endogenous homology-directed repair (HDR) mechanism exploit donor DNA templates. (Modified from Graham DB, Root DE, Genome Biology, 2015.).

maximize its efficiency, it contains a nuclear localization sequence, that allows maximal nuclear targeting of the nuclease (Jao et al., 2013).

Cas9 activity results in a double strand break upstream the PAM sequence, that will be repaired by two endogenous mechanisms: i) Non-Homologous End Joining (NHEJ), which leads to random insertion/deletion (indels) mutations and it is the most common repair mechanism, and ii) Homology-Directed Repair (HDR), which is more difficult to achieve and needs an exogenous template to fill the generated gap (Ran et al., 2013) (see Figure 8).

1.16. MORPHOLINO VS CRISPR-CAS9

In 2015, Lawson and colleagues reported that in a pool of more than 80 mutated genes, only the 20% of mutant phenotypes resemble that of the corresponding morphants (Kok et al., 2015). This result pointed out the problem the interpretation of data obtained with the MOs, underlining the possibility of a high off-target effect rate in MOs based studies. In addition, in a recent work, Stainier and co-workers showed that in general mutants present a milder phenotype compared embryos knocked down for the same gene with the MO approach (Rossi et al., 2015). However, transcriptomic analysis revealed the up-regulation of a set of genes that was present in mutants but not in morphant embryos, suggesting the activation of compensatory pathways. From these works we can conclude that it seems that, for the study of gene function, there is not a perfect or best approach, but it is necessary to evaluate case by case and identify the best strategy, that could be the simultaneous use of both approaches, as we will show in this work.

Both CRISPR-Cas9 and MO-injection can have off-target effects and both approaches must have the appropriate controls.

To study the effect on early development, the fastest tool is certainly MO-injection, useful to rapidly screen deleterious phenotypes, that have to be carefully evaluated and the right control experiments must be performed, as described previously in chapter 1.11. In addition, the generation of a

corresponding mutant line will allow the validation of the MO used for previous experiments in a *null* genetic background: additional phenotypes seen in mutants injected with MO targeted against the mutated gene, are surely due to off-target effects (Stainier et al., 2017).

2. RESULTS

2.1. MORPHOLINO ANTISENSE OLIGONUCLEOTIDES EFFICIENTLY DOWNREGULATE MCU IN ZEBRAFISH EMBRYOS

To investigate the role of *mcu* during development we decided to use transient reverse genetic approach, taking advantage of modified antisense oligonucleotides called morpholino (MOs). MOs have been largely employed in the last decades to downregulate target genes during early stages of development to study gene function during vertebrate embryogenesis (Corey and Abrams, 2001b; Rosen et al., 2009).

The injection of interfering MOs in fertilized eggs allows the transient disruption of the target gene function in the developing embryos allowing the characterization of the effect of gene silencing along zebrafish development. We started by injecting one- to two-cell stage zebrafish embryos with two independent *mcu*-specific MOs. The first MO targets the translation start site of mcu transcript and we will call it atg-*mcu*MO. The second targets the splicing site between the second exon and the second intron of mcu mRNA and we will call it spl-*mcu*MO. The injection of both MOs resulted in the efficient knockdown of Mcu protein (Figure A). Both MOs do not show a significant embryonic lethality, assessed by embryo survival at 24 hours post injection (Figure B). In addition, when the same dose of atg-*mcu*MO e spl-*mcu*MO was used, the atg-*mcu*MO displayed a higher efficiency of downregulation and therefore we decided to perform all the subsequent injections with this MO molecule at the dose 1.75 µg/µl.

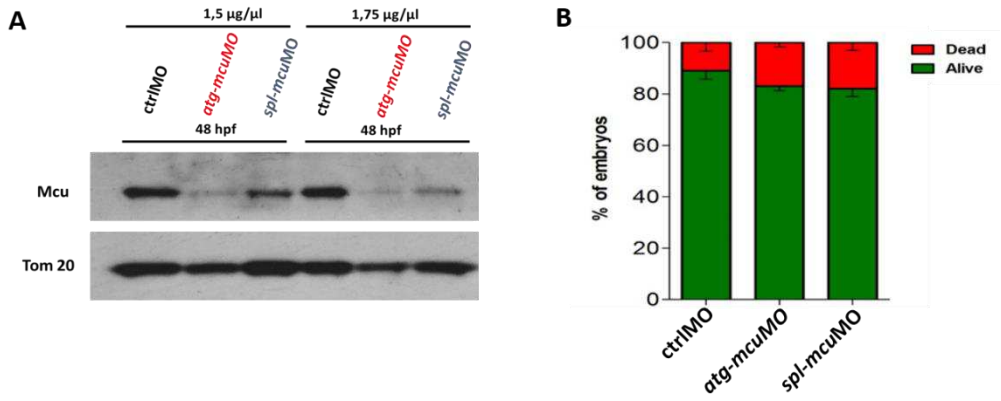

Figure 8. Injection of *mcu*-targeted Morpholino in fertilized zebrafish eggs efficiently downregulates Mcu protein expression without affecting embryo survival. A) Western blot analysis of protein lysates from embryo at 48 hpf injected with different concentrations of ctrlMO, atg-mcuMO and spl-mcuMO. 50µg of total lysate were loaded on a 4-12% Bis-Tris gel and the expression of Mcu was evaluated using a specific antibody. B) Survival of embryos at 24 hpf injected with the 1.75 µg/µl MO dose. Data are represented as percentages of total embryos and are the mean of 3 independent injection experiments.

The time course analysis of Mcu protein level was performed by Western blot of embryo extracts at different time points after MO injection. This analysis revealed a significant downregulation of Mcu starting from 30 hpf, whilst at 24 hpf, which is usually considered the time point with the maximal MO interfering activity, Mcu protein was still detectable at a remarkable level. Unexpectedly, we also found that our *mcu*-targeting MOs maintain their efficacy even several days after injection, producing a consistent blunting of *mcu* expression up to 8 days post-injection (Figure 9).

We then choose 48 hours after injection as the optimal time point to study the effects of Mcu ablation in morphant embryos and we therefore started

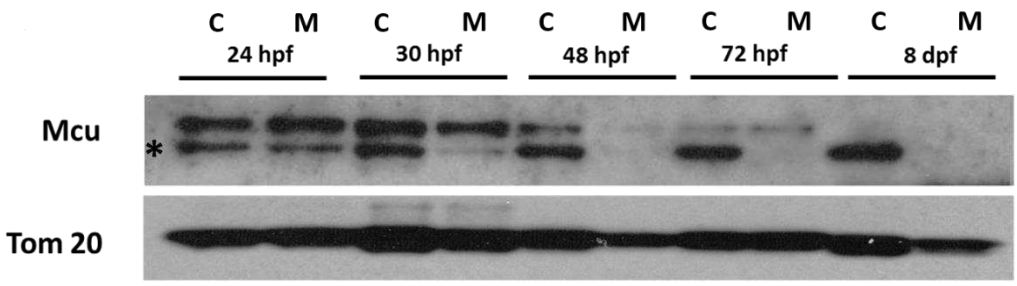

Figure 9. Efficient Mcu downregulation occurs from 30 hpf and last up to 8 dpf. Western blot analysis of protein extracted from embryos and larvae at different developmental stages, injected with atg-*mcu*MO (M) or ctrlMO (C).Tom 20 is used as mitochondrial loading control. The specific band of Mcu is evidenced with a star.

assessing the morphological and functional phenotype of injected embryos at 48 hpf.

Embryonic cell death was assessed by Acridine Orange (AO) staining on injected embryos (Tucker and Lardelli, 2007). Despite AO signal level was comparable between *mcu* morphants and control embryos, we registered a significant but transient increase in AO signal in atg-*mcu*MO injected embryos at 24 hpf, in particular in the neural tube and in the head region. As the activation of the p53-dependent apoptotic pathway upon the injection of MOs is one of the reported off-target effects of antisense oligonucleotides which may be responsible for undesired neuronal cell death, independently of the specific gene that has been targeted (Robu et al., 2007), we decided to co-inject

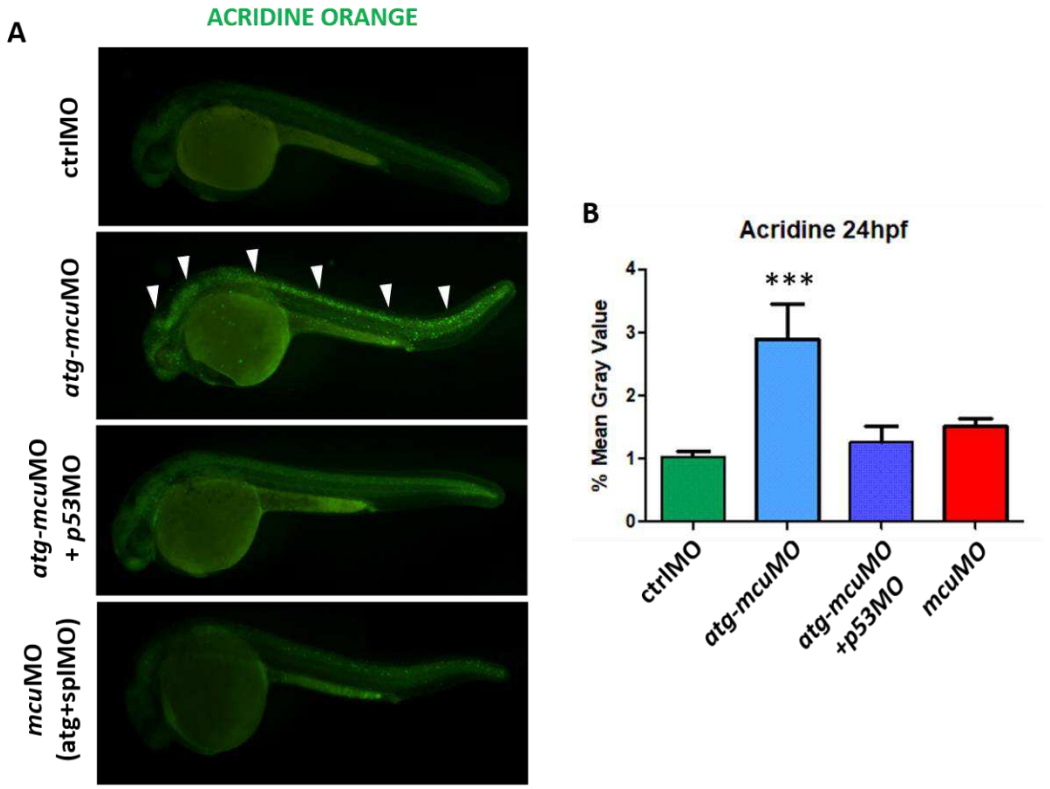

Figure 10. Detection of cell death by Acridine Orange staining in embryos injected with different MOs at 24 hpf. A) Representative images of Acridine Orange staining at 24 hpf performed on embryos injected with ctrlMO, atg-*mcu*MO alone, atg-*mcu*MO together with *p53*MO and *mcu*MO (atg-*mcu*MO with spl-*mcu*MO at sub-effective doses). White arrows indicate the presence of cell death in the neural tube and head regions of atg-*mcu*MO-injected embryos. B) Quantification of AO fluorescence in morphant embryos, expressed as the percentage of fluorescence respect to that of control embryos (***p<0.001).

the *p53*MO together with atg-*mcu*MO to understand if this was the case. After co-injection of atg-*mcu*MO/*p53*MO, AO fluorescence was comparable to ctrlMO-injected embryos, thus leading us to consider it an off-target effect due to the MO injection dose. We performed AO measurements with increasing doses of atg- and spl-*mcu*MO and both MOs, at high doses, showed a significant increase in AO signal. For this reason, we decided to optimize the injection protocol to achieve the best downregulation efficiency with almost no off-target effects. We performed co-injection of the two MOs, at sub effective doses, as suggested by literature (Bill et al., 2009; Eisen and Smith, 2008) to achieve our goal (Figure 10). We checked the knock down efficiency by Western blot analysis and the dose atg-*mcu*MO 0.9 µgr/µl + spl-*mcu*MO 1 µgr/µl ended up to be be the desired one, yielding the lowest toxicity and off-target effects combined with an efficient downregulation, and it has been therefore used for all the subsequent experiments, it will be referred to as *mcu*MO hereafter (Figure 11).

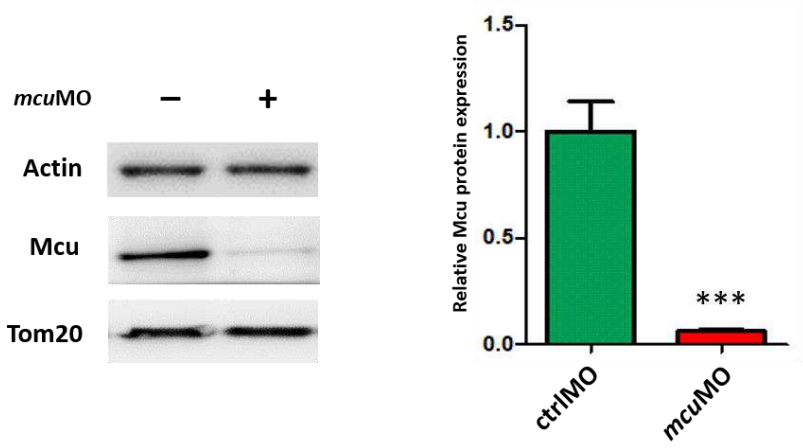

Figure 11. Co-injection of sub-effective doses of two distinct *mcu*-targeting morpholino leads to high Mcu downregulation efficiency. A), Western blot analysis of protein extracts from embryos at 48 hpf injected with *mcu*MO (atg-*mcu*MO 0.9 µg/µl + spl-*mcu*MO 1 µg/µl). 50µg of total protein lysate were loaded on a 4-12% Bis-Tris gel and the expression of Mcu was evaluated using a specific antibody. Actin is used as loading control and Tom 20 as a mitochondrial protein reference. B) Quantification of the relative Mcu protein expression level normalized to Actin.

2.2. GENERAL MORPHOLOGY OF ZEBRAFISH EMBRYOS IS PRESERVED AFTER MCU DOWNREGULATION

Embryo development was followed during the first hours after fertilization and no significant defect in body plan and organ morphology was detected in Mcu downregulated embryos compared to controls, regardless they were injected with atg-*mcu*MO or *mcu*MO (Figure 12 A).

Despite that, to a deep observation, *mcu* morphants did display some slight abnormalities even if they develop normally. Indeed, the majority of embryos (around 70%) appeared smaller than controls, presenting a curvature in the tail region, a reduced eye diameter and a relatively enlarged yolk sack. All these parameters allowed us to classify this as mild phenotype. However, nearly 30% of *mcu* silenced embryos looked normal. Only a small, non-statistically significant percentage of embryos displayed a severe phenotype with gross morphological alterations, complete bending of the tail and pronounced cardiac edema.

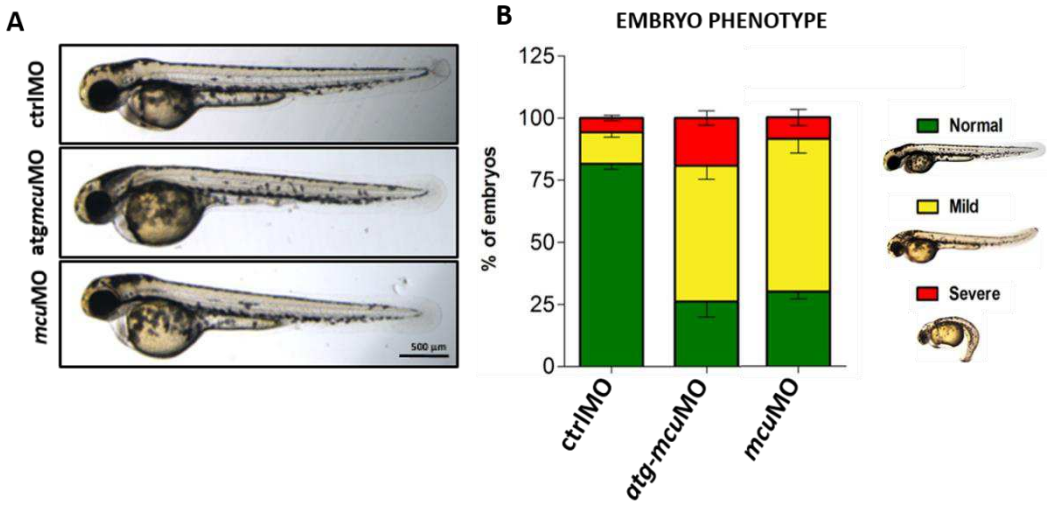

Figure 12. Mcu downregulation does not lead to morphological defects at early developmental stages. A) Representative bright field images of injected embryos. Scale bar= 500 µm. B) Quantification of the percentages of the different phenotypes observed in embryos injected with ctrlMO, atg-*mcu*MO and *mcu*MO. Green bars represent normal phenotype; yellow bars represent mild morphological abnormalities and red bars represent severely altered phenotype.

Quantification of the longitudinal axis length, of the dorso-ventral axis length and of the eye surface of control and *mcu* morphants at 48 hpf showed that *mcu* morphant length was not significantly different from controls, while the dorso-ventral axis and the eye-area were significantly reduced (see Figure 13).

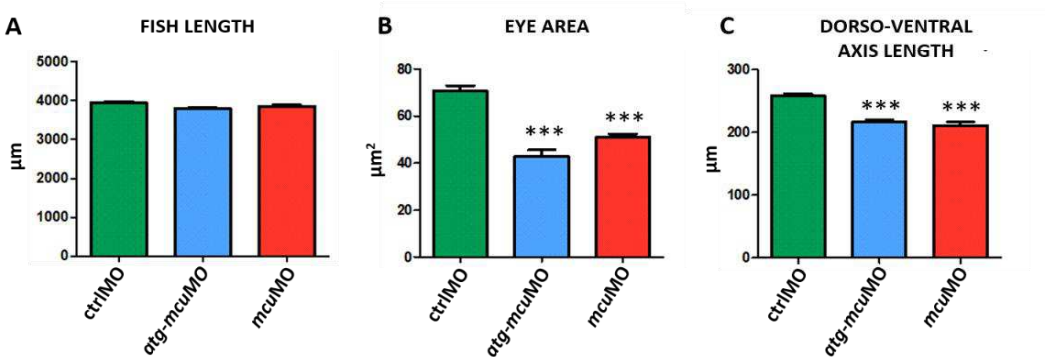

Figure 13. Mcu morphant embryos have a significantly reduced dorso-ventral axis and smaller eyes compared to controls. A) Measurements of MO-injected embryo body length. B) Measurements of the surface of the eye of MO-injected embryos. C) Measurements of the dorso-ventral axis length in MO-injected embryos. All the measurements were performed at 48 hpf, *** $p<0.001$.

2.3. MCU DOWNREGULATION DOES NOT ALTER MITOCHONDRIAL MORPHOLOGY

Mcu ablation in mice does not seem to affect mitochondria distribution and morphology (Mammucari et al., 2015; Pan et al., 2013). Nevertheless, we wanted to verify whether also in our system this is the case. We then used two methods to assess mitochondrial morphology in *mcu*MO-injected embryos: i) the first approach consisted in injecting *mcu*MO in transgenic embryos expressing a green fluorescent protein (GFP) targeted to the mitochondrial membrane of blood vessels, *Tg(kdrl:mlsGFP)*, and ii) the second was the co-injection of *mcu*MO with a plasmid encoding for a mitochondria-targeted GFP. Mitochondria of the blood vessels in the forebrain of *mcu*MO-injected embryos at 48 hpf showed no significant morphological differences compared to controls (Figure 14). Similarly, mitochondria of skeletal muscle fibers expressing mitochondria-targeted GFP from *mcu*MO-injected embryos were not distinguishable from those in control animals (Figure 14). Thus, both in

vessels and in skeletal muscle, mitochondrial morphology is not significantly affected by Mcu downregulation.

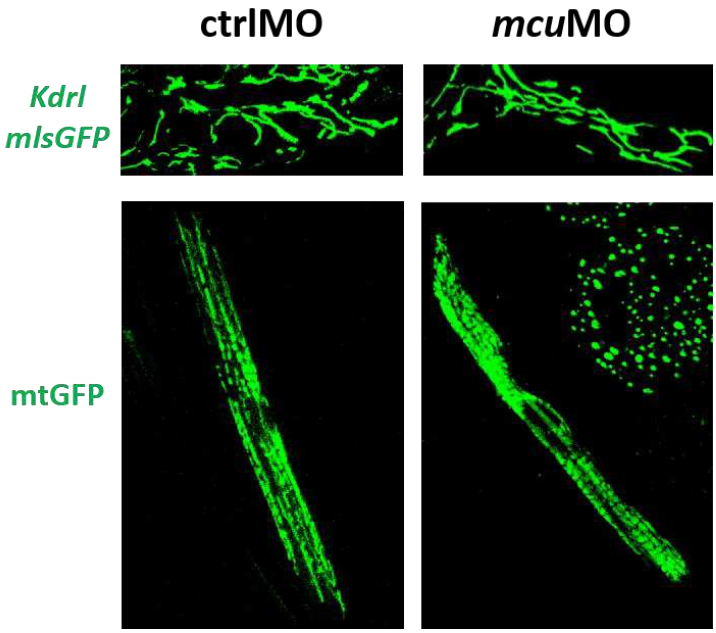

Figure 14. Mitochondrial morphology is not affected in zebrafish embryos upon Mcu downregulation. Analysis of mitochondrial morphology on embryos injected with *mcu*MO and ctrlMO at 48 hpf. In the upper panel, representative confocal images of mitochondria in the forebrain blood vessels of morphant embryos from the transgenic *Tg(kdrl:mlsGFP)* zebrafish line. In the lower panel, mitochondria of skeletal muscle fibers expressing mitochondrial-targeted GFP are visualized by green fluorescence with a confocal microscope. Fertilized zebrafish eggs were co-injected with MOs together with a plasmid encoding for a mtGFP.

2.4. MCU DOWNREGULATION DAMPENS MITOCHONDRIAL Ca^{2+} UPTAKE AND ALTERS CYTOSOLIC Ca^{2+} DYNAMICS IN ISOLATED ZEBRAFISH MUSCLE FIBERS

In order to evaluate the effect of Mcu downregulation on global Ca^{2+} dynamics we developed a protocol to monitor intracellular Ca^{2+} in isolated skeletal muscle fibers from zebrafish larvae. Briefly, we adapted an already described protocol (Horstick et al., 2013) to obtain isolated myofibers from zebrafish larvae at 72 hpf (Figure 15 A). We confirmed that myofibers deriving from *mcu*MO injected embryos were depleted of Mcu, and that they displayed normal mitochondria distribution and morphology (Figure 15 B). As expected

from the data obtained in mammalian skeletal muscle fibers, Mcu downregulation causes a reduction of myofiber size also in the zebrafish model, as assessed by the smaller diameter of *mcu*MO-injected myofibers compared to control fibers (Figure 15 A).

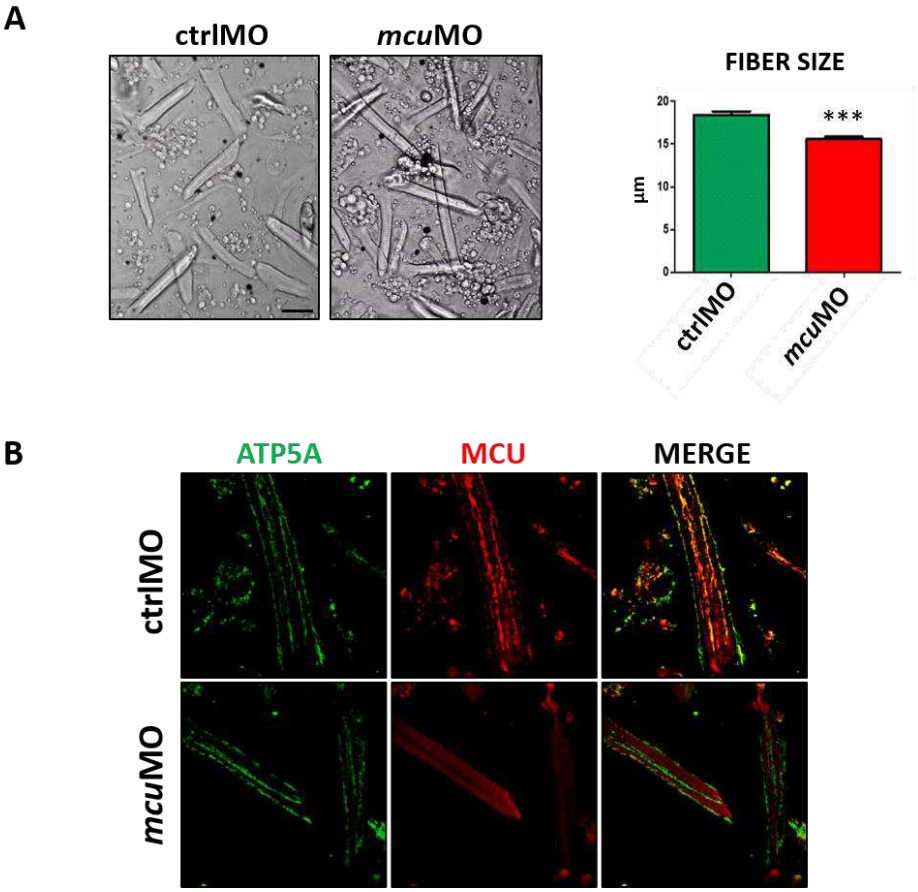

Figure 15. Isolation of skeletal muscle fibers from MO-injected larvae at 72hpf. A) Brightfield images of zebrafish isolated myofibers from control and *mcu*-morphant larvae. The diameter of myofibers was measured and the quantification shown in the graph. Scale bar=20µm (n=50 myofibers were counted for each group; ***, p<0.001). B) Immunofluorescence analysis of isolated myofibers with antibodies against Mcu and the mitochondrial marker Atp5a (subunit 5 of ATP synthase) evidenced the lack of Mcu protein in the majority of *mcu* morphant fibers.

Myofiber preparations from *mcu*MO-injected and control embryos were then incubated with mitochondrial (Rhod-2) and cytosolic (Fura-2) Ca^{2+} probes after 24 hours of culture. Cultured fibers were challenged with caffeine to elicit Ca^{2+} release from the sarcoplasmatic reticulum and mitochondrial Ca^{2+} uptake and cytosolic Ca^{2+} elevation were measured, respectively. As described in the mouse muscle fiber model, the downregulation of *mcu* leads to a significant

blunting of mitochondrial Ca^{2+} uptake upon caffeine stimulation also in zebrafish skeletal myofibers.

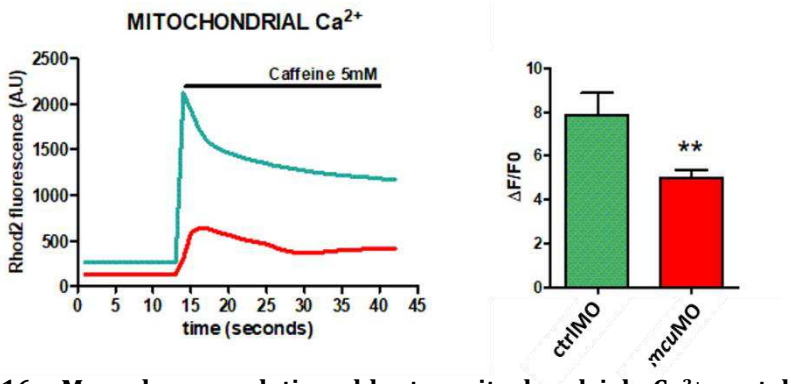

Figure 16. Mcu downregulation blunts mitochondrial Ca^{2+} uptake. Left panel, representative traces of mitochondrial Ca^{2+} level before and after caffeine stimulation measured with Rhod-2 and expressed as background-subtracted fluorescent intensity on isolated myofibers from *mcu*MO-injected (red) or control (green) larvae at 72 hpf. Right panel, quantification of the Rhod-2 signal expressed as increased fluorescence relative to the basal level, before the stimulus. (n=30 fibers, **, p<0.01).

We also analysed the effect of Mcu downregulation on cytosolic Ca^{2+} dynamics, observing a slight but significant increase in the maximal cytosolic Ca^{2+} elevation upon caffeine stimulation of fibers from mcuMO-injected embryos. Despite that, basal Ca2+ level in the cytosol of resting fibers is not different in *mcu*MO fibers compared to controls (Figure 17).

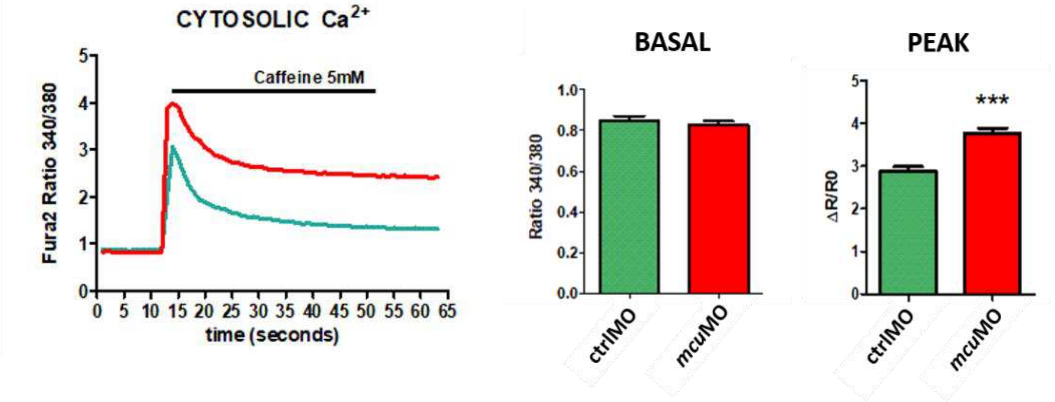

Figure 17. Mcu downregulation alters cytosolic Ca^{2+} dynamics. In the upper image, representative traces of cytosolic Ca^{2+} measurements performed on isolated myofibers loaded with Fura-2 and challenged with caffeine. In the lower part, quantification of the Fura-2 signal expressed as increased fluorescence relative to the basal level, before the stimulus, and after caffeine stimulation. (n=30; ***, p<0.001).

2.5. MCU DOWNREGULATION LEADS TO AN IMPAIRMENT OF THE LOCOMOTOR ACTIVITY OF THE DEVELOPING FISH

In order to characterize the effects of Mcu downregulation from a functional point of view, we monitored the locomotor activity of control and *mcu*MO-injected zebrafish during development by assessing their swimming behaviour at two different stages. Namely, at 48 hpf we measure the ability of embryos to escape after a mechanical stimulus produced by gently tapping the embryo tail with a capillary tip (touch-test) (Brustein et al., 2003; Saint-Amant and Drapeau, 1998; Wolff et al., 2003). Although at the age of 48 hpf zebrafish embryos rest most of the time, the gentle touching of the tail induces a fast and forward-directed movement away from the stimulus source in most of the control animals (more than 85% were classified as displaying a "normal" behaviour).

Only a minimal percentage of control embryos had an aberrant response (less than 10% showed movements either with a reduced distance length or an altered direction) and very few (5%) did not move at all (Figure 18). Differently, most of *mcu*MO-injected embryos (72%) were classified as having an altered response to applied stimuli and the 15% was not able to move (Figure 18).

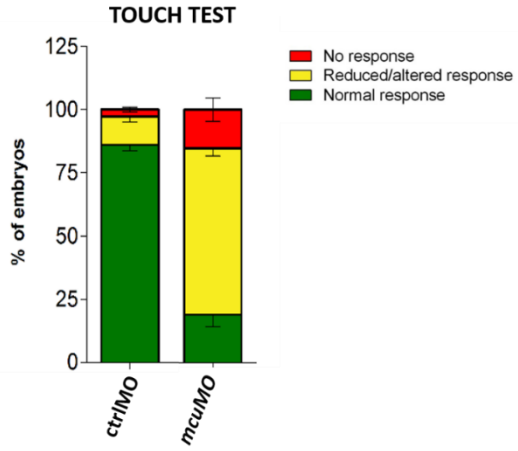

Figure 18. Mcu downregulation impairs the touch-evoked escape response of zebrafish embryos at 48 hpf. Touch test assay was performed on *mcu*MO-injected and control embryos at 48 hpf. Embryos were put in a petri dish and the tail was gently touched with a capillary tip, escape response was classified as normal (green), altered/reduced (yellow) or no response (red). (n = 250 embryos were assessed from 5 independent MO injections).

At later stages, both control and of *mcu*MO-injected embryos were similarly able to freely swim. We then wondered whether the locomotor defect observed in 48 hpf *mcu* morphant embryos may have recovered over time during development. To test this, we analysed the swimming behaviour of larvae at 5 dpf, where we have already shown that Mcu is largely absent from *mcu*MO-injected individuals (Fig. 19). In order to do this, we performed tracking experiments using C-trax and MAtLab softwares (usually implemented for tracking Drosophila flight behaviour), which has been expressly adapted to record and analyse zebrafish movements (see chapter 4.16 for details).

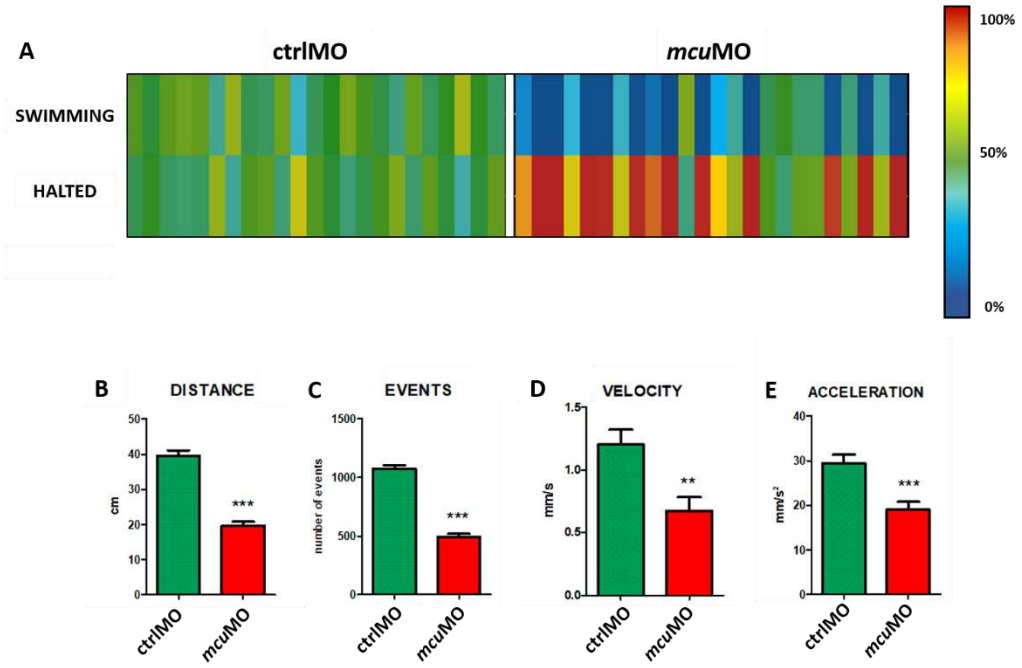

Figure 19. Mcu downregulation impairs spontaneous locomotor activity at 5 dpf. Spontaneous locomotor activity was assessed tracking the swimming behaviour of *mcu*MO-injected and control larvae at 5 dpf. A) Representative heat map of zebrafish larvae activity expressed as percentage of total recording time. Blue=0% of time, green=50% of time, red=100% of time spent moving or in halted position. Every rectangle represents anindividual. B) Quantification of the total distance covered by the larvae in 10 minute recording***, $p<0.001$. C) Quantification of the number of events/movements initiated by larvae***, $p<0.001$. D) Quantification of the mean swimming velocity of larvae, *mcu* morphants **, $p<0.01$. E) Quantification of the mean swimming acceleration of larvae***, $p<0.001$.

We recorded 10 minute videos of 5 dpf control and *mcu*MO-injected larvae freely swimming in 10 cm-diameter petri dishes and tracked the movement of each individual animal with C-trax and analized the tracking with MatLab.

As the heat map (Figure 19 A) shows, there is a strinking difference between control and *mcu* morphant fish movements even at developmental stages later than 48 hpf. In particular, control larvae spend almost half of the time exploring the arena and half in an halted position, while *mcu*MO-injected larvae are mostly halted, and the total distance covered during the swimming of control animals is the double of that of *mcu* morphants. A more detailed analysis of the movement parameters evidences that all the components of the movement appear to be altered in *mcu* morphants: the acceleration and the velocity in *mcu*MO-injected larvae are significantly lower than in control larvae (Figure 19 B-E). In conclusion, our results highlight a persistent deficit of fish locomotor activity as the consequence of Mcu downregulation. These locomotor defects, enduring for the first days of development, without improvements, led us to consider a possible damage of the skeletal muscle component or a neuronal impairement, or an involvement of both components (Brustein et al., 2003; Naganawa and Hirata, 2011b; Umeda and Shoji, 2017).

2.6. MCU KNOCK DOWN AFFECTS SKELETAL MUSCLE DEVELOPMENT AND DIFFERENTIATION

To the aim to identify which are the locomotor system components mostly affected by Mcu silencing and primarily responsible for the swimming defects recorded in *mcu*MO-injected embryos, we considered the skeletal muscle tissue and the motor neuron cell population as the two main elements defining the locomotor output of zebrafish (Brustein et al., 2003; Naganawa and Hirata, 2011b; Umeda and Shoji, 2017). We started firstly by analysing skeletal muscle structure.

We performed phalloidin staining of control and *mcu*MO-injected embryos, to visualize the actin filaments and appreciate eventual alterations of the sarcomeric organization in Mcu dowregulated embryos.

As depicted in Figure 20, *mcu*MO-injected embryos at 48 hpf did not present major defects in actin myofibrils arrangement compared to controls. However, to a careful observation it is possible to visualize some minor differences. Myofibers of Mcu downregulated embryos appear less compact, with curvatures in some regions and with more inter-myofibrillar space (Figure 20). Myo Tendineous Junction is nicely visualized with actin staining, and the overall structure is present and seems to be unaffected.

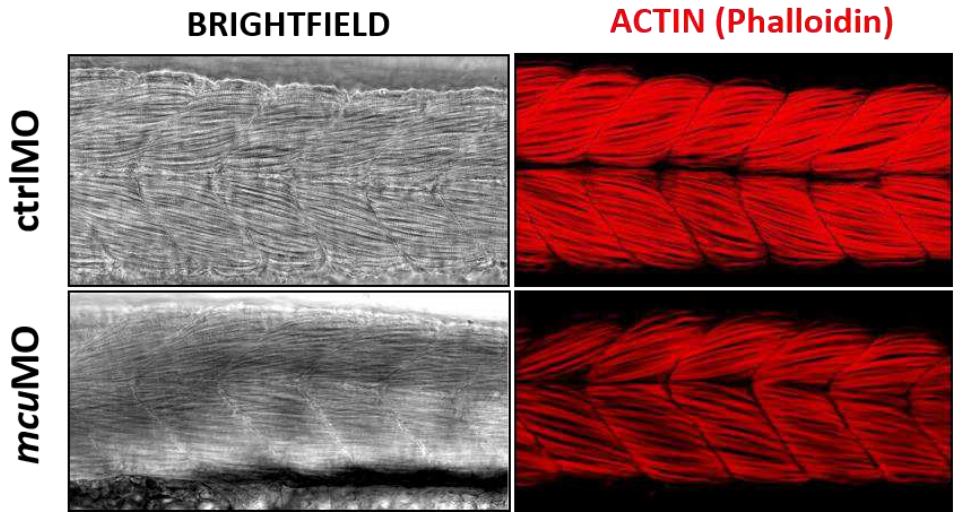

Figure 20. Mcu downregulation alters skeletal muscle structure in developing zebrafish embryo. Representative confocal images of actin filaments stained with rhodamine-conjugated Phalloidin evidences from 48 hpf embryos injected with control or *mcu*MO. Somites corresponding to the central part of the trunk (at the yolk extension region) were imaged.

We also assessed general skeletal muscle organization by measuring the birefringence index of embryo musculature at 48 hpf. The birefringence (i.e the optical property of anisotropic materials to refract polarized light due to the presence of repetitive and structurally organized elements; typical examples of biological birefringent structures are: skeletal muscle sarcomeres and extracellular matrix collagen fibrils) is a property of undamaged skeletal muscles and its measurement is commonly used to assess muscle integrity. At

48 hpf the birefringence of *mcu*MO-injected embryo muscles was significantly reduced (80% reduction) when comparared to controls (Figure 21). This suggests a deranged myofiber organization and overall structure of Mcu downregulated muscles.

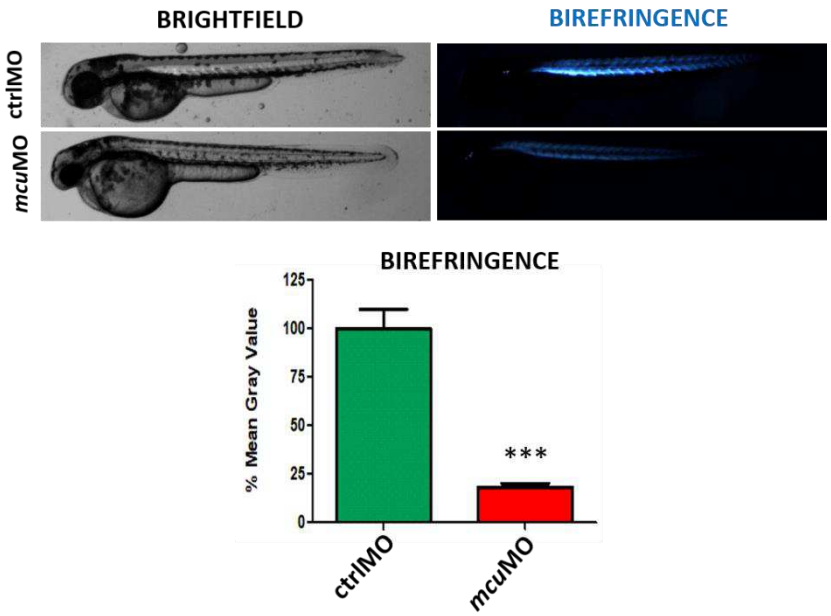

Figure 21. Mcu downregulation alters myofibril organization. Birefringence assessment in 48 hpf zebrafish embryos. In the upper part, birefringence of muscles ordered architecture in control and *mcu*MO-injected embryos can be visualized. The polarized light passing through control embryos indicates that they are highly birefringent, whilst *mcu* morphant muscle structure has a very low birefrengence percentage (despite they show an overall normal morphology, as in brightfield images). In the lower part there is the quantification of the mean value of birefringence, normalized to control value. Mcu downregulated embryos have a significant decrease in muscle birefringence (n=57, *** $p<0.001$).

Next, to assess whether *mcu* knock down might affect skeletal muscle fiber-type specification and patterning, we performed immunofluorescence staining of slow- and fast-type fibers in control and *mcu*MO-injected embryos at 48 hpf. Both types of fibers are present in *mcu* morphants, however they display a similar altered phenotype compared to control fibers, with a significant reduction of alignment within the myotome. In particular, slow fibers of *mcu* morphants display a more severe degree of alteration as they appear highly disorganized, twisted and wavy, and some of them are missing, thus leaving more cell-free spaces in *mcu* morphants. Fast fibers, located deeper in the myotome appear less affected, but still presenting a reduced diameter and

thinner and wavy myofiber compared to control fast fibers (Figure 22). Taken together, these data shows that both fiber-types are affected by the silencing of Mcu expression and this leads to a significant alteration of skeletal muscle structure in 48 hpf embryos.

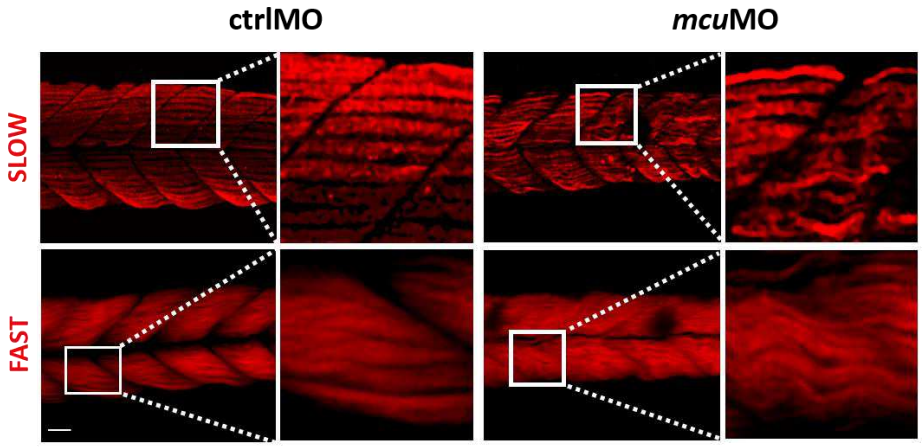

Figure 22. Both slow and fast fibers are affected by Mcu downregulation in the developing zebrafish embryo. Representative images of skeletal muscle somites at the level of the yolk extension, after immunolabeling with antibodies against slow (upper panels) and fast (lower panels) myosin heavy chain (MyHC) to identify slow and fast fiber-types in ctrlMO- and *mcu*MO-injected embryos at 48 hpf. The insert on the right represents a particular of the left panel at higher magnification. Scale bar=50µm.

In order to verify if this altered muscular phenotype is transient or maintained also at later stages in developing *mcu* morphant fish, we performed histological investigation to assess the muscular and overall morphology of control and *mcu*MO-injected embryos. Hematoxilin-Eosin staining on transverse and longitudinal paraffin sections of 5 dpf control and *mcu* morphant larvae revealed an evident reduction of the dorso-ventral axis in *mcu* morphants, accompanied by a general reduction of the muscle mass and a lower number of fibers respect to controls. Moreover, transverse sections evidenced a disarrangement of muscle fibers within the myotome, with abnormal nuclei distribution and enlarged intercellular space (Figure 23).

To better evaluate the ultrastructural alterations observed in Mcu downregulated zebrafish, we performed transmission electron microscopy analysis of skeletal muscle tissue from ctrlMO- and *mcu*MO-injected larvae

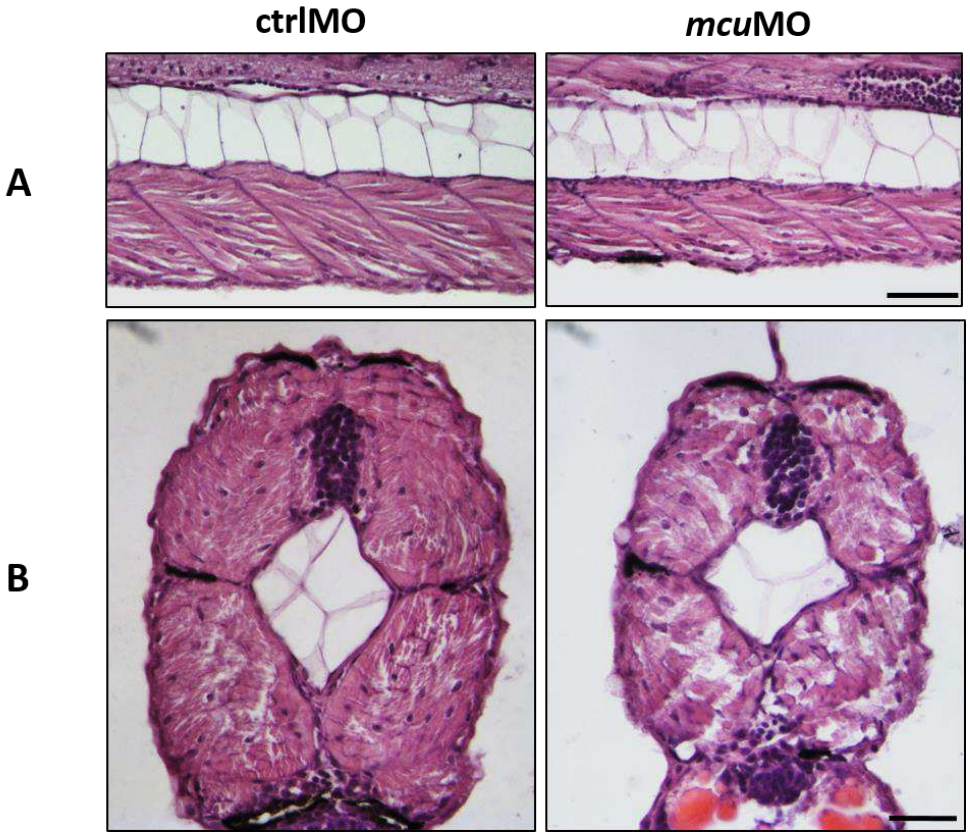

Figure 23. Mcu downregulation leads to skeletal muscle structure alteration in 5dpf developing zebrafish larvae. Representative images of Hematoxylin-Eosin staining of (A) longitudinal and (B) transverse paraffin sections of 5 dpf larvae from control and *mcu*MO-injected fertilized eggs. Scale bars=500 μm (A), 1 mm (B).

(Figure 24). The compact ordered structure that is visible in control sections is completely altered in Mcu downregulated myofibers.

The Z and M line are correctly aligned in controls as well as in *mcu* morphants, however in the last ones the ordered alignment of myofibrils in interrupted by SR enlargement and accumulation of vesicles. Mitochondria are present and tightly packed along control myofibers, in *mcu* morphants instead mitochondria appear less electron-dense, with a lower number of cristae (Figure 24 C).

All the results obtained up to now, indicate a strong involvement of Mcu in skeletal muscle development and in the maintenance of correct tissue function.

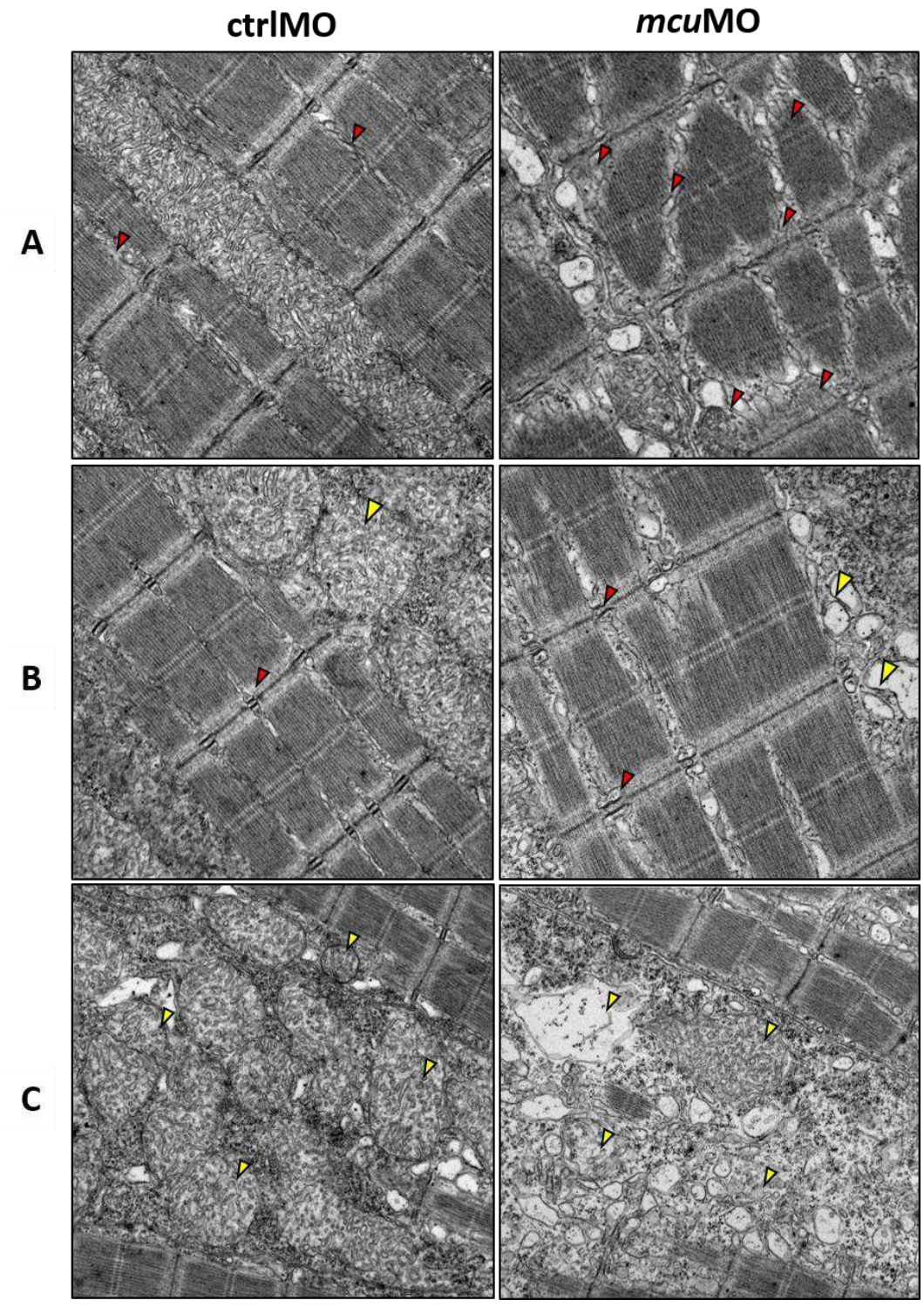

Figure 24. Mcu downregulation alters myofibrillar and mitochondrial ultrastructure in 5 dfp developing zebrafish. Transmission electron microscopy analysis was performed on ctrlMO and *mcu*MO-injected larvae at 5 dpf and three representative images for each group are presented. Note that myofibrillar arrangement, sarcomeric SR vesicle distribution (red arrowhead) and mitochondria cristae morphology (yellow arrowhead) are significant altered in mcu morphant larvae. Scale bar=1 μm.

2.7. MCU DOWNREGULATION IMPAIRS NEUROMUSCULAR DEVELOPMENT IN ZEBRAFISH EMBRYOS

The locomotor system is made of two components: muscular and neuronal tissue (Brustein et al., 2003; Low et al., 2012; Umeda and Shoji, 2017). Skeletal muscle fibers and motor neurons develop in tight contact and they reciprocally depend one from the other for proper specification, differentiation and function (Brennan et al., 2005) (see chapter 1.12 for a detailed description of the skeletal muscle – motor neuron interaction during development). We thus moved to investigate the possible involvement of the motor neuronal component in the locomotor defects recorded in *mcu*MO-injected zebrafish embryos. To do this, we took advantage of a transgenic line present in the zebrafish facility of the University of Padova, the *Tg (hb9:mGFP)* where the *hb9* (*mnx1*) promoter drives the expression of a GFP on the membrane of motor neuron cell population. We injected ctrlMO and *mcu*MO at 1-2 cell-stage zebrafish embryos and we monitored the motor neuron axon branching and maturation. No significant differences were detected at 24 hpf, compatible with the lack of Mcu downregulation at that time point.

An alteration of the motor neuron branching and axonal elongation became evident at 48 hpf, when *mcu*MO-injected embryos display a lower number of developing axons together with abnormal branching compared to control (Figure 25). Indeed, axons of *mcu*MO embryos frequently fail to extend into the myotome and appear extremely shorter than the control. We could exclude this is due simply to a delay in motor neuron development, since the defect is still present and the innervation pattern even more compromised at 72 hpf. We counted the number of missing axon, starting from the first somite of the trunk, and *mcu* morphants have a significantly lower number of motor neurons compared with controls at the same developmental stage and the number of axons that are completely missing (which we considered as “gaps”) increased over time. This means that axons fail to develop and did not develop later.

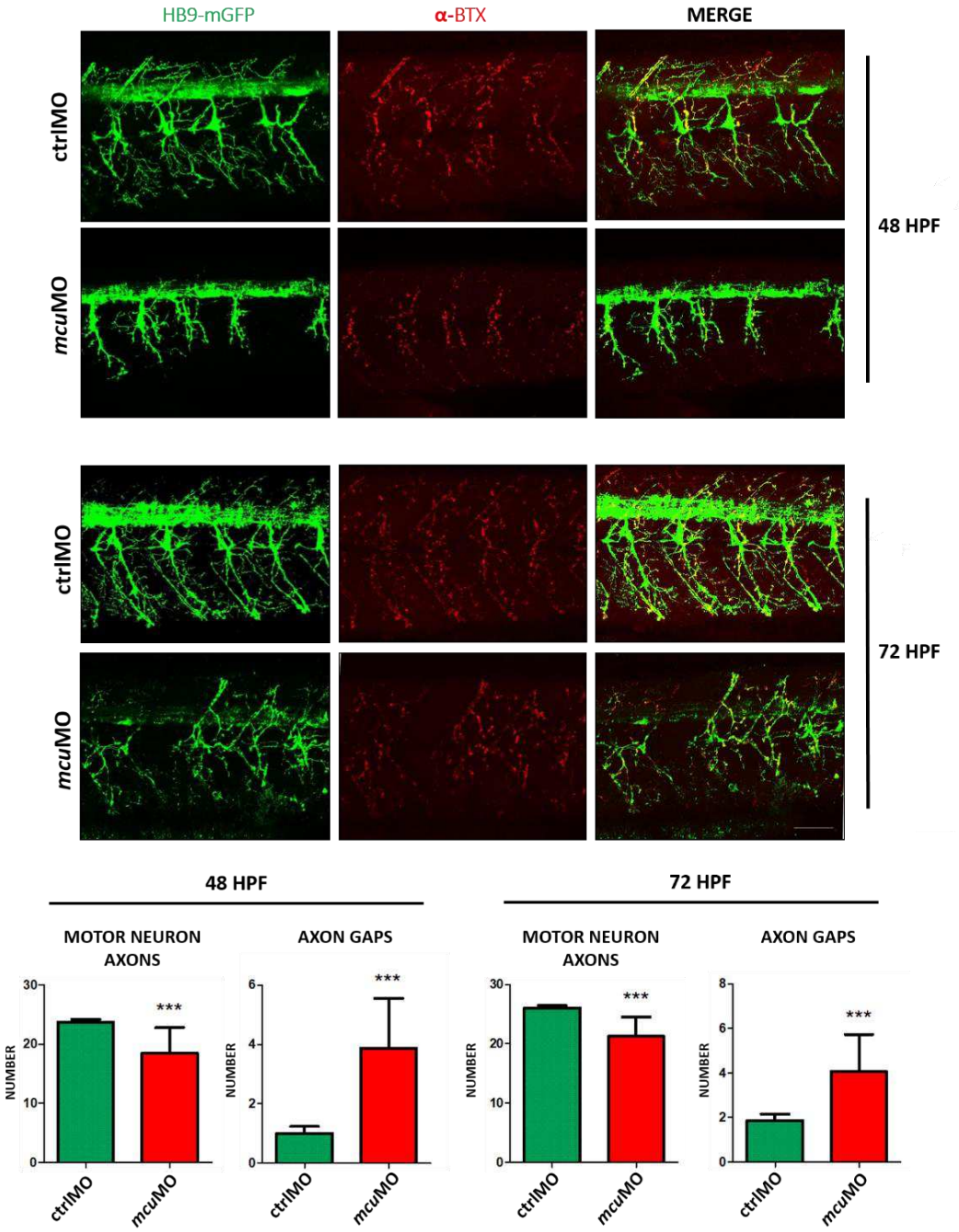

Figure 25. Mcu downregulation impairs neuromuscular development. Representative confocal images of the trunck somites of *Tg(hb9:mGFP)* whole larvae injected with ctrlMO and *mcu*MO after labelling of AchR with TRITC-conjugated α-bungarotoxin at 48 and 72 hpf. Motor neurons are marked by the expression of mitochondria-targeted GFP (mtGFP) in green. AchRs are identified by TRITC signal in red. The graphs represent the quantification of the total number of motor neuron axons and the number of missing axons (gaps) at the two developmental stages analyzed. The number of total motor neuron axons is significantly lower in *mcu* morphants compared to control at the same developmental stage, and the axon gaps present at 48 hpf are not replaced by growing motor neurons at later stages (***, $p<0.001$, n=20).

To analyse the neuromuscular junction (NMJ) number and distribution, we labelled acetylcholine receptors (AchRs) with TRITC-conjugated α-Bungarotoxin and analysed ctrlMO- and *mcu*MO-injected whole embryos at two different time points at confocal microscope. AchR clusters partially colocalize with motor neuron nicely overlapping with neuronal GFP along the axon paths at the NMJ in control animals. Differently, AchRs clustering is reduced and their distribution significantly altered in *mcu*MO-injected fish both at 48 and 72 hpf. From these data, we concluded that Mcu downregulation impairs the development of the motor neuron network and interferes with the establishment of NMJs.

2.8. MCU DOWNREGULATION AFFECTS MUSCLE PRECURSOR CELLS MIGRATION AND DIFFERENTIATION

In order to identify the primary cause of the neuromuscular phenotype and discriminate if it relies on the muscular or neuronal component, we started analysing some crucial steps of the process of skeletal muscle differentiation in control and *mcu* morphants. In particular, we explored the early events in the specification of muscle fiber-type in ctrMO and *mcu*MO- injected developing embryo by characterizing one of the crucial element in the establishment of the neuromuscular system in zebrafish, which is the adaxial cell population (Devoto et al., 1996). Adaxial cells are a sub population of muscle pioneer cells that, at around 30 hpf arise from the mesoderm laterally to the zebrafish notochord and migrate to the surface of the myotome were they will develop into the slow muscle fibers layer that will surround the more internal mass of fast fibers. Beside their relevance as the progenitors of the slow musculature (Cortés et al., 2003; Devoto et al., 1996; Honjo and Eisen, 2005; Hughes, 2004; Jackson and Ingham, 2013a), adaxial cells are also of crucial importance for the axon growth and pathfinding during motor neuron maturation. In order to monitor the number and distribution of these adaxial cells in our experimental model, we performed immunofluorescence analysis using antibodies against Engrailed, a transcription factor specifically

expressed by adaxial cells at this stage. In control embryos the Engrailed-positive adaxial cells are clustered along the mid-line of the dorso-ventral axis, whilst in *mcu* morphants the positive signal almost completely disappears, with a reduction in adaxial cell number, dicreased clusterization and evident mislocalization of the Engrailed expression (Figure 26). Our results inidicates that Mcu downregulation is accompanied by deficit of the adaxial cell population and/or of the signalling that regulates their migration and differentiation, which may be the primary cause of the neuromuscular phenotype observed in *mcu*MO-injected embryos.

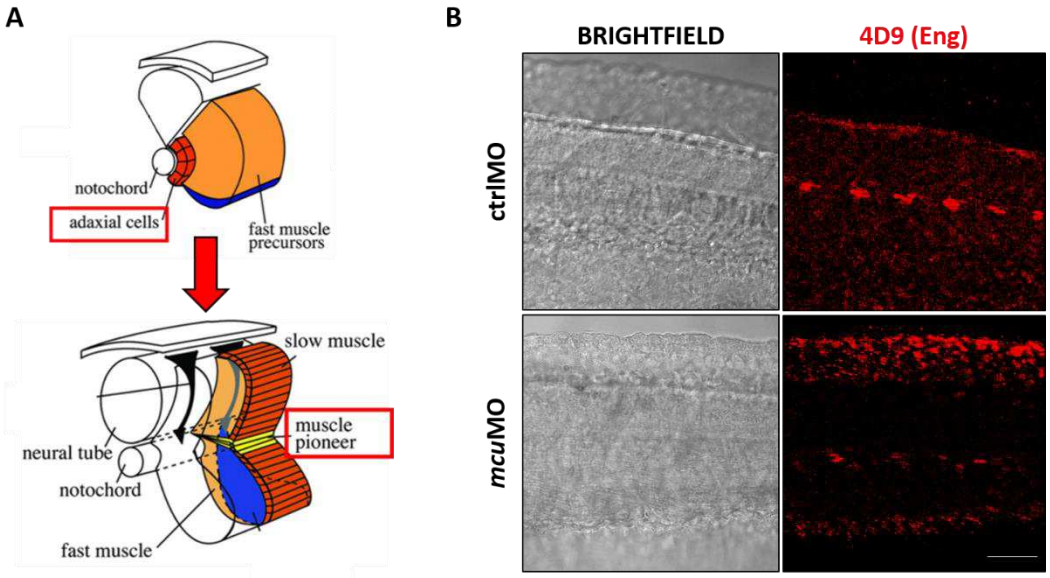

Figure 26. Mcu downregulation impact on adaxial cells population specification. A) Schematic representation of adaxial cells localization and subsequent migration and differentiation (adapted from *Honjo and Eisen, 2005*). B) Immunofluorescence analysis using anti-Engrailed antibodies of 30 hpf embryos injected with ctrlMO and *mcu*MO. Scale bar=50 µm

2.9. MCU KNOCK DOWN IMPINGES ON EMBRYO METABOLISM AND OXIDATIVE STRESS RESPONSE DURING ZEBRAFISH DEVELOPMENT

Mitochondria, being the primary site of cellular energy production, hosting multiple essential biochemical processes and consistently participating to the regulation of the pleiotropic Ca^{2+} signaling, are at the center of cellular metabolism. Moreover, mitochondrial Ca^{2+} accumulation in the mitochondrial matrix has a functional role in stimulating Krebs cycle enzymes and boosting

ATP production. Considering the increasing energy demand of the developing embryo during early developmental growth (Dumollard et al., 2007; Huang et al., 2013b), the investigation of the mechanisms underlying mitochondria metabolism, and in particular the regulation of mitochondrial Ca^{2+} uptake during embryogenesis, is a topic of major interest for a developmental biologist.

We then explored the contribution of Mcu to the embryo response to stress and, in particular, we analyzed the embryonic survival rate to oxidative insults (such as mitochondrial complex I inhibition by rotenone and H_2O_2 exposure) in control and *mcu*MO-injected embryos. First, we treated embryos at 48 hpf with low concentrations of rotenone and hydrogen peroxide and we monitored embryo survival after 8 and 20 hours of treatment. We registered a significant decrease in *mcu* morphants survival already after 8 hours of treatment and after 20 hours less than 30% of *mcu* morphants survived, compared to over 70% of controls (Figure 27). We concluded that Mcu downregulation sensitizes developing embryos to oxidative stress.

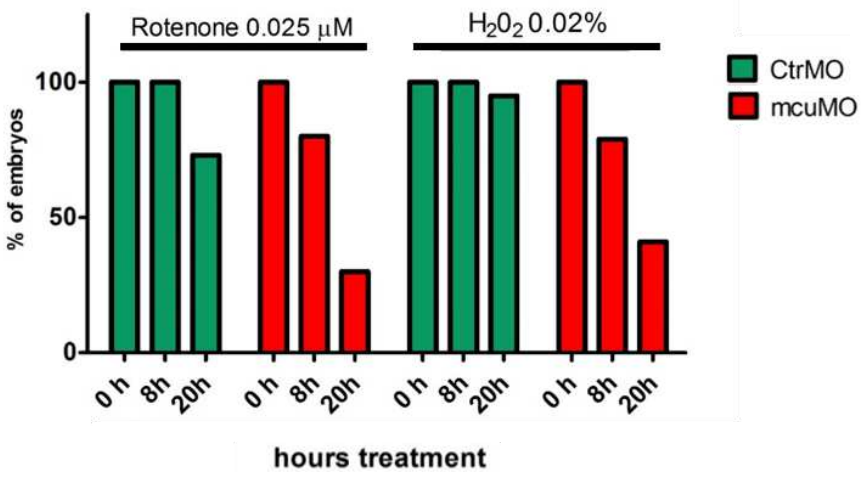

Figure 27. Mcu downregulation sensitizes developing embryos to oxidative stress. 48 hpf control and *mcu*MO-injected embryos were placed in a solution containing embryo medium (fish water) added with 0.025 µM rotenone or 0.02% H_2O_2 and embryo survival was assessed at two different time points: 8 and 20 hours after the additions. Embryo survival is expressed as percentage of living embryos over the total of embryos in the plate (n=30 embryos per condition were considered).

Considering these first results, we wondered whether this increase sensitivity to respiratory chain blockers and ROS was due to an imbalanced basal activity of the respiratory chain of *mcu* morphants that might not cope with their increased energy demand. In order to evaluate this, we performed SeaHorse© experiments to analyze oxygen consumption rate (OCR) in whole zebrafish embryos (Stackley et al. 2011). We choose 4 dpf as an appropriate time point for our analysis, permitting an easier manipulation when fitting the embryo to the special assay plates, where living zebrafish samples need to be immobilized and embryos at early stages, including 72 hpf, are easily damaged. We started the SeaHorse© protocol measuring basal OCR in fish water for 15 minutes, and then we added the uncoupler Carbonyl cyanide 4-(trifluoromethoxy)phenylhydrazone (FCCP) to dissolve the electrical potential of the inner mitochondrial membrane so to maximally stimulating the respiratory chain oxygen consumption and thus calculating the embryo maximal respiration.

After FCCP addition, a combination of rotenone (complex I inhibitor) and antimycin A (complex III inhibitor) is supplemented to the sample in order to blunt mitochondrial oxygen consumption via the blockade of the respiratory complexes (Figure 28). *Mcu* morphants displayed a significant decrease in basal OCR (-20%) and also a decrease in the maximal respiration (-48%) compared to controls.

These data underline the importance of mitochondrial Ca^{2+} signaling for embryo survival to cope with environmental stress condition and with the increasing metabolic demand that are critical and unavoidable during the development of zebrafish and, more generally, of an organism.

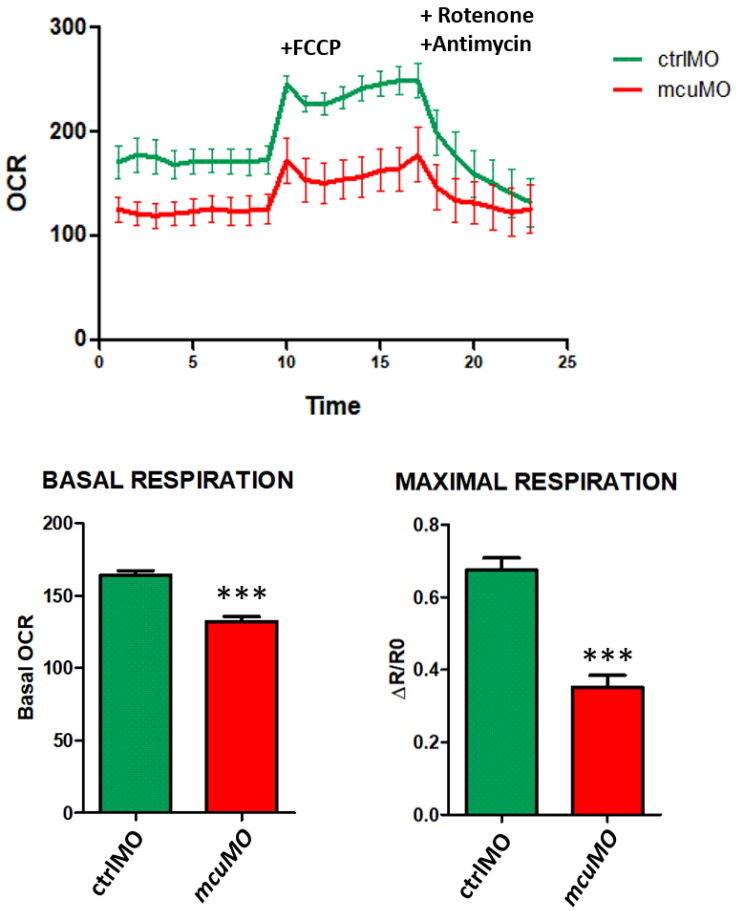

Figure 28. Mcu knock down significantly lowers basal and maximal respiration in zebrafish larvae. Oxygen consumption rate of whole individual zebrafish larvae ctrlMO- and *mcu*MO-injected, was measured with SeaHorse XF at 4 dpf. Larvae were fit in appropriate islet capture plates and OCR was measure in basal conditions and after sequential additions of FCCP (mitochondria uncoupler) and rotenone + antimycinA (inhibitors of complex I and III, respectively). In the graph are reported the quantification of the basal (left) and the maximal (right) respiration (*** $p<0.001$, n=30 larvae per condition were assessed from three independent experiments).

2.10. GENERATION OF ZEBRAFISH *MCU* MUTANT LINE

In order to accomplish the analysis of Mcu role during later zebrafish developmental stages to adulthood and in early embryogenesis before the 30 hpf stage, where *mcu*MO revealed to be unefficient in downregulating Mcu, we undertook the generation of a *mcu* mutant fish line in parallel to the study of transient *mcu* downregulation using MO approach. We exploited CRISPR/Cas9 technology to modify the zebrafish *mcu* locus, a technique that had been largely used in the last years for genomic editing in different organisms,

including zebrafish (Auer et al., 2014; Gagnon et al., 2014; Li et al., 2016b). The protocol for the generation of zebrafish mutant alleles by CRISPR/Cas9 technology involves multiple steps. Firstly, a single guide RNA (sgRNA) optimized for the targeting of the specific gene of interest has to be designed following heuristic rules, which take into account multiple parameters and multiple databases helping in the sgRNA selection are currently available. After synthesis, sgRNAs are injected directly into the zebrafish zygote either with in vitro-synthesized mRNA encoding a nuclear localized Cas9 or with commercially available Cas9 protein with a nuclear localization sequence. Injection of the zygote or early blastula-stage embryo thus generates highly mosaic zebrafish embryos. These latter will grow into mosaic adults that will be outcrossed to wild-type lines to obtain a progeny hopefully containing heterozygous individuals, which can be raised and crossed to generate homozygous mutants (Figure 29 A). Germline mutations can be identified in the offspring in both cases using standard molecular biology methods.

To design zebrafish *mcu* targeted sgRNAs, we implemented the second version of CHOPCHOP (Labun et al., 2016) and selected 6 possible sgRNAs for our genome editing experiments. We then followed the protocol published from Gagnon and colleagues (Gagnon et al., 2014) and after synthetizing the sgRNAs we injected the sgRNA/Cas9 protein in the zebrafish zygotes (data not shown). To increase nuclease cutting efficiency we inject fertilized eggs with a nuclear-targeted Cas9 protein (nCas9n) instead of *Cas9* mRNA molecules. We then performed DNA extraction from injected embryos and with specific primers we amplified the genomic region of interest. To identify the eventual generation of insertion/deletion mutations (indels) by the CRISPR/Cas9 system we used the Heteroduplex Mobility Assay (HMA), a method based on the fact that PCR amplicons which contain indels of various length, are not fully complementary and therefore may generate heteroduplexes after annealing. Heteroduplexes could be distinguished from homoduplexes using poly-acrylamide gel electrophoresis, since the former migrates more slowly than the latter. This method has been successfully used to verify presence of indels

in various examples of genomic editing approaches (Ansai et al., 2014; Ota et al., 2014; Shigeta et al., 2016). We evaluated the editing efficiency of our sgRNAs and we selected the guide targeting on exon 1 of *mcu* locus as the most suitable for our experiments (Figure 29 B). We injected fertilized eggs with sgRNA#4 together with nCas9 protein and collected the developing embryos of this first generation (F_0), raised them to adulthood and outcrossed them with wild type AB/Tuebingen fish (WT), to clean the genetic background of the line and reduce the possibility of off-targets. This generation of F_1 fish were screened for germline transmission of the *mcu* genomic mutations. Briefly, fin clipping of F_1 fish provided tissue for genotyping and, after genomic DNA extraction and PCR amplification, we identify possible mutant alleles as those displaying amplicons of multiple different lengths of in the resolving gel electrophoresis. The amplicons of the selected alleles were then sequenced to precisely identify the nature and extent of the mutation (Figure 29 C-D). A number of germline mutations screened did not lead to the generation of null alleles (insertion or deletion of three or multiple of three base pairs). However, we isolated two founders, one with an insertion of 20 bp ($mcu^{ins20/+}$) and one with a deletion of 14 bp ($mcu^{del14/+}$) that we isolated for future breeding. These heterozygous fish were then outcrossed with WT and their F_2 offspring raised to adulthood and crossed to obtain homozygous $mcu^{ins20/\ ins20}$ and $mcu^{del14/del14}$ (or simply $mcu^{mut/mut}$) fish (Figure 29). The frameshift mutations were predicted to lead to the formation of a premature stop codon (after 124 AA for the 14 bp deletion and 22 AA for 20 bp insertion).

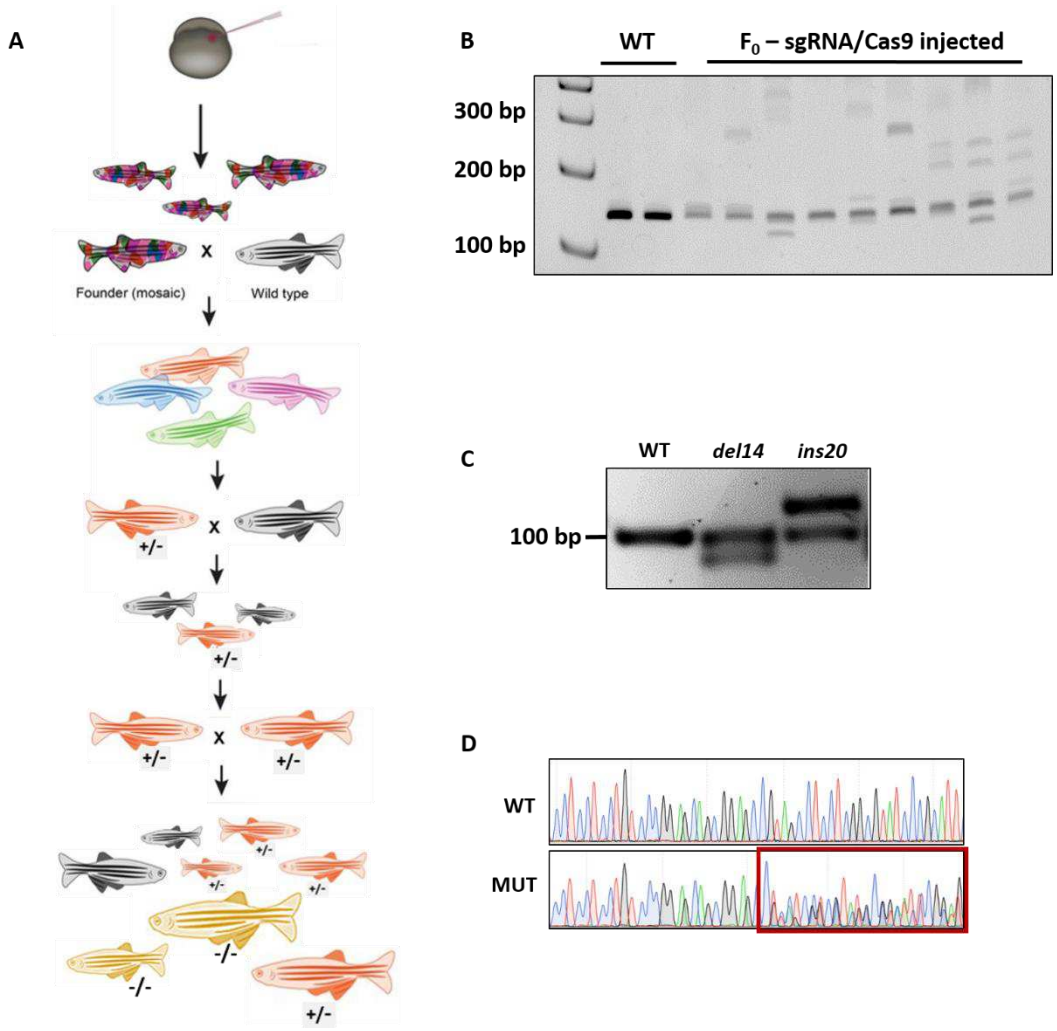

Figure 29. Generation of *mcu*^{mut} line. A) Schematic visualization of the protocol to obtain genomic mutant zebrafish with CRISPR/Cas9 technology. First, we designed the mcu-targeting sgRNAs that were injected in zebrafish fertilized eggs together with the nuclear-targeted Cas9 protein. The resulting F_0 fish were outcrossed with WT fish to obtain F_1 population carrying different mutation. After screening of F_1 adults, we identified two fish carrying a deletion of 14 bp and an insertion of 20 bp, respectively. These F_1 heterozygous fish were outcrossed with WT fish to purify the genetic background and reduce possible off-target transmission. Each of the F_2 heterozigous fish were then incrossed to obtain the F_3 population which may eventually contains the homozygous fish. B) Representative poly-acrylamide gel to identify the genomic editing efficiency of sgRNA/Cas9 injections. The PCR product of 160 bp was analysed by HMA, WT band are visualized as one marked band, as the amplicons have all the same length and form only homoduplexes. The PCR products from fin clipping of F_0 fish evidence multiple bands, due to heteroduplexes formations. C) Representative agarose gel electrophoresis used to discriminate different indels after genomic DNA PCR amplification. The first lane represents the single band of WT fish (amplicon length of 99 bp), the second and the third lanes show 2 amplicon bands of different lengths (one band corresponding to WT DNA and an additional band corresponding to the mutated alleles; namely the *mcu*^{del14} deletion, which migrates faster, and the *mcu*^{ins20} insertion, which migrates slower than the WT. D) The exact length of the indels was confirmed by sequencing, in the chromatogram the double peak corresponding to the presence of wt allele and mutant allele at the same position during sequencing is shown for *mcu*^{del14} F_0 fish.

2.11. MCU EXPRESSION IS ABLATED IN *MCU*^{DEL14} AND *MCU*^{INS20} MUTANT LINES

To confirm the absence of Mcu in our mutant lines, we performed Western blot analysis and we observed not detectable Mcu expression either in *mcu*$^{del14/del14}$ and *mcu*$^{ins20/ins20}$ whole extracts from 5 dpf larvae (Figure 30).

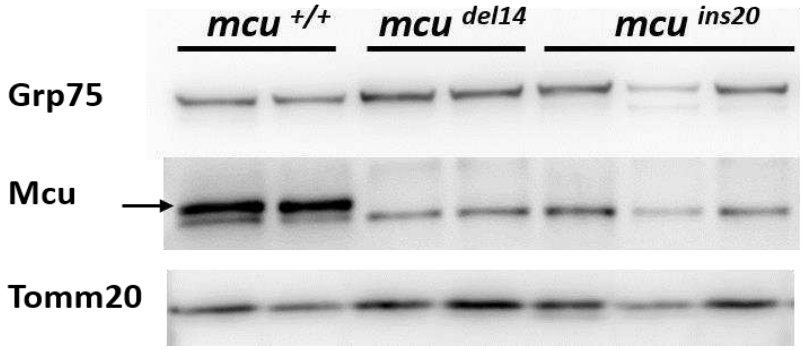

Figure 30. Mcu protein is absent in both zebrafish *mcu*^{del14} and *mcu*^{ins20} mutant lines. Western blot analysis of lysate from 5 dpf larvae of different genotypes. Mcu protein expression is ablated in both mutant lines. Tomm 20 is used as mitochondrial loading control. Mcu antibody detects two bands in zebrafish whole embryo extracts, the specific one is indicated by the arrow.

2.12. MITOCHONDRIAL Ca^{2+} UPTAKE IS BLUNTED IN *MCU*^{DEL14}*/MCU NULL* MUTANT LARVAE

To confirm that absence of Mcu band in Western blot experiments indeed corresponds to a functional impairement of Mcu activity, we measured mitochondrial Ca^{2+} uptake in skeletal muscle fibers from *mcu*^{del14} */mcu null* larvae at 4 dpf, as described for *mcu*MO-injected embryos. The experiment was conducted using Rhod-2 probe to measure mitochondrial Ca^{2+} levels in isolated muscle fibers after 24 hours in culture. Ca^{2+} release from the sarcoplasmatic reticulum (SR) was induced by the addition of the ryanodine receptor agonist caffeine and mitochondrial Ca^{2+} uptake recorded as increase in Rhod-2 fluorescence. Rhod-2 measurements clearly evidenced that mitochondrial Ca^{2+} accumulation upon caffeine challenge is significantly dampened in *mcu*$^{del14/del14}$ compared to control fibers (Figure 31). These

findings are expected for cells lacking Mcu and consistent with those of other *MCU* knockout models (Gherardi et al., 2018; Mammucari et al., 2015; Pan et al., 2013) demonstrating that mitochondrial Ca^{2+} uptake is Mcu-dependent also in zebrafish skeletal muscle.

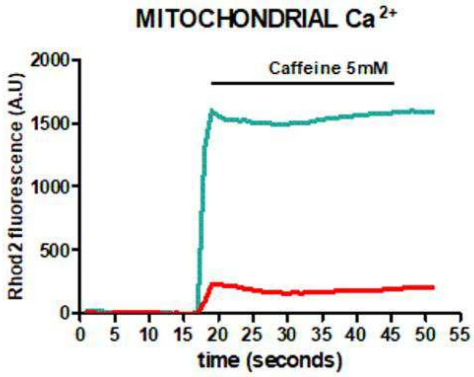

Figure 31. Mcu ablation dampens mitochondrial Ca^{2+} uptake. Representative traces of mitochondrial Ca^{2+} measurements performed on isolated myofibers using Rhod-2 before and after caffeine stimulation in isolated muscle fibers from WT (green) and *mcu*$^{del14/del14}$ (red) larvae at 4dpf.

2.13. MCU ABLATION DOES NOT SIGNIFICANTLY ALTER EMBRYO MORPHOLOGY AT EARLY DEVELOPMENTAL STAGES

After confirming the absence of Mcu protein and the efficient dampening of mitochondrial Ca^{2+} uptake in *mcu null* mutants, we initially analyzed the progression of *mcu* mutant fish development during early embryonic stages. This would allow to assess the eventual occurrence of morphological alterations that were masked in our *mcu*MO-injected embryos due to the presence of a strong maternal mitochondrial component. Even zebrafish embryos, in the absence of Mcu, do not show significant alterations in the first days of development (Figure 32), similarly to what has been reported for the *MCU*$^{-/-}$ mice (Pan et al., 2013). Despite that, at 48 hpf both *mcu*$^{del14/del14}$ *and* *mcu*$^{ins20/ins20}$ embryos showed a significant reduction in length compared to the WT sibling and a small percentage of them (15% in *mcu*$^{del14/del14}$ and 12% in *mcu*$^{ins20/ins20}$ offspring) displayed cardiac edema . Although *mcu* mutant larvae

reach adulthood without evident morphological abnormalities, only half of the expected mendelian ratio was found in the adults.

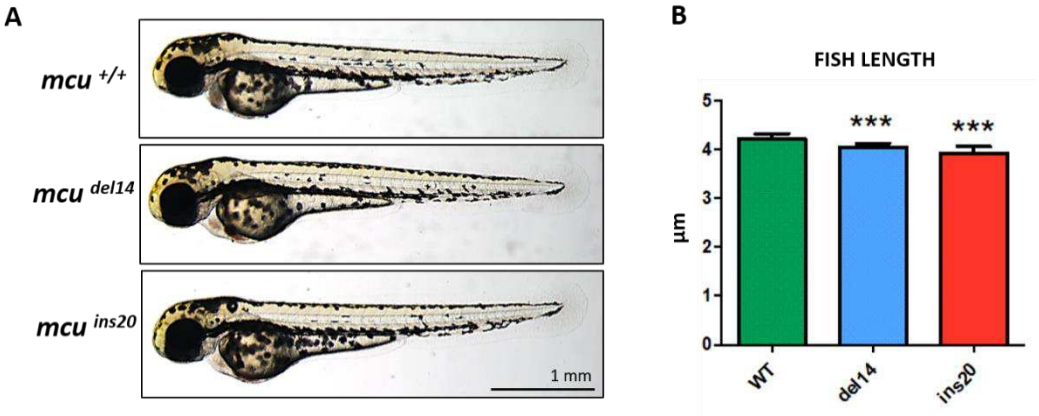

Figure 32. Mcu ablation does not significantly alter embryo development. A) Representative images of 48 hpf embryos of different genotypes, as indicated. Scale bar 1mm. B) Quantification of embryo length, showing a little but significant reduction in the antero-posterior body axis length of *mcu* mutant embryos at 48 hpf (n=30 embryo per genotype were measured, *** $p<0.001$).

2.14. MCU ABLATION LEADS TO LOCOMOTOR IMPAIRMENT IN *MCU* MUTANT FISH

In the course of our preliminary observation of *mcu* mutant fish behaviour, we noticed a reduction of $mcu^{-/-}$ embryo motility after hatching, which lead us to further investigate the locomotor ability of the mutant fish. We thus performed the touch-evoked escape response test in WT and mutant embryos at 48 hpf, as we did for MO-injected embryos. While only a limited percentage (10%) of WT animals had an altered response, the majority of mutant embryos (70% of mcu^{del14} embryos and 80% of mcu^{ins20} (Figure 33), showed an altered response to touch test.

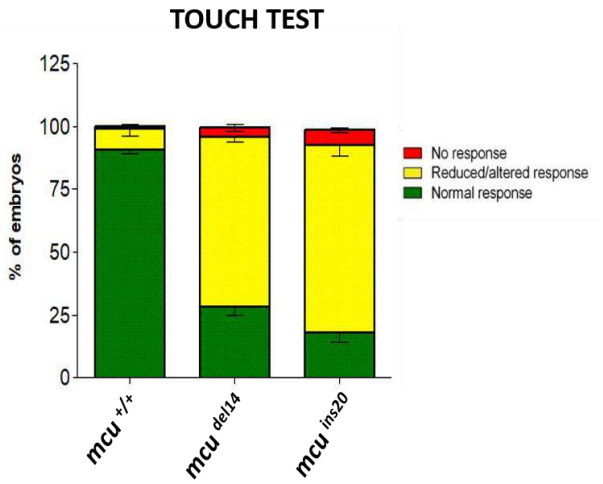

Figure 33. Locomotor impairment is evident in Mcu devoided embryos. Touch test assay was performed on mutant embryos and their WT siblings at 48 hpf. Embryos were put in a petri dish and the tail was gently touched with a capillary tip, escape response was classified as normal (green), altered/reduced (yellow) or no response (red). n = 50 embryos were assessed from 2 independent offsprings.

In order to discriminate if this locomotor defect was related to a specific stage or to a delay in the development, we performed analysis of the swimming behaviour by tracking *mcu*^{del14} larvae movement at 5 dpf. The analysis of locomotor ability of *mcu*^{ins20} larvae is ongoing. From the tracking profile it is clearly evident the difference between the swimming behaviour of mutant larvae and their WT siblings (Figure 34 A). While the latter move all over the arena exploring all the space available, the former concentrate their movements at the center and explore just a limited area of the arena (see Figure 34 A). The heat map depicting with color-based code the amount of time spent either moving or in an halted position, evidences that *mcu*^{del14} larvae spend significant time in an halted position (40% of total recording time), whilst their WT siblings are far more active, moving for more than 80% of the time. Various tracking parameters and components of the movement are now being considered to have a clearer picture of the *mcu* mutant locomotor impairment. However, preliminary data already show that mutant larvae cover a shorter distance at each movement compared to the WT animals and all the cinematic parameters are altered. Overall, our results highlight a

significant deficit of fish locomotor activity as the consequence of Mcu ablation.

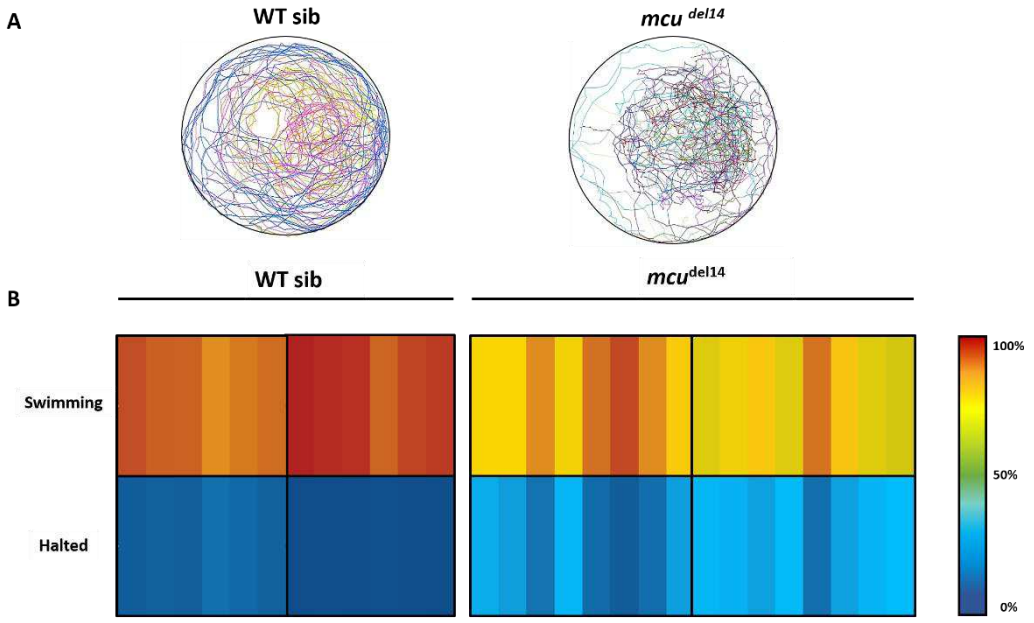

Figure 34. Mcu ablation impairs spontaneous locomotor activity at 5 dpf. Spontaneous locomotor activity was assessed tracking the swimming behaviour of *mcu*$^{del14/del14}$ mutant and wt larvae at 5 dpf. A) Tracking profile of wt and mutant larvae movements within the 10 minutes recording of *mcu*$^{del14/del14}$ (n=12 wt larvae, n=16 mutant larvae mutant larvae were analysed). B) Representative heat map of zebrafish larvae activity expressed as percentage of total 10 minute recording time spent moving (Swimming, upper panels) or in an halted position (Halted, bottom panels). Blue=0% of time, green=50% of time, red=100% of time.. Every rectangle represents an individual.

2.15. THE ABSENCE OF MCU LEADS TO SKELETAL MUSCLE DEFECTS

To verify whether the locomotor deficiency reported at 48 hpf and 5 dpf was due to an impairment of skeletal muscle tissue, we performed ultrastructural analysis of skeletal muscle fibers and their component in 5dpf wt and *mcu* mutant larvae.

Notably, the compact and ordered structure of myofibrillar sarcomeres that is visible in WT sections, is completely altered in Mcu depleted larvae. Although both the Z and M line are correctly aligned, the systematic arrangement of myofibrils is interrupted by an increased number and enlarged size of SR vesicles in the absence of Mcu, as notable in both *mcu*^{del14} and 80 *mcu*^{ins20} mutant larvae (Figure 35). Heterozygous *mcu*$^{del14/+}$ larvae present an

intermediate phenotype (Figure 35). Triads (terminal cisternae of the SR together with their associated T tubule) appear enlarged in the heterozygous larvae, and their structure and distribution are strongly aberrant in homozygous larvae, compared to controls (see Figure 35). Mitochondria are present and tightly packed in highly mitochondria rich regions along myofibers, independently of the genotype. However, in some cases, *mcu* hetero- and homozygous mutant fish show altered mitochondrial cristae morphology and distribution and, interestingly, the presence of these deranged mitochondria and the presence of absolutely normal mitochondria may co-exist within the same myofiber and even in the very same mitochondria enriched region within a muscle fiber.

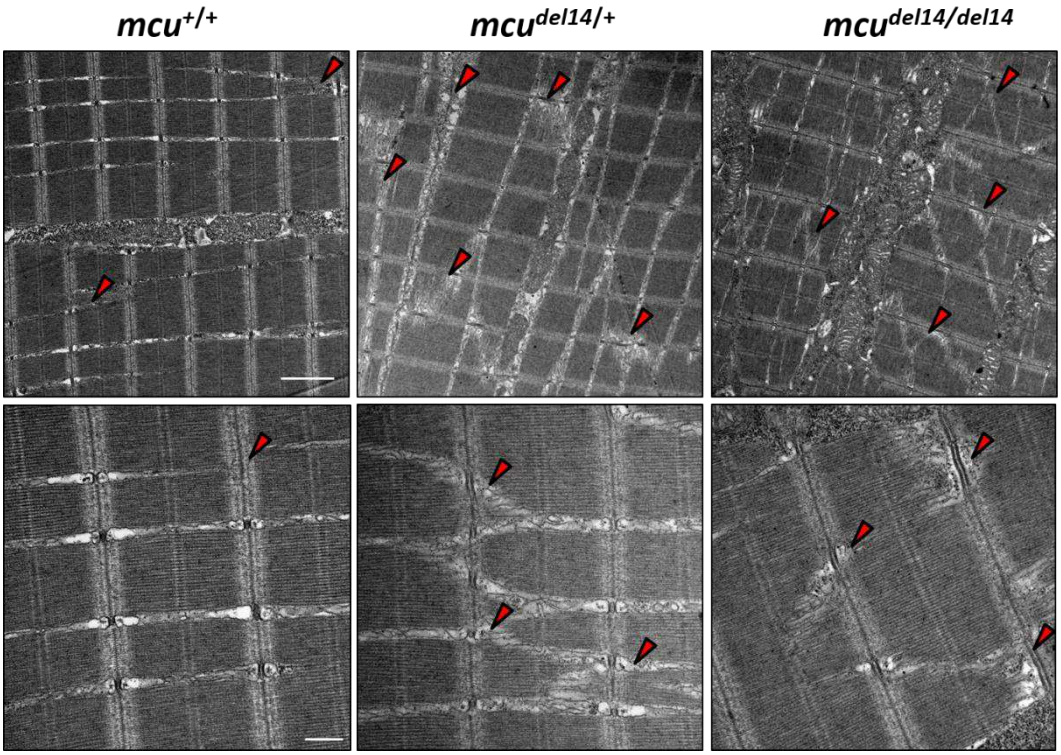

Figure 35. Mcu ablation alters myofibrillar ultrastructure in 5 dfp zebrafish. Representative images of transmission electron microscopy analysis performed on *mcu*$^{del14/del14}$, *mcu*$^{del14/+}$ and WT *mcu*$^{+/+}$ sibling larvae at 5dpf. Note that myofibrillar arrangement, sarcomeric SR vesicle distribution (red arrowhead) and triads (terminal cisternae + T-tubule) are significantly altered in both heterozygous and homozygous mutant larvae. Scale bar = 2 µm (top panels), 500 nm (bottom panels).

Concluding, our findings on *mcu* mutant fish confirm the fundamental role of Mcu in skeletal muscle development and in the maintenance of the physiological function of this tissue.

2.16. ADULT *MCU* MUTANT ZEBRAFISH SHOW ADIPOSE TISSUE ACCUMULATION AND SKELETAL MUSCLE ALTERATIONS

Heterozygous and homozygous *mcu* mutant larvae reach adulthood without displaying significant morphological defects, though WT siblings appear slightly leaner. To note, the incross of *mcu* heterozygous fish to obtain homozygous mutants did not yield the expected mendelian ratio. In fact only 11% of $mcu^{del14/del14}$ and the 15% of $mcu^{ins20/ins20}$ animals reach adulthood, far from the expected 25%. Moreover, we found only 10% of homozygous females. However 4 mpf mutant fish are fertile, can breed and lay eggs.

Despite from a preliminary macroscopic observation *mcu* mutant fish were not significantly different from WT siblings, a more detailed morphological analysis of tissues and organs was conducted on 4 months old fish. Transverse paraffin sections of WT, heterozygous and homozygous mcu^{del14} mutant were stained with Hematoxylin-Eosin unveiling abnormal adipose tissue depositions surrounding and internal to skeletal muscle masses and in the ventral part of the myotome.

Skeletal muscle mass is compact, with an ordered pattern of myofiber distribution and without fat infiltrate in WT animals. In *mcu* mutant muscle, on the contrary, the array of myofiber is less homogeneously distributed, less compact and display significant fat deposition. Also subcutaneous adipose tissue amount is higher in *mcu* mutant compared to WT fish (Figure 36).

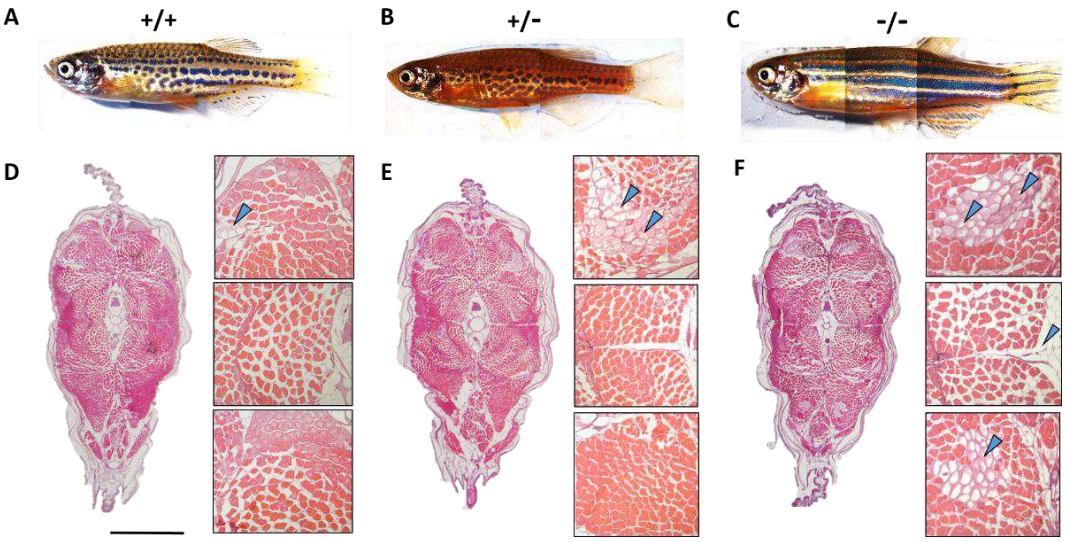

Figure 36. Mcu ablation leads to no major morphological defects, but an increased adipose tissue deposition is found in *mcu*^{del14} fish at 4 mpf. A-C) Representative images of adult WT (A), *mcu*$^{del14/+}$ (B), and *mcu*$^{del14/del14}$ (C) fish at 4 mpf. D-F) Hematoxylin-Eosin staining of transversal paraffin sections of WT (D), *mcu*$^{del14/+}$ heterozygous (E) and *mcu*$^{del14/del14}$ homozygous (F) fish at 4 mpf. Representative images of the entire trunk sections at the level posterior to the anus and details of the musculature of this region at 20-fold higher magnification (see the three insets per group) are presented. Adipose tissue deposition is indicated by blue arrowheads (scale bar=1mm, the enlargements are 20x magnifications of different regions of the corresponding section).

Hematoxylin-Eosin staining on longitudinal sections of WT and homozygous *mcu*$^{del14/del14}$ fish. In these sections, the presence of visceral adipose tissue accumulation in the ventral region is far more evident in *mcu*$^{del14/del14}$ mutant compared to control fish (Figure 37 C-F).

Interestingly, the intestinal folds and villi of mutant fish present some differences compared to WT. In particular, the apical part of the intestinal fold is extremely damaged in mutants. Given the importance of the gut contribution to the general nutrient metabolism and, more in particular, to lipid absorption, accumulation and utilization (Sheng et al., 2018) we postulate that the intestinal defect of mcu mutants may participate in the establishing altered lipid metabolism which may lead to increased fat deposition, as we indeed reported (Figure 36 and Figure 37).

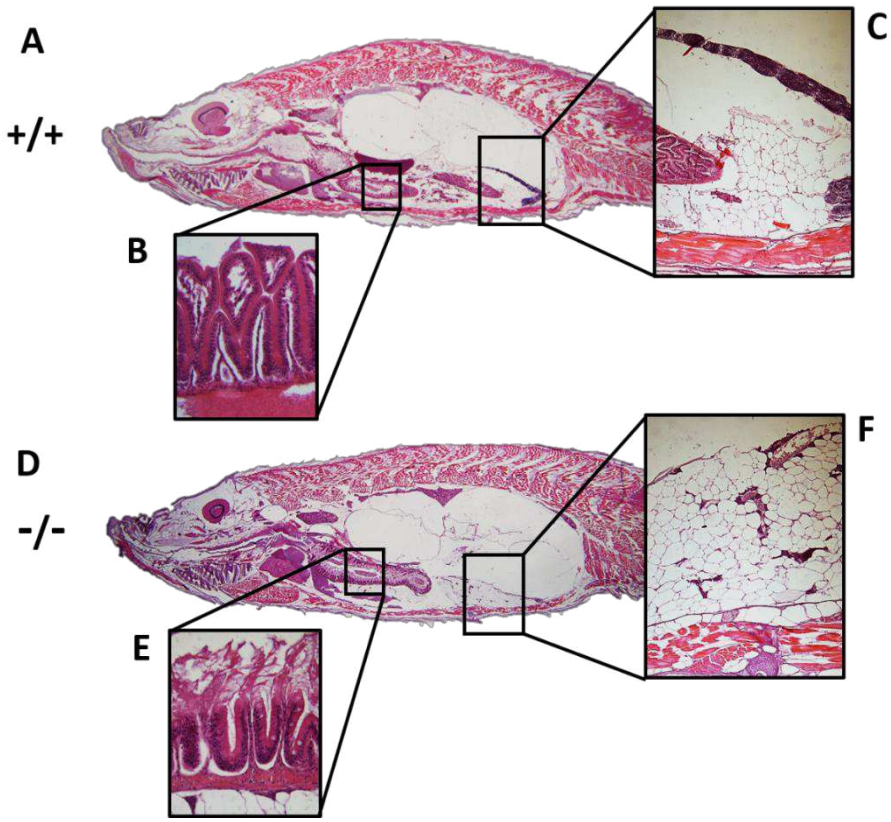

Figure 37. Mcu mutant fish display adipose tissue accumulation and intestinal fold impairment at 4 mpf. Hematoxylin-Eosin staining of longitudinal paraffin sections of WT (A) and homozygous *mcu*$^{del14/del14}$ fish (D) at 4 mpf. Representative images on an entire section are reported. B,E) Magnification of intestinal villi of WT (B) and *mcu*$^{del14/del14}$ (E) fish. C,F) Magnification of adipose tissue accumulation in the ventral region (40x magnifications of different regions of the corresponding section).

3. DISCUSSION AND CONCLUSIONS

Mitochondrial Ca^{2+} signaling has many roles in cell function, metabolism and survival (Granatiero et al., 2017; Raffaello et al., 2016). Recently, the channel responsible for Ca^{2+} entry into the mitochondria, the mitochondrial calcium uniporter (MCU) (Baughman et al., 2011; De Stefani et al., 2011a), and its regulators (MICU1, MICU2, MICU3, MCUb and EMRE) (see chapter 1.4, 1.5, 1.6 for detailed description of the complex components) have been identified. In the last years, several cellular and mouse models for the study of the MCU complex have been generated, demonstrating the importance of mitochondrial Ca^{2+} in physiological and pathological conditions (De Stefani et al., 2016). MCU plays a fundamental role in cancer progression (Tosatto et al., 2016), neuronal activity and survival (Qiu et al., 2013), heart function (Williams et al., 2015; Wu et al., 2015) and skeletal muscle trophism (Mammucari et al., 2018). Moreover, the ablation of MCU in the pure C57BL/6 mouse strain leads to embryonic lethality, pointing to a possible involvement of the uniporter in early developmental stage (Harrington and Murphy, 2015; Pendin et al., 2014). In this context, our work aimed to explore the contribution of MCU and mitochondrial Ca^{2+} uptake to organogenesis and embryonic development. To do this we decided to exploit *Danio rerio,* commonly known as zebrafish, as animal model for our study. In the last years, it has revealed to be an extremely powerful experimental research model in various areas of biology and biomedicine, due to the many advantageous features of this organism, such as: rapid development, external fertilization, transparency of eggs and embryos, large progenies, ease of genetic manipulation. In addition, genome

organization and the major signaling pathways involved in organogenesis and development are highly conserved from lower vertebrates to humans (Fuentes et al., 2018; Granato and Nüsslein-Volhard, 1996; Nasevicius and Ekker, 2000), making zebrafish extremely useful for studying embryogenesis as well as modelling human diseases (Elmonem et al., 2018; Lin, 2012; Naert and Vleminckx, 2018; Sakai et al., 2018). We focused our attention on the pore forming subunit Mcu, and we adopted two different reverse genetic strategies to explore its contribution to zebrafish development and physiology: i) the downregulation of Mcu using antisense oligonucleotides in fertilized eggs, and ii) the generation of a stable *mcu* mutant zebrafish animal.

In situ hybridization data previously obtained in our laboratory showed an ubiquitous *mcu* mRNA expression, with an increased regionalization at late larval stages, and reported the presence of the Mcu protein already at early embryonic stages. We designed morpholino-modified antisense oligonucleotides (MOs) to specifically target *mcu* mRNA in developing embryos. MO strategy has already been successfully used to study gene function during development (Bill et al., 2009; Corey and Abrams, 2001; Rosen et al., 2009) (see chapters 1.13 and 1.14 for a detailed description of MO strategy). Unexpectedly, we obtained a very strong Mcu downregulation only after 30 hpf, with a maximal MO interfering activity at 48 hpf, whilst the downregulation of most MO-targets has been reported to occur efficiently already at 24 hpf. However, it has been reported that maternal organelles are distributed among the blastomeres according to a partitioning mechanism in the oocyte, and that mtDNA replication is halted during the very early stages of zebrafish development, as the total amount of mtDNA measured per embryo remains stable through to at least 24 hpf (Artuso et al., 2012). In addition, Mcu is an IMM integral protein, with a relatively long half-life, suggesting that zebrafish zygotic mitochondria may receive a strong contribution from maternal Mcu proteins, which cannot be targeted by MO molecules during the first zygotic divisions. Thus, the *mcu* mRNA will be accessible to the atg- and spl-*mcu*MO only after the beginning of zygotic transcription and Mcu protein

downregulation will be relevant only when its turnover rate will allow the replacement of maternal Mcu with newly synthetized protein. This may explain why Mcu downregulation is detected only from 30 hpf and becomes significant from 48 hpf. For this reason, in order to study the effect of Mcu knock down in morphant embryos we choose 48 hpf (corresponding to 48 hours after microinjection) as the optimal time point for our observations.

Thus, we started our analysis by assessing the phenotype of injected embryos at 48 hpf, reporting no major morphological abnormalities but a significant impairment of locomotor activity in both atg- and spl-*mcu*MO-injected embryos.

The analysis of embryonic cell death has also been performed at different time points after MO injection, using Acridine Orange staining (Tucker and Lardelli, 2007), which revealed the occurrence of an enhanced cell loss in embryos injected with the atg-*mcu*MO and spl-*mcu*MO respect to controls. Cell death was mainly localized in the neural tube and head region of the 24 hpf *mcu* morphants and diminished over time, becoming nearly undetectable at 48 hpf. Thus, this transient cell death did not overlap with Mcu downregulation profile. Neural cell death at 24 hpf was recently reported to be one of the possible off-target effects of MO injection, due to aspecific p53-mediated apoptosis activation in response to MO molecule and independent of the target gene (Robu et al., 2007). To verify if the aspecific *p53* pro-apototic pathway activation was also occurring in our model, we blocked p53 with a targeted MO. In atg-*mcu*MO/*p53*MO co-injected embryos, neuronal cell death was comparable to controls, confirming that the increased neuronal cell loss in *mcu* morphant embryos was due to off-target p53 activation due to MO molecule. To overcome this issue, we developed and optimized a MO-injection protocol, which consists in co-injecting a mixture of the atg- and spl- *mcu*MOs, each at sub-effective dose (Bill et al., 2009; Eisen and Smith, 2008; Robu et al., 2007). This approach proved to be successful, leading to an efficient Mcu protein knockdown with negligible off-target neuronal cell death, and was then used for all the following experiments.

We next wanted to demonstrate that Mcu downregulation indeed affects mitochondrial Ca^{2+} uptake in developing zebrafish. MCU ablation or knock down has already been shown to impact on mitochondrial Ca^{2+} uptake, leading to its abrogation or dampening (Hamilton et al., 2018; Mammucari et al., 2015; Pan et al., 2013; De Stefani et al., 2011b). Prudent and colleagues, in their study of Bcl-wav role in zebrafish notochord axis formation, described a model for Mcu downregulation through MO-mediated knock down (Prudent et al., 2013). The authors reported a reduction in mitochondrial Ca^{2+} uptake in *mcu* morphant embryos at 75% epiboly stage, which corresponds to 8 hpf, much earlier than 30 hpf, time point at which we detect an efficient Mcu downregulation upon MO injection. In a second study, *mcu*MO injection was used to downregulate Mcu in *pink*^{1Y431*} mutant zebrafish, in order to reduce mitochondrial Ca^{2+} uptake in dopaminergic zebrafish neurons (Soman et al., 2017). However, no Ca^{2+} measurements have been provided from the authors. Similarly, another group used Mcu overexpression to increase mitochondrial Ca^{2+} uptake, but the experimental evidence is again missing (Shimizu et al., 2015).

To perform Ca^{2+} measurements in our study, we developed a protocol consisting in the isolation of skeletal muscle fibers from zebrafish larvae (adapted from Horstick et al., 2013, described in details in chapter 4.6, 4.7, 4.8) where cytosolic and mitochondrial Ca^{2+} dynamics were monitored by the specific Ca^{2+} probes Fura-2 and Rhod-2, respectively. We demonstrated that Mcu downregulation is indeed accompanied by altered Ca^{2+} dynamics in myofibers derived from zebrafish embryos. In particular, we recorded a blunting of mitochondrial Ca^{2+} uptake following agonist stimulation and an increase in cytosolic Ca^{2+} transients, probably due to a reduced mitochondrial buffering capacity, as it has already been reported in other MCU knockout models (Lombardi et al., 2017; Luongo et al., 2015).

Following, we checked mitochondrial morphology with different approaches, demonstrating that it was not altered upon Mcu downregulation, in line with previous findings (Mammucari et al., 2015; Pan et al., 2013), excluding an

involvement of Mcu in the arrangement, distribution and position of mitochondria in developing zebrafish embryos.

We proceeded analyzing *mcu* morphants from a macroscopic and morpho-functional point of view. No major abnormalities or morphological defects have been observed. The progression of the development is overall similar in Mcu downregulated and control embryos, although they display a slight reduction in size (15% decrease in dorso-ventral axis length compared to controls), similarly to what has been found in total *MCU*$^{-/-}$ mice (Pan et al., 2013). Interestingly, the functional analysis of embryo locomotor activity by the touch-evoked escape response assay at 48 hpf revealed an impairment of *mcu* morphant response to mechanical stimulation. This reveals an important role of Mcu-mediated regulation of cellular Ca^{2+} dynamics in the establishment of a functional locomotor system in the developing zebrafish embryo.

Locomotor impairment is a hallmark of a number of pathological conditions, in particular of those affecting the skeletal muscle and the nervous system (Drapeau et al., 2002; Granato et al., 1996; Low et al., 2012; Saint-Amant and Drapeau, 1998). For this reason, we investigated the skeletal muscle component in developing *mcu* morphants, both at embryonic and larval stage. A reduction in fiber size and an increased inter-myofibrillar space, as revealed by actin and myosin staining, together with a deranged array of sarcomeric units, assessed by birefringence assay, were observed in myofibers of Mcu downregulated embryos. As in mammals, zebrafish skeletal muscle is composed of two types of fibers, fast and slow, which differ for both physiological (velocity of contraction) and metabolic (glycolytic versus oxidative) properties (see chapter 1.11). In zebrafish, slow fibers form a thin layer of mononucleated muscle cells at the periphery of the myotome, which mainly consists of multinucleated fast fibers (Gurevich et al., 2015; Jackson and Ingham, 2013). Ca^{2+} has been reported to be one of the most important second messengers implicated in the control of many biological functions both at the cellular and tissue level, including the regulation muscle formation (for a detailed review see Webb and Miller, 2011). Given the altered Ca^{2+} dynamics

recorded in *mcu* morphants and considering the recent findings on the effect of MCU modulation in mammalian muscle tissue homeostasis (Gherardi et al., 2018; Mammucari et al., 2015), we wondered whether Mcu downregulation and the associated blunting of mitochondrial Ca^{2+} uptake could affect skeletal muscle development and fiber-type specification in zebrafish embryos. We observed evident alterations in the morphology and arrangement of both slow and fast *mcu*MO myofibers. With respect to the fiber-type specificity, slow fibers appeared more affected than the fast. However, this difference is somehow expected if one considers the divergent regulatory and transcriptional pathways characterizing the two fiber-types (Buckingham and Vincent, 2009; Devoto et al., 1996; von Hofsten et al., 2008), which may explain their different sensitivity to Ca^{2+} signals. In light of this, it would be exceedingly interesting to analyze the fiber-type specific gene expression profile, to understand the molecular mechanism by which alterations in Ca^{2+} dynamics can differently affect the nuclear transcription program of distinct fiber-types, as it has already been shown the importance of Ca^{2+} in modulating gene expression (van Haasteren et al., 1999). Neverthless, these investigations are beyond the scope of the present thesis and need to be addressed in the future.

It should be kept in mind that skeletal muscle tissue is not the only component determining locomotor activity; indeed, the nervous system, in particular the motor neuronal network, plays also a relevant role (Saint-Amant and Drapeau, 1998).

The evaluation of the motor neuron population in *mcu*MO-injected *Tg(hb9:mGFP)* embryos, evidenced a compromised motor neuron network in the presence of reduced Mcu levels. Developing motor neurons are strongly dependent on the sustenance and growth factors provided by surrounding tissues, especially by the migrating muscle pioneer cells, which originate from adaxial cells (Beattie, 2000; Devoto et al., 1996; Zeller et al., 2002). Our hypothesis is that the impairment in axon pathfinding displayed by *mcu* morphant embryos may be due to the defective action/differentiation of the adaxial cell population. The analysis of adaxial cells in *mcu*MO-injected

embryos showed a remarkable mislocalization of these cells, and a strong reduction in their number compared to control embryos. This confirms the fact that their deficit may contribute to the defective skeletal muscle-motor neuron developmental axis observed in Mcu-deficient embryos, as we initially hypothesized. An alternative explanation concerns the role of Ca^{2+} as a fundamental mediator of neuronal firing activity and signaling (Belgacem and Borodinsky, 2011), which suggests that an altered Ca^{2+} homeostasis in developing neuronal cells may itself impinge on axon growth. As third possibility, we cannot exclude that the observed phenotype is due to a combination of both mechanisms. Future experiments specifically addressing this issue will help to elucidate which of the proposed hypothesis holds true.

An additional aspect needs to be considered in order to explain the defective muscle development and the impairment in axon pathfinding, which involves Sonic Hedgehog (*shh* or *hh*). Hh is a fundamental signaling pathway that governs many developmental processes and is today considered as a paradigm for classical morphogens playing fundamental roles in various processes, from embryogenesis to cancer (Lee et al., 2016). Dysfunction in the Hh pathway leads to several developmental abnormalities and diseases, making it an important therapeutic target. Interestingly, in zebrafish, *Shh* pathway is reported to play a role both in muscle fiber-type specification during somitogenesis and axon guidance (Blagden et al., 1997; HUGHES et al., 1998; Ingham and Kim, 2005; Wolff et al., 2003; Yam and Charron, 2013; Yam et al., 2009). Moreover, it has been recently shown that intracellular Ca^{2+} signaling controls the level of Shh-dependent gene expression in target cells, thus affecting their final developmental outcome in the zebrafish embryo (Klatt Shaw et al., 2018). Since we demonstrated that Mcu downregulation not only dramatically dampens mitochondrial Ca^{2+} uptake, but also alters intracellular Ca^{2+} dynamics, we could envisage that this dysregulation in Ca^{2+} signaling may impinge on the Shh pathway, thus causing the neuro-muscular developmental axis alterations observed in *mcu* morphants. However, this eventuality still needs to be investigated.

Another important issue we wanted to address was the effect of Mcu downregulation on metabolism and energetics of developing zebrafish embryo, given the fundamental role of mitochondrial Ca^{2+} in the regulation of crucial TCA cycle dehydrogenases and of the respiratory chain activity (Griffiths and Rutter, 2009; Tarasov et al., 2012). In the very early stages of development, zebrafish embryo metabolism relies uniquely on the presence of the yolk sac, which provides all the nutrients required to its sustenance (Quinlivan and Farber, 2017). At a macroscopic observation, the yolk sac of *mcu* morphants appeared larger compared to controls at 5 dpf and both basal and maximal respiration result significantly lower than those of control larvae. This is compatible with a lower energy production of Mcu downregulated animals, since the dampening of mitochondrial Ca^{2+} uptake may cause a reduction in the TCA cycle activity and ATP synthesis, and subsequent lowering in energy demand. This translates into reduced consumption of yolk content. Our results are in line with very recent findings obtained in our laboratory in skeletal muscle specific knockout mice (*skMCU*$^{-/-}$), where MCU loss can limit the supply of reducing equivalents to the electron transport chain, thus lowering OCR already in basal conditions (Gherardi et al., 2018). The impairment in the respiratory chain could finally lead to mitochondrial dysfunction, thus making embryos more sensitive to oxidative stress when treated with respiratory chain inhibitors (rotenone, complex I inhibitor) or ROS-inducing agent (hydrogen peroxide). Together, these results highlight the fundamental contribution of Mcu and mitochondrial Ca^{2+} uptake to metabolism and energy production in the developing zebrafish embryo. In this context, it would be interesting to analyze the yolk composition at different developmental stages (Quinlivan and Farber, 2017), to understand which is the substrate preference of control and *mcu* morphant animals. We plan to undertake these investigations in the future.

The ultrastructural analysis performed on 5 dpf larvae revealed an altered myofiber ultrastructure in *mcu* morphants compared to controls, with the presence of abundant sarcoplasmic reticulum vesicles, abnormally crossing

the actin filaments and interrupting the ordered myofibrillar structure, enlarged and disarranged triads and less electron-dense mitochondria with a lower amount of cristae, despite some of them retain a normal ultrastructure. Concerning the myofiber ultrastructural alterations and SR enlargement, we hypothesize that they may arise as a consequence of the prolonged alteration in Ca^{2+} dynamics. The SR is responsible for the active storage, release and re-uptake of Ca^{2+} ions and altering the function of that machinery and its involved proteins can cause skeletal muscle related pathologies (Dorn and Maack, 2013; García-Pérez et al., 2008; Rossi and Dirksen, 2006). To unveil the contribution of the SR to the *mcu* morphant defects, additional investigation of the SR-Ca^{2+} storage capacity and evaluation of the expression of Ca^{2+}-related channels and proteins have been already planned.

To better characterize the role of Mcu during zebrafish embryogenesis overcoming the maternal mitochondrial contribution issue and at later developmental stages, including adulthood, the generation of a stable *mcu* mutant zebrafish was needed. In addition, this could be used to validate and integrate the MO approach and the stable *mcu* mutant phenotype will be reinforced and corroborated by the *mcu* morphant model, since mutants and morphants often exhibit distinct phenotypes (Kok et al., 2015; Robu et al., 2007). In 2001, a zebrafish *mcu* mutant line has been generated with gene trap technique, and was described not to display particular developmental defects (Trinh et al., 2011). Nowadays, the widespread availability of site-specific nucleases enables targeted genome editing in zebrafish. In particular, we used the CRISPR–Cas9 system (see chapter 1.16 for details). We generated two *mcu* mutant lines, one with a deletion of 14 bp (mcu^{del14}) and one with an insertion of 20 bp (mcu^{ins20}) in exon 1 of *mcu* locus. Both lines lack Mcu protein expression, but we have no data about the protein level of other MCU complex components due to the lack of specific antibodies for the zebrafish isoforms. However, we already planned qPCR experiments to assess their mRNA expression. Ca^{2+} measurements on isolated muscle fibers, demonstrated the blunting of mitochondrial Ca^{2+} uptake in mcu^{del14} fibers, similarly to what is

already reported for knock out mouse models (Gherardi et al., 2018; Luongo et al., 2015; Pan et al., 2013) and in line with what previously obtained with the MO model.

Mitochondrial Ca^{2+} uptake measurements were performed with the mitochondrial Ca^{2+} probe Rhod-2. Despite Rhod-2 can mislocalize outside the mitochondrial compartment (cytosol and nucleus), the cytosolic concentration of the probe is generally far lower than that in the mitochondria and mitochondrial Ca^{2+} measurements usually are not significantly affected by the eventual cytosolic signal of the probe (Boitier et al., 1999; Collins et al., 2001). Nevertheless, we still observed a residual Rhod-2 signal in response to agonist stimulation, which was difficult to definitively localize to the mitochondria of *mcu* mutant fibers. It is possible that the agonist induced mitochondrial Rhod-2 signal, which is forcedly very low due to the lack of Mcu-mediated Ca^{2+} uptake in mitochondria of *mcu* mutant fibers, may be masked by the relatively enhanced Rhod-2 signal in the cytosol. Another explanation for the residual mitochondrial Ca^{2+} uptake in the absence of Mcu has been recently proposed by envisaging the entry of Ca^{2+} into the mitochondria through a mechanism independent of the uniporter activity (Hamilton et al., 2018). Further analysis will elucidate this point.

Homozygous embryos of both mutant lines display a little but significant decrease in total length at 48 hpf, in line with the findings obtained in the *MCU* knockout mice (Pan et al., 2013) and supporting the role of Mcu in controlling trophism, as demonstrated in muscle tissue (Mammucari et al., 2015). We confirmed the involvement of Mcu in locomotor function, both with touch-evoked escape response and tracking of spontaneous locomotor activity at 5 dpf. The characterization of the tracking profile and the detailed analysis of all the kinetic parameters of mutant larvae will help to shed light on the possible involvement of specific neuronal components. Regarding skeletal muscle development, preliminary data revealed a general impairment of skeletal muscle tissue in mutant larvae. Transmission electron microscopy analysis clearly shows ultrastructural alteration in *mcu* mutants (both homozygous

and heterozygous) that are very similar to what observed in the *mcu*MO-injected animals. Notably, in addition to SR derangement, triads display an aberrant structure in the homozygous mutant.

The fish of both mutant lines reach adulthood and are fertile. However, only the 11% of *mcu*^{del14} and 15% of *mcu*^{ins20} adult fish are found, a percentage far from the expected mendelian ratio. This underlines the fundamental contribution of Mcu not only in the first stages of development and organogenesis, but also to later stages of juvenile-to-adult progression, where the increasing energy demand of growing larvae plays a major role. Very interestingly, preliminary histological assessment of adult mutant fish, shows an abnormal accumulation of adipose tissue in the ventral region and in the myotome. These abnormal adipose deposits are present in homozygous fish and, to a lesser extent, also in heterozygous fish. This could reasonably be due to metabolic alterations, as data recently published by our laboratory in the mouse model (Gherardi et al., 2018) also suggest. As already reported in *mcu* morphants, preliminary data suggest that the absence of MCU reduces mitochondrial respiration also in *mcu* mutants (lower mitochondrial Ca^{2+} uptake induces lower OXPHOS and ATP production, thus reducing utilization of substrates and subsequent lowering of energy demand). We hypothesize that the unused substrates accumulate, thus favoring lipid deposition which, in turn associated with an altered mitochondrial metabolism, may be responsible for the metabolic changes and activation of systemic signaling, including inflammation and modulation of gene expression (Anderson et al., 2011; Carten et al., 2011; Esteves et al., 2016; Semova et al., 2012). In this context, it would be interesting to analyze the level of myokines and cytokines (Leal et al., 2018) in mutant larvae, to understand the cross-talk between skeletal muscle and adipose tissue in zebrafish and the possibility of Ca^{2+} modulation of metabolic rewiring (Flynn et al., 2009; Hölttä-Vuori et al., 2010; Vargas, 2018).

In conclusion, our work has been aimed to explore the role of mitochondrial Ca^{2+} uptake in vertebrate development. To date, our results highlight its fundamental contribution to the differentiation and maturation of both skeletal muscle tissue and motor neuron network and highlight the dramatic impact of Ca^{2+} dysregulation, due to the lack of Mcu, in metabolism of developing embryos and larvae. The characterization of the *mcu* mutants that we generated, together with the multiple advantages of the zebrafish model, including the easiness of manipulation and the increasing availability of zebrafish transgenic/mutant disease models, will help to further elucidate the involvement of mitochondrial Ca^{2+} in vertebrate organogenesis, physiology and, importantly, pathology. Last, the *mcu* mutant zebrafish that we generated could be an extremely powerful model to modulate Ca^{2+} dynamics in pathological conditions where mitochondrial Ca^{2+} overload has been proved to be detrimental, such as Parkinson's disease and dystrophies just to mention two of them (Berger and Currie, 2012; Tranchant and Anheim, 2016; Zhang et al., 2015).

4. MATERIALS AND METHODS

4.1. ZEBRAFISH MAINTENANCE

Wild type, mutant and transgenic zebrafish were staged and maintained according to standard procedures (Kimmel et al., 1995) . Embryos were raised at 28 °C in Petri dishes containing fish water (50X: 25g Instant Ocean, 39.25 g $CaSO_4$ and 5g $NaHCO_3$ for preparing 1 liter) and kept in a 12:12 light-dark (LD) cycle. For screening and in vivo imaging, embryos and larvae were anesthetized with 0.04% tricaine (Sigma-Aldrich, E10521). The *Tg(kdrl:mlsGFP)* transgenic line was kindly provided by Prof. Didier Stainier (Max Planck Institute).

4.2. MORPHOLINO INJECTION

All the MOs were ordered from Gene Tools (Philomath, OR, USA). The antisense MOs used for the reverse genetic experiments in zebrafish have been designed against the ATG translation start site of *mcu* mRNA and against the splicing site in exon2-intron2 junction.

atg-*mcu*MO sequence: 5'-ATC TAC ACA CTT TCG CAG CCA TCT C-3'

spl-*mcu*MO sequence: 5'-TCA AGA GTA AAG CAC TGA CCT GGG C-3'

Additional MO used: ctrlMO 5'-CCT CTT ACC TCA GTT ACA ATT TAT A-3', *p53*MO (Robu et al., 2007)

All the MOs were reconstituted at 1 mM in nuclease-free water. Different MOs concentrations were tested in a range between 1 and 2.5 µg/µl. MOs

and plasmids (see below) were injected into the yolk at 1/2-cell stage. Injected embryos were raised to the desired stage for observations or collected for subsequent analysis.

4.3. GENERATION OF THE *MCU* MUTANT LINE

Mcu mutants were generated using the CRISPR/Cas9-mediated genome editing. Gene-specific guide RNA (sgRNA) were designed against an optimal CRISPR site in exon 21 of *mcu* (NM_001077325) using CHOPCHOP software (available at: https://chopchop.rc.fas.harvard.edu). BLAST analysis of the target sequence revealed no specific binding with other genes. sgRNA was generated according to previously described methods (Gagnon et al., 2014) and *in vitro* transcribed using MEGAshortscript T7 kit (Life Technologies, AM1354). Cas9 commercially available protein was used for efficient sgRNA injection. Fertilized eggs were injected with 1 nl of a solution containing 300 ng/µl Cas9 protein and 60 ng/µl sgRNA.

sgRNA sequence: GGGATACGCCGAGGAGGCTACGG

Genomic DNA was extracted from 3 dpf larvae individually injected to verify the presence of mutations and confirm the activity of the guide. Injected embryos were raised to adulthood and F_0 founders selected by genotyping. Embryos were collected from the outcrosses between these F_0 founders and WT were raised and genotyped to confirm germline transmission of the mutation (F_1 generation). Heterozygous mutants with the same mutation were selected and crossed, to obtain homozygous mutant embryos (F_2 generation).

4.4. GENOTYPING *MCU*$^{-/-}$ MUTANTS

Larvae or adult fish were anesthetized in tricaine and a small fragment of the caudal fin was cut with a sharp blade. Genomic DNA was extracted using reference protocol (Meeker et al., 2007). the target sites were amplified by PCR Master Mix (Thermo Fisher, K0172). Mutations in F_0 were detected using heteroduplex mobility assay (HMA) (Ansai et al., 2014).

PCR conditions were as follows: 15 min at 95 °C, 35 cycles at 95 °C for 30 s, 64 °C for 30 s and 72 °C for 30 s. PCR amplicons were electrophoresed on a 4-12% polyacrylamide gel (Life Technologies). For verification, PCR products from fish harbouring indel mutations were subjected to sequencing. Poly Peak Parser software (http://yosttools.genetics.utah.edu/PolyPeakParser/) was used for identification and sequence characterization of heterozygous mutant carriers generated by genome editing. Screening primers for heterozygous and homozygous fish were designed to amplify a 99-bp region across sgRNA target region. PCR products were resolved in 3% agarose low EEO gel (Fisher BioReagents, BP160-500) in order to identify *mcu*$^{+/+}$, *mcu*$^{+/-}$ and *mcu*$^{-/-}$ samples (both for the 14 bp deletion and the 20 bp insertion, as they derive both from the same sgRNA targeting).

Primer for sequencing (long amplicon of 169 bp):

FOR1l: GCACTTGCGTCCTCTCGG

REV1l: TTTTGTGCCCTGATGCCTCT

Short primers for gel electrophoresis (short amplicon of 99 bp)

FOR1s: ATGGCTGCGAAAGTGTGTAG

REV1s: CTGTGAGGAGACACCGAATG

4.5. ACRIDINE ORANGE ASSAY

Embryos at different timepoints were stained with AO to identify cell death. The assay has been performed at 24/30/48 hpf, as reported in literature (Tucker and Lardelli, 2007).

4.6. MYOFIBER ISOLATION FROM 72 HPF ZEBRAFISH LARVAE

Larvae at 72 hpf were dissociated according to the protocol provided by Dowling and colleagues some years ago, with some modifications (Horstick et al., 2013). Briefly, 20 larvae per tube (at least 60 per condition, divided in 3 tubes) were dissociated in Collagenase A (Roche) to a final concentration 4

mg/ml collagenase diluted in Leibovitz L-15 media (SIGMA). Dissociation has been carefully monitored to prevent over (or under) digestion of fish. Times for digestion will vary depending on intensity of trituration, number of embryos per tube, and age of embryos. It is also often less (in comparison to wild types) for embryos or larvae with skeletal muscle alterations. After centrifuging and filtration, fresh L-15 media supplemented with FBS, P/S and fungizone has been added to fibers. Myofibers were then allowed to settle on poly-L-lysine coated coverslips o/N. The day after plating, live imaging Ca^{2+} measurements were performed on myofibers were fixed for IF analysis following the protocol cited above.

4.7. CYTOSOLIC CA^{2+} MEASUREMENTS IN ISOLATED ZEBRAFISH FIBERS

Myofibers were loaded with 2 μM Fura-2-AM (Life Technologies) diluted in Krebs-Ringer modified buffer containing 0.02% pluronic acid and 250 μM sulfinpyrazone for 20 min at 37 °C and then washed with Krebs-Ringer modified buffer. Images were acquired every 1s with a Zeiss Axiovert 200 microscope equipped with a Fluotar 40x/1.3 N.A. oil immersion objective (Zeiss) and a high-sensitivity 16-bit Evolve 512 Delta EMCCD (Photometrics). Exposure time was set to 150ms. Excitation was performed with a DeltaRAM V highspeed monochromator (Photon Technology International) equipped with a 75 W xenon arc lamp. The system is controlled by MetaMorph 7.5 (Molecular Devices). Images were collected by alternatively exciting the fluorophore at 340 and 380 nm and fluorescence emission recorded through a 515/30 nm band-pass filter (Semrock). Changes in fluorescence (340/380 nm ratio) were expressed as ΔR/R0, where ΔR = (R-R0), R is the ratio at time t and R0 is the ratio at the beginning of the experiment.

4.8. MITOCHONDRIAL Ca^{2+} MEASUREMENTS IN ISOLATED ZEBRAFISH FIBERS

Myofibers were loaded with Rhod-2 (Life Technologies) diluted in Krebs-Ringer modified buffer containing 0.02% pluronic acid for 15 min at 37 °C and then washed with Krebs-Ringer modified buffer for 15 minutes. Images were acquired every 1s with a Zeiss Axiovert 200 microscope equipped with a Fluotar 40x/1.3 N.A. oil immersion objective (Zeiss) and a high-sensitivity 16-bit Evolve 512 Delta EMCCD (Photometrics). Exposure time was set to 100ms. Excitation was performed with a DeltaRAM V highspeed monochromator (Photon Technology International) equipped with a 75 W xenon arc lamp. The system is controlled by MetaMorph 7.5 (Molecular Devices). Images were collected by exciting the fluorophore at 550 and the fluorescence emission at 580 recorded. For all the experiments, exposure time was set to 150 ms and images were acquired every 1s. Changes in mitochondrial Ca^{2+} levels were expressed as arbitrary unit (A.U.), R0 is the signal at the beginning of the experiment. Analysis was performed with the Fiji distribution of ImageJ. Images were background corrected frame by frame by subtracting the mean pixel value of a cell-free region of interest.

4.9. MEASUREMENT OF OXYGEN CONSUMPTION RATE (OCR)

OCR was measured on 4 dpf zebrafish larvae with a Seahorse XF24 extracellular flux analyzer. Embryos were placed into the XF24 microplate well (1 fish per well) and blocked with a capture screen in the presence of 670 µl of fish water. The basal respiration was measured for 20 minutes at 28.5 °C, while the maximal respiration was measured upon FCCP 0.5 µM. Respiratory rates are average±SD of at least 20 individual embryos per condition. Images were acquired with Leica SP5, Nikon C2 or Zeiss LSM 700 confocal microscopes and analysed with the ImageJ/Fiji software.

4.10. HISTOLOGY: HAEMATOXILIN & EOSIN STAINING

Larvae at 5 dpf and adult zebrafish were fixed for 24 h in Bouin's solution, following established protocols (Facchinello et al., 2017). The samples were dehydrated progressively in ethanol and embedded in paraffin. Transverse and longitudinal sections of 7 μm were made on Jung AG Heidelberg microtome. Slices were then deparaffinised, rehydrated and stained with Haematoxylin and Eosin and finally mounted with Eukitt (BioOptica) for microscopic examination. Images were acquired at a 5000B Leica microscope equipped with a DC500 digital camera.

4.11. WESTERN BLOTTING

Proteins were extracted from larvae at different developmental stages (Kimmel et al., 1995). Lysis was performed in ice-cold RIPA buffer (125 mM NaCl, 25 mM TRIS-Cl pH 7.4, 1 mM EGTA-TRIS pH 7.4, 1% Triton-X100, 0.5% sodium deoxycholate, 0.1% SDS and Complete EDTA-free protease inhibitor cocktail (Roche) on ice. Crude lysate was cleared by centrifuging 30 min at 13,200 rpm and proteins in the supernatant quantified using the BCA Protein Assay Kit (Pierce). Equal amounts of proteins (50 μg) were loaded on 4-12% Bis-Tris NuPage gels (Life Technologies) SDS/PAGE and blotted on PVDF Immobilon-P membranes (Millipore). Dried membranes were then washed with TBS buffer (Tris–HCl 50 mM pH 7.5, NaCl 50 mM) with 1% (w/v) bovine serum albumin (BSA, Sigma) and incubated over night with the indicated primary antibodies at 4 °C: anti-MCU (SIGMA, HPA016480, rabbit, 1:1000), anti-GRP75 (Santa Cruz, sc-133137, mouse, 1:5000), anti-Tomm20 (SIGMA, HPA011562, rabbit, 1:2000), anti-β-Actin (Santa Cruz, sc-69879, mouse, 1:1000). Secondary HRP-conjugated antibodies (Bio-Rad) were incubated for 1 h at room temperature and protein bands detected by chemiluminescence on a UVITEC Alliance Mini HD9. Quantitation of the signal was performed with ImageJ.

4.12. IMMUNOHYSTOCHEMISTRY

For immunohistochemistry, 48 hpf embryos were fixed overnight at 4°C in phosphate-buffered saline (PBS) containing 4% paraformaldehyde. Following acetone treatment for 7 min at –20°C, they were rinsed in distilled water and transferred to a PBS solution containing 1% Triton-X, 2% goat serum and the antibody of choice for overnight incubation at 4°C. The larvae were then washed extensively in PBS containing 0.5% Triton-X for 2 h, after which 1:500 Alexa 488or 555-conjugated secondary antibody was added. Following overnight incubation at 4°C embryos were washed extensively in PBS containing 0.5% Triton-X. Antibodies utilized were anti-F59 (DSHB, 1:50), anti-F310 (DSHB, 1:50), monoclonal anti-engrailed (4D9, DSHB; 1:20). ACh receptors (AChRs) were labeled with 0.1 μM alpha-bungarotoxin which was added to the secondary antibody incubation. Phalloidin staining was performed on embryos at 48 hpf using Rhodamine conjugated Phalloidin (Thermo Fisher). All embryos were imaged with a Leica SP5 confocal microscope.

4.13. ELECTRON MICROSCOPY

5dpf zebrafish embryos, were fixed with Karnovsky fixative (2.5% glutaraldehyde and 2% paraformaldheyde in 0.1 M cacodylate buffer) O/N at 4 ◦ C, washed with 0.1 M cacodylate buffer, post-fixed with osmium tetroxide for 2 h, and embedded in EPON 812 as previously described (Parsons et al., 2002). Ultrathin sections were viewed on a Zeiss 902 electron microscope.

4.14. BIREFRINGENCE ANALYSIS

Muscle birefringence was analyzed at 48 hpf. Briefly, embryos were anesthetized with 0.02% tricaine (SIGMA), embedded in 2% methylcellulose (SIGMA) and finally placed on a glass to analyze muscle light refraction with polarizing filters. Images were acquired with a Leica M165FC

stereomicroscope. The integrated area of birefringence pixels was calculated using ImageJ software, as described (Smith et al., 2013).

4.15. TOUCH TEST

Touch evoked escape response was induced in 48 hpf zebrafish embryos, gently touching the end of the tail with capillary tips. The startle response was classified as normal (embryos having a prompt response, rapidly swimming away from the stimulus), altered (embryo moving just for little distances or in circle) and no response when even if applied twice, the stimulus didn't induce any movement.

4.16. TRACKING EXPERIMENTS

Tracking experiments have been performed on zebrafish larvae at 5 dpf. All experiments were carried out between 9.30-11.30 am. For each session, a group of 8 to 12 individuals was transferred in a transparent plexiglass chamber for video recording. The chamber (maximum height at the centre = 3.5 mm; diameter = 109 mm) was designed to I) confine larvae in 2D space, II) not allow the larvae to reach the edge of the arena. In this open chamber larvae were free to swim in fishwater (5 mm deep) at the temperature of 28°C without obstacles or stimulations. The fish's chamber was placed at the centre of a circular arena uniformly illuminated by white LEDs and the video was acquired by a digital camera (Chameleon 2, Point Grey Research Inc, Richmond, BC, Canada) connects to a PC via USB cable. Before the recording session, larvae were left to acclimate in the darkness for 5 min. After this period the light was switched on and camera triggered for video acquisition (15 frames per s). The video recording lasted 10 min and was acquired on PC using a software provided by the same camera manufacture (FlyCapture). The videos obtained were off-line analysed by the open source software CTRAX (California Institute of Technology Fly Tracker) for the fish positions tracking. Errors made by tracking process were corrected and computed using specific

MATLAB scripts, provided by the developers of CTRAX (Branson et al., 2009). Further analyses utilized home made MATLAB and R scripts.

4.17. STATISTICAL ANALYSIS

Statistical analysis was performed using Graph Pad Prism V6.0. Data are presented as the means ± SEM, unless otherwise specified. Significance was calculated by Student's t-test.

5. REFERENCES

Alam, M.R., Groschner, L.N., Parichatikanond, W., Kuo, L., Bondarenko, A.I., Rost, R., Waldeck-Weiermair, M., Malli, R., and Graier, W.F. (2012). Mitochondrial Ca2+ uptake 1 (MICU1) and mitochondrial ca2+ uniporter (MCU) contribute to metabolism-secretion coupling in clonal pancreatic β-cells. J. Biol. Chem. *287*, 34445–34454.

Anderson, J.L., Carten, J.D., and Farber, S.A. (2011). Zebrafish lipid metabolism: from mediating early patterning to the metabolism of dietary fat and cholesterol. Methods Cell Biol. *101*, 111–141.

Ansai, S., Inohaya, K., Yoshiura, Y., Schartl, M., Uemura, N., Takahashi, R., and Kinoshita, M. (2014). Design, evaluation, and screening methods for efficient targeted mutagenesis with transcription activator-like effector nucleases in medaka. Dev. Growth Differ. *56*, 98–107.

Antony, A.N., Paillard, M., Moffat, C., Juskeviciute, E., Correnti, J., Bolon, B., Rubin, E., Csordás, G., Seifert, E.L., Hoek, J.B., et al. (2016). MICU1 regulation of mitochondrial Ca(2+) uptake dictates survival and tissue regeneration. Nat. Commun. *7*, 10955.

Artuso, L., Romano, A., Verri, T., Domenichini, A., Argenton, F., Santorelli, F.M., and Petruzzella, V. (2012). Mitochondrial DNA metabolism in early development of zebrafish (Danio rerio). Biochim. Biophys. Acta - Bioenerg. *1817*, 1002–1011.

Auer, T.O., Duroure, K., De Cian, A., Concordet, J.-P., and Del Bene, F. (2014). Highly efficient CRISPR/Cas9-mediated knock-in in zebrafish by homology-independent DNA repair. Genome Res. *24*, 142–153.

Babin, P.J., Goizet, C., and Raldúa, D. (2014). Zebrafish models of human motor neuron diseases: Advantages and limitations. Prog. Neurobiol. *118*, 36–58.

Bano, D., Young, K.W., Guerin, C.J., LeFeuvre, R., Rothwell, N.J., Naldini, L., Rizzuto, R., Carafoli, E., and Nicotera, P. (2005). Cleavage of the Plasma Membrane Na+/Ca2+ Exchanger in Excitotoxicity. Cell *120*, 275–285.

Baradaran, R., Wang, C., Siliciano, A.F., and Long, S.B. (2018). Cryo-EM structures of fungal and metazoan mitochondrial calcium uniporters. Nature *559*, 580–584.

Baughman, J.M., Perocchi, F., Girgis, H.S., Plovanich, M., Belcher-Timme, C.A., Sancak, Y., Bao, X.R., Strittmatter, L., Goldberger, O., Bogorad, R.L., et al. (2011a). Integrative genomics identifies MCU as an essential component of the mitochondrial calcium uniporter. Nature *476*, 341–345.

Baughman, J.M., Perocchi, F., Girgis, H.S., Plovanich, M., Belcher-Timme, C.A., Sancak, Y., Bao, X.R., Strittmatter, L., Goldberger, O., Bogorad, R.L., et al. (2011b). Integrative genomics identifies MCU as an essential component of the mitochondrial calcium uniporter. Nature *476*, 341–345.

Beattie, C.E. (2000). Control of motor axon guidance in the zebrafish embryo. Brain Res. Bull. *53*, 489–500.

Belgacem, Y.H., and Borodinsky, L.N. (2011). Sonic hedgehog signaling is decoded by calcium spike activity in the developing spinal cord. Proc. Natl. Acad. Sci. U. S. A. *108*, 4482–4487.

Berger, J., and Currie, P.D. (2012). Zebrafish models flex their muscles to shed light on muscular dystrophies. Dis. Model. Mech. *5*, 726–732.

Berger, J., Sztal, T., and Currie, P.D. (2012). Quantification of birefringence readily measures the level of muscle damage in zebrafish. Biochem. Biophys. Res. Commun. *423*, 785–788.

Bernardi, P. (1999). Mitochondrial transport of cations: channels, exchangers, and permeability transition. Physiol. Rev. *79*, 1127–1155.

Beutner, G., Sharma, V.K., Giovannucci, D.R., Yule, D.I., and Sheu, S.S. (2001). Identification of a ryanodine receptor in rat heart mitochondria. J. Biol. Chem. *276*, 21482–21488.

Bick, A.G., Calvo, S.E., and Mootha, V.K. (2012). Evolutionary diversity of the mitochondrial calcium uniporter. Science *336*, 886.

Bill, B.R., Petzold, A.M., Clark, K.J., Schimmenti, L.A., and Ekker, S.C. (2009). A primer for morpholino use in zebrafish. Zebrafish *6*, 69–77.

Blagden, C.S., Currie, P.D., Ingham, P.W., and Hughes, S.M. (1997). Notochord induction of zebrafish slow muscle mediated by Sonic hedgehog. Genes Dev. *11*, 2163–2175.

Blum, M., De Robertis, E.M., Wallingford, J.B., and Niehrs, C. (2015). Morpholinos: Antisense and Sensibility. Dev. Cell *35*, 145–149.

Boitier, E., Rea, R., and Duchen, M.R. (1999). Mitochondria exert a negative feedback on the propagation of intracellular Ca2+ waves in rat cortical astrocytes. J. Cell Biol. *145*, 795–808.

Branson, K., Robie, A.A., Bender, J., Perona, P., and Dickinson, M.H. (2009). High-throughput ethomics in large groups of Drosophila. Nat. Methods *6*, 451–457.

Brennan, C., Mangoli, M., Dyer, C.E.F., and Ashworth, R. (2005). Acetylcholine and calcium signalling regulates muscle fibre formation in the zebrafish embryo. J. Cell Sci. *118*, 5181–5190.

Brookes, P.S., Parker, N., Buckingham, J.A., Vidal-Puig, A., Halestrap, A.P., Gunter, T.E., Nicholls, D.G., Bernardi, P., Lemasters, J.J., and Brand, M.D. (2008). UCPs — unlikely calcium porters. Nat. Cell Biol. *10*, 1235–1237.

Brustein, E., Saint-Amant, L., Buss, R.R., Chong, M., McDearmid, J.R., and Drapeau, P. (2003). Steps during the development of the zebrafish locomotor network. J. Physiol. *97*, 77–86.

Buckingham, M., and Vincent, S.D. (2009). Distinct and dynamic myogenic populations in the vertebrate embryo. Curr. Opin. Genet. Dev. *19*, 444–453.

Carten, J.D., Bradford, M.K., and Farber, S.A. (2011). Visualizing digestive organ morphology and function using differential fatty acid metabolism in live zebrafish. Dev. Biol. *360*, 276–285.

Chang, D.C., and Meng, C. (1995). A localized elevation of cytosolic free calcium is associated with cytokinesis in the zebrafish embryo. J. Cell Biol. *131*, 1539–1545.

Chaudhuri, D., Sancak, Y., Mootha, V.K., and Clapham, D.E. (2013). MCU encodes the pore conducting mitochondrial calcium currents. Elife *2*, e00704.

Cheng, Y., and Perocchi, F. (2015). ProtPhylo: identification of protein-phenotype and protein-protein functional associations via phylogenetic profiling. Nucleic Acids Res. *43*, W160-8.

Collins, T.J., Lipp, P., Berridge, M.J., and Bootman, M.D. (2001). Mitochondrial Ca(2+) uptake depends on the spatial and temporal profile of cytosolic Ca(2+) signals. J. Biol. Chem. *276*, 26411–26420.

Cooper, G.M. (2000). Mitochondria.

Corey, D.R., and Abrams, J.M. (2001a). Morpholino antisense oligonucleotides: tools for investigating vertebrate development. Genome Biol. *2*, REVIEWS1015.

Corey, D.R., and Abrams, J.M. (2001b). Morpholino antisense oligonucleotides: tools for investigating vertebrate development. Genome Biol. *2*, REVIEWS1015.

Cortés, F., Daggett, D., Bryson-Richardson, R.J., Neyt, C., Maule, J., Gautier, P., Hollway, G.E., Keenan, D., and Currie, P.D. (2003). Cadherin-Mediated Differential Cell Adhesion Controls Slow Muscle Cell Migration in the Developing Zebrafish Myotome. Dev. Cell *5*, 865–876.

Coutelle, O., Blagden, C.S., Hampson, R., Halai, C., Rigby, P.W.J., and Hughes, S.M. (2001). Hedgehog Signalling Is Required for Maintenance of myf5 and myoD Expression and Timely Terminal Differentiation in Zebrafish Adaxial Myogenesis. Dev. Biol. *236*, 136–150.

Csordás, G., Várnai, P., Golenár, T., Roy, S., Purkins, G., Schneider, T.G., Balla, T., and Hajnóczky, G. (2010). Imaging Interorganelle Contacts and Local Calcium Dynamics at the ER-Mitochondrial Interface. Mol. Cell *39*, 121–132.

Csordás, G., Golenár, T., Seifert, E.L., Kamer, K.J., Sancak, Y., Perocchi, F., Moffat, C., Weaver, D., de la Fuente Perez, S., Bogorad, R., et al. (2013). MICU1 controls both the threshold and cooperative activation of the mitochondrial Ca^{2+} uniporter. Cell Metab. *17*, 976–987.

Dahm, R., and Geisler, R. (2006). Learning from Small Fry: The Zebrafish as a Genetic Model Organism for Aquaculture Fish Species. Mar. Biotechnol. *8*, 329–345.

DELUCA, H.F., and ENGSTROM, G.W. (1961). Calcium uptake by rat kidney mitochondria. Proc. Natl. Acad. Sci. U. S. A. *47*, 1744–1750.

Denton, R.M. (2009). Regulation of mitochondrial dehydrogenases by calcium ions. Biochim. Biophys. Acta - Bioenerg. *1787*, 1309–1316.

Denton, R.M., Randle, P.J., and Martin, B.R. (1972). Stimulation by calcium ions of pyruvate dehydrogenase phosphate phosphatase. Biochem. J. *128*, 161–163.

Devoto, S.H., Melançon, E., Eisen, J.S., and Westerfield, M. (1996). Identification of separate slow and fast muscle precursor cells in vivo, prior to somite formation. Development *122*,

3371–3380.

Dickinson, M.E., Flenniken, A.M., Ji, X., Teboul, L., Wong, M.D., White, J.K., Meehan, T.F., Weninger, W.J., Westerberg, H., Adissu, H., et al. (2016). High-throughput discovery of novel developmental phenotypes. Nature *537*, 508–514.

Dimmer, K.S., Navoni, F., Casarin, A., Trevisson, E., Endele, S., Winterpacht, A., Salviati, L., and Scorrano, L. (2008). LETM1, deleted in Wolf-Hirschhorn syndrome is required for normal mitochondrial morphology and cellular viability. Hum. Mol. Genet. *17*, 201–214.

Dorn, G.W., and Maack, C. (2013). SR and mitochondria: Calcium cross-talk between kissing cousins. J. Mol. Cell. Cardiol. *55*, 42–49.

Drago, I., and Davis, R.L. (2016). Inhibiting the Mitochondrial Calcium Uniporter during Development Impairs Memory in Adult Drosophila. Cell Rep. *16*, 2763–2776.

Drapeau, P., Saint-Amant, L., Buss, R.R., Chong, M., McDearmid, J.R., and Brustein, E. (2002). Development of the locomotor network in zebrafish. Prog. Neurobiol. *68*, 85–111.

Dumollard, R., Duchen, M., and Carroll, J. (2007). The Role of Mitochondrial Function in the Oocyte and Embryo. Curr. Top. Dev. Biol. *77*, 21–49.

Eisen, J.S., and Smith, J.C. (2008). Controlling morpholino experiments: don't stop making antisense. Development *135*, 1735–1743.

Elmonem, M., Berlingerio, S., van den Heuvel, L., de Witte, P., Lowe, M., Levtchenko, E., Elmonem, M.A., Berlingerio, S.P., van den Heuvel, L.P., de Witte, P.A., et al. (2018). Genetic Renal Diseases: The Emerging Role of Zebrafish Models. Cells *7*, 130.

Esteves, A., Knoll-Gellida, A., Canclini, L., Silvarrey, M.C., André, M., and Babin, P.J. (2016). Fatty acid binding proteins have the potential to channel dietary fatty acids into enterocyte nuclei. J. Lipid Res. *57*, 219–232.

Facchinello, N., Skobo, T., Meneghetti, G., Colletti, E., Dinarello, A., Tiso, N., Costa, R., Gioacchini, G., Carnevali, O., Argenton, F., et al. (2017). nr3c1 null mutant zebrafish are viable and reveal DNA-binding-independent activities of the glucocorticoid receptor. Sci. Rep. *7*, 4371.

Fan, C., Fan, M., Orlando, B.J., Fastman, N.M., Zhang, J., Xu, Y., Chambers, M.G., Xu, X., Perry, K., Liao, M., et al. (2018). X-ray and cryo-EM structures of the mitochondrial calcium uniporter. Nature *559*, 575–579.

Feng, X., Adiarte, E.G., and Devoto, S.H. (2006). Hedgehog acts directly on the zebrafish dermomyotome to promote myogenic differentiation. Dev. Biol. *300*, 736–746.

Fieni, F., Lee, S.B., Jan, Y.N., and Kirichok, Y. (2012). Activity of the mitochondrial calcium uniporter varies greatly between tissues. Nat. Commun. *3*, 1317.

Flynn, E.J., Trent, C.M., Rawls, J.F., and Rawls, J.F. (2009). Ontogeny and nutritional control of adipogenesis in zebrafish (Danio rerio). J. Lipid Res. *50*, 1641–1652.

Foyouzi-Youssefi, R., Arnaudeau, S., Borner, C., Kelley, W.L., Tschopp, J., Lew, D.P., Demaurex, N., and Krause, K.H. (2000). Bcl-2 decreases the free Ca2+ concentration within the endoplasmic reticulum. Proc. Natl. Acad. Sci. U. S. A. *97*, 5723–5728.

Fuentes, R., Letelier, J., Tajer, B., Valdivia, L.E., and Mullins, M.C. (2018). Fishing forward and reverse: Advances in zebrafish phenomics. Mech. Dev.

Gagnon, J.A., Valen, E., Thyme, S.B., Huang, P., Akhmetova, L., Ahkmetova, L., Pauli, A., Montague, T.G., Zimmerman, S., Richter, C., et al. (2014). Efficient mutagenesis by Cas9 protein-mediated oligonucleotide insertion and large-scale assessment of single-guide RNAs. PLoS One *9*, e98186.

García-Pérez, C., Hajnóczky, G., and Csordás, G. (2008). Physical Coupling Supports the Local Ca $^{2+}$ Transfer between Sarcoplasmic Reticulum Subdomains and the Mitochondria in Heart Muscle. J. Biol. Chem. *283*, 32771–32780.

Gherardi, G., Nogara, L., Ciciliot, S., Fadini, G.P., Blaauw, B., Braghetta, P., Bonaldo, P., De Stefani, D., Rizzuto, R., and Mammucari, C. (2018). Loss of mitochondrial calcium uniporter rewires skeletal muscle metabolism and substrate preference. Cell Death Differ. 1.

Giacomello, M., Drago, I., Bortolozzi, M., Scorzeto, M., Gianelle, A., Pizzo, P., and Pozzan, T. (2010). Ca2+ hot spots on the mitochondrial surface are generated by Ca2+ mobilization from stores, but not by activation of store-operated Ca2+ channels. Mol. Cell *38*, 280–290.

Gilland, E., Miller, A.L., Karplus, E., Baker, R., and Webb, S.E. (1999). Imaging of multicellular large-scale rhythmic calcium waves during zebrafish gastrulation. Proc. Natl. Acad. Sci. U. S. A. *96*, 157–161.

Giorgi, C., Baldassari, F., Bononi, A., Bonora, M., De Marchi, E., Marchi, S., Missiroli, S., Patergnani, S., Rimessi, A., Suski, J.M., et al. (2012). Mitochondrial Ca2+ and apoptosis. Cell Calcium *52*, 36–43.

Glasgow, E., and Tomarev, S.I. (1998). Restricted expression of the homeobox gene prox 1 in developing zebrafish. Mech. Dev. *76*, 175–178.

Goessling, W., North, T.E., and Zon, L.I. (2007). New Waves of Discovery: Modeling Cancer in Zebrafish. J. Clin. Oncol. *25*, 2473–2479.

Goldsmith, P. (2004). Zebrafish as a pharmacological tool: the how, why and when. Curr. Opin. Pharmacol. *4*, 504–512.

Gramaglia, D., Gentile, A., Battaglia, M., Ranzato, L., Petronilli, V., Fassetta, M., Bernardi, P., and Rasola, A. (2004). Apoptosis to necrosis switching downstream of apoptosome formation requires inhibition of both glycolysis and oxidative phosphorylation in a BCL-XL- and PKB/AKT-independent fashion. Cell Death Differ. *11*, 342–353.

Granatiero, V., De Stefani, D., and Rizzuto, R. (2017). Mitochondrial Calcium Handling in Physiology and Disease. In Advances in Experimental Medicine and Biology, pp. 25–47.

Granato, M., and Nüsslein-Volhard, C. (1996). Fishing for genes controlling development. Curr. Opin. Genet. Dev. *6*, 461–468.

Granato, M., van Eeden, F.J., Schach, U., Trowe, T., Brand, M., Furutani-Seiki, M., Haffter, P., Hammerschmidt, M., Heisenberg, C.P., Jiang, Y.J., et al. (1996). Genes controlling and mediating locomotion behavior of the zebrafish embryo and larva. Development *123*.

Griffiths, E.J., and Rutter, G.A. (2009). Mitochondrial calcium as a key regulator of

mitochondrial ATP production in mammalian cells. Biochim. Biophys. Acta - Bioenerg. *1787*, 1324–1333.

Grunwald, D.J., and Streisinger, G. (1992). Induction of recessive lethal and specific locus mutations in the zebrafish with ethyl nitrosourea. Genet. Res. *59*, 103–116.

Gurevich, D., Siegel, A., and Currie, P.D. (2015). Skeletal Myogenesis in the Zebrafish and Its Implications for Muscle Disease Modelling. (Springer, Berlin, Heidelberg), pp. 49–76.

van Haasteren, G., Li, S., Muda, M., Susini, S., and Schlegel, W. (1999). Calcium Signalling and Gene Expression. J. Recept. Signal Transduct. *19*, 481–492.

Hamilton, J., Brustovetsky, T., Rysted, J.E., Lin, Z., Usachev, Y.M., and Brustovetsky, N. (2018). Deletion of mitochondrial calcium uniporter incompletely inhibits calcium uptake and induction of the permeability transition pore in brain mitochondria. J. Biol. Chem. jbc.RA118.002926.

Harrington, J.L., and Murphy, E. (2015). The mitochondrial calcium uniporter: mice can live and die without it. J. Mol. Cell. Cardiol. *78*, 46–53.

Hayashi, T., Rizzuto, R., Hajnoczky, G., and Su, T.-P. (2009). MAM: more than just a housekeeper. Trends Cell Biol. *19*, 81–88.

Hoffman, N.E., Chandramoorthy, H.C., Shanmughapriya, S., Zhang, X.Q., Vallem, S., Doonan, P.J., Malliankaraman, K., Guo, S., Rajan, S., Elrod, J.W., et al. (2014). SLC25A23 augments mitochondrial Ca^{2+} uptake, interacts with MCU, and induces oxidative stress-mediated cell death. Mol. Biol. Cell *25*, 936–947.

von Hofsten, J., Elworthy, S., Gilchrist, M.J., Smith, J.C., Wardle, F.C., and Ingham, P.W. (2008). Prdm1- and Sox6-mediated transcriptional repression specifies muscle fibre type in the zebrafish embryo. EMBO Rep. *9*, 683–689.

Holmström, K.M., Pan, X., Liu, J.C., Menazza, S., Liu, J., Nguyen, T.T., Pan, H., Parks, R.J., Anderson, S., Noguchi, A., et al. (2015). Assessment of cardiac function in mice lacking the mitochondrial calcium uniporter. J. Mol. Cell. Cardiol. *85*, 178–182.

Hölttä-Vuori, M., Salo, V.T. V, Nyberg, L., Brackmann, C., Enejder, A., Panula, P., and Ikonen, E. (2010). Zebrafish: gaining popularity in lipid research. Biochem. J. *429*, 235–242.

Honjo, Y., and Eisen, J.S. (2005). Slow muscle regulates the pattern of trunk neural crest migration in zebrafish. Development *132*, 4461–4470.

Horstick, E.J., Gibbs, E.M., Li, X., Davidson, A.E., and Dowling, J.J. (2013). Analysis of embryonic and larval zebrafish skeletal myofibers from dissociated preparations. J. Vis. Exp. e50259.

Howe, K., Clark, M.D., Torroja, C.F., Torrance, J., Berthelot, C., Muffato, M., Collins, J.E., Humphray, S., McLaren, K., Matthews, L., et al. (2013). The zebrafish reference genome sequence and its relationship to the human genome. Nature *496*, 498–503.

Huang, G., Vercesi, A.E., and Docampo, R. (2013a). Essential regulation of cell bioenergetics in Trypanosoma brucei by the mitochondrial calcium uniporter. Nat. Commun. *4*, 2865.

Huang, P., Zhu, Z., Lin, S., and Zhang, B. (2012). Reverse Genetic Approaches in Zebrafish. J. Genet. Genomics *39*, 421–433.

Huang, S.-H., Huang, K.-S., Yu, C.-H., and Gong, H.-Y. (2013b). Metabolic profile analysis of a single developing zebrafish embryo via monitoring of oxygen consumption rates within a microfluidic device. Biomicrofluidics *7*, 64107.

Hughes, S.M. (2004). Muscle Differentiation: A Gene for Slow Muscle? Curr. Biol. *14*, R156–R157.

HUGHES, BLAGDEN, LI, and GRIMALDI (1998). The role of hedgehog proteins in vertebrate slow and fast skeletal muscle patterning. Acta Physiol. Scand. *163*, S7–S10.

Hung, V., Zou, P., Rhee, H.-W., Udeshi, N.D., Cracan, V., Svinkina, T., Carr, S.A., Mootha, V.K., and Ting, A.Y. (2014). Proteomic mapping of the human mitochondrial intermembrane space in live cells via ratiometric APEX tagging. Mol. Cell *55*, 332–341.

Hutson, L.D., and Chien, C.-B. (2002). Wiring the zebrafish: axon guidance and synaptogenesis. Undefined.

Ingham, P.W., and Kim, H.R. (2005). Hedgehog signalling and the specification of muscle cell identity in the Zebrafish embryo. Exp. Cell Res. *306*, 336–342.

Jackson, H.E., and Ingham, P.W. (2013a). Control of muscle fibre-type diversity during embryonic development: The zebrafish paradigm. Mech. Dev. *130*, 447–457.

Jackson, H.E., and Ingham, P.W. (2013b). Control of muscle fibre-type diversity during embryonic development: The zebrafish paradigm. Mech. Dev. *130*, 447–457.

Jao, L.-E., Wente, S.R., and Chen, W. (2013). Efficient multiplex biallelic zebrafish genome editing using a CRISPR nuclease system. Proc. Natl. Acad. Sci. U. S. A. *110*, 13904–13909.

Jiang, D., Zhao, L., and Clapham, D.E. (2009). Genome-Wide RNAi Screen Identifies Letm1 as a Mitochondrial Ca2+/H+ Antiporter. Science (80-.). *326*, 144–147.

Jones, R.G., Bui, T., White, C., Madesh, M., Krawczyk, C.M., Lindsten, T., Hawkins, B.J., Kubek, S., Frauwirth, K.A., Wang, Y.L., et al. (2007). The proapoptotic factors Bax and Bak regulate T Cell proliferation through control of endoplasmic reticulum Ca(2+) homeostasis. Immunity *27*, 268–280.

Kelly, A., and Hurlstone, A.F. (2011). The use of RNAi technologies for gene knockdown in zebrafish. Brief. Funct. Genomics *10*, 189–196.

Khorchid, A., and Ikura, M. (2002). How calpain is activated by calcium. Nat. Struct. Biol. *9*, 239–241.

Kimmel, C.B., Ballard, W.W., Kimmel, S.R., Ullmann, B., and Schilling, T.F. (1995). Stages of embryonic development of the zebrafish. Dev. Dyn. *203*, 253–310.

Kirichok, Y., Krapivinsky, G., and Clapham, D.E. (2004). The mitochondrial calcium uniporter is a highly selective ion channel. Nature *427*, 360–364.

Klatt Shaw, D., Gunther, D., Jurynec, M.J., Chagovetz, A.A., Ritchie, E., and Grunwald, D.J. (2018). Intracellular Calcium Mobilization Is Required for Sonic Hedgehog Signaling. Dev. Cell *45*, 512–525.e5.

Kok, F.O., Shin, M., Ni, C.-W., Gupta, A., Grosse, A.S., van Impel, A., Kirchmaier, B.C., Peterson-

Maduro, J., Kourkoulis, G., Male, I., et al. (2015). Reverse Genetic Screening Reveals Poor Correlation between Morpholino-Induced and Mutant Phenotypes in Zebrafish. Dev. Cell *32*, 97–108.

Kovács-Bogdán, E., Sancak, Y., Kamer, K.J., Plovanich, M., Jambhekar, A., Huber, R.J., Myre, M.A., Blower, M.D., and Mootha, V.K. (2014). Reconstitution of the mitochondrial calcium uniporter in yeast. Proc. Natl. Acad. Sci. U. S. A. *111*, 8985–8990.

Kwong, J.Q., Lu, X., Correll, R.N., Schwanekamp, J.A., Vagnozzi, R.J., Sargent, M.A., York, A.J., Zhang, J., Bers, D.M., and Molkentin, J.D. (2015). The Mitochondrial Calcium Uniporter Selectively Matches Metabolic Output to Acute Contractile Stress in the Heart. Cell Rep.

Labun, K., Montague, T.G., Gagnon, J.A., Thyme, S.B., and Valen, E. (2016). CHOPCHOP v2: a web tool for the next generation of CRISPR genome engineering. Nucleic Acids Res. *44*, W272–W276.

Lawson, N.D., and Wolfe, S.A. (2011). Forward and reverse genetic approaches for the analysis of vertebrate development in the zebrafish. Dev. Cell *21*, 48–64.

Leal, L.G., Lopes, M.A., and Batista, M.L. (2018). Physical Exercise-Induced Myokines and Muscle-Adipose Tissue Crosstalk: A Review of Current Knowledge and the Implications for Health and Metabolic Diseases. Front. Physiol. *9*, 1307.

Lee, K.W., Webb, S.E., and Miller, A.L. (1999). A Wave of Free Cytosolic Calcium Traverses Zebrafish Eggs on Activation. Dev. Biol. *214*, 168–180.

Lee, R.T.H., Zhao, Z., and Ingham, P.W. (2016a). Hedgehog signalling. Development *143*, 367–372.

Lee, S.K., Shanmughapriya, S., Mok, M.C.Y., Dong, Z., Tomar, D., Carvalho, E., Rajan, S., Junop, M.S., Madesh, M., and Stathopulos, P.B. (2016b). Structural Insights into Mitochondrial Calcium Uniporter Regulation by Divalent Cations. Cell Chem. Biol. *23*, 1157–1169.

Lewis-Smith, D., Kamer, K.J., Griffin, H., Childs, A.-M., Pysden, K., Titov, D., Duff, J., Pyle, A., Taylor, R.W., Yu-Wai-Man, P., et al. (2016). Homozygous deletion in MICU1 presenting with fatigue and lethargy in childhood. Neurol. Genet. *2*, e59.

Li, M., Zhao, L., Page-McCaw, P.S., and Chen, W. (2016a). Zebrafish Genome Engineering Using the CRISPR-Cas9 System. Trends Genet. *32*, 815–827.

Li, M., Zhao, L., Page-McCaw, P.S., and Chen, W. (2016b). Zebrafish Genome Engineering Using the CRISPR-Cas9 System. Trends Genet. *32*, 815–827.

Lin, Y.-Y. (2012). Muscle diseases in the zebrafish. Neuromuscul. Disord. *22*, 673–684.

Liu, J.C., Liu, J., Holmström, K.M., Menazza, S., Parks, R.J., Fergusson, M.M., Yu, Z.-X., Springer, D.A., Halsey, C., Liu, C., et al. (2016). MICU1 Serves as a Molecular Gatekeeper to Prevent In Vivo Mitochondrial Calcium Overload.

Logan, C. V, Szabadkai, G., Sharpe, J.A., Parry, D.A., Torelli, S., Childs, A.-M., Kriek, M., Phadke, R., Johnson, C.A., Roberts, N.Y., et al. (2014). Loss-of-function mutations in MICU1 cause a brain and muscle disorder linked to primary alterations in mitochondrial calcium signaling. Nat. Genet. *46*, 188–193.

Lombardi, A.A., Arif, E., Luongo, T.S., and Elrod, J.W. (2017). Genetic Ablation of Fibroblast Mitochondrial Calcium Uptake Increases Myofibroblast Transdifferentiation and Exacerbates Fibrosis in Myocardial Infarction. Biophys. J. *112*, 96a.

Low, S.E., Woods, I.G., Lachance, M., Ryan, J., Schier, A.F., and Saint-Amant, L. (2012). Touch responsiveness in zebrafish requires voltage-gated calcium channel 2.1b. J. Neurophysiol. *108*, 148–159.

Luongo, T.S., Lambert, J.P., Yuan, A., Zhang, X., Gross, P., Song, J., Shanmughapriya, S., Gao, E., Jain, M., Houser, S.R., et al. (2015). The Mitochondrial Calcium Uniporter Matches Energetic Supply with Cardiac Workload during Stress and Modulates Permeability Transition. Cell Rep. *12*, 23–34.

Makarova, K.S., Haft, D.H., Barrangou, R., Brouns, S.J.J., Charpentier, E., Horvath, P., Moineau, S., Mojica, F.J.M., Wolf, Y.I., Yakunin, A.F., et al. (2011). Evolution and classification of the CRISPR-Cas systems. Nat. Rev. Microbiol. *9*, 467–477.

Mallilankaraman, K., Doonan, P., Cárdenas, C., Chandramoorthy, H.C., Müller, M., Miller, R., Hoffman, N.E., Gandhirajan, R.K., Molgó, J., Birnbaum, M.J., et al. (2012a). MICU1 Is an Essential Gatekeeper for MCU-Mediated Mitochondrial Ca2+ Uptake that Regulates Cell Survival. Cell *151*, 630–644.

Mallilankaraman, K., Cárdenas, C., Doonan, P.J., Chandramoorthy, H.C., Irrinki, K.M., Golenár, T., Csordás, G., Madireddi, P., Yang, J., Müller, M., et al. (2012b). MCUR1 is an essential component of mitochondrial Ca2+ uptake that regulates cellular metabolism. Nat. Cell Biol. *14*, 1336–1343.

Mammucari, C., Gherardi, G., Zamparo, I., Raffaello, A., Boncompagni, S., Chemello, F., Cagnin, S., Braga, A., Zanin, S., Pallafacchina, G., et al. (2015). The mitochondrial calcium uniporter controls skeletal muscle trophism in vivo. Cell Rep. *10*, 1269–1279.

Mammucari, C., Raffaello, A., Vecellio Reane, D., Gherardi, G., De Mario, A., and Rizzuto, R. (2018). Mitochondrial calcium uptake in organ physiology: from molecular mechanism to animal models. Pflugers Arch. *470*, 1165–1179.

Mannella, C. a (2006). Structure and dynamics of the mitochondrial inner membrane cristae. Biochim. Biophys. Acta *1763*, 542–548.

Mannella, C.A., Buttle, K., Rath, B.K., and Marko, M. (1998). Electron microscopic tomography of rat-liver mitochondria and their interaction with the endoplasmic reticulum. Biofactors *8*, 225–228.

De Marchi, U., Castelbou, C., and Demaurex, N. (2011). Uncoupling protein 3 (UCP3) modulates the activity of Sarco/endoplasmic reticulum Ca2+-ATPase (SERCA) by decreasing mitochondrial ATP production. J. Biol. Chem. *286*, 32533–32541.

Marraffini, L.A., and Sontheimer, E.J. (2010). CRISPR interference: RNA-directed adaptive immunity in bacteria and archaea. Nat. Rev. Genet. *11*, 181–190.

Martell, J.D., Deerinck, T.J., Sancak, Y., Poulos, T.L., Mootha, V.K., Sosinsky, G.E., Ellisman, M.H., and Ting, A.Y. (2012). Engineered ascorbate peroxidase as a genetically encoded reporter for electron microscopy. Nat. Biotechnol. *30*, 1143–1148.

McQuibban, A.G., Joza, N., Megighian, A., Scorzeto, M., Zanini, D., Reipert, S., Richter, C., Schweyen, R.J., and Nowikovsky, K. (2010). A Drosophila mutant of LETM1, a candidate gene for seizures in Wolf-Hirschhorn syndrome. Hum. Mol. Genet. *19*, 987–1000.

Meeker, N.D., Hutchinson, S.A., Ho, L., and Trede, N.S. (2007). Method for isolation of PCR-ready genomic DNA from zebrafish tissues. Biotechniques *43*, 610–614.

Mitchell, P. (1961). Coupling of phosphorylation to electron and hydrogen transfer by a chemi-osmotic type of mechanism. Nature *191*, 144–148.

Mitchell, P. (1966). Chemiosmotic Coupling in Oxidative and Photosynthetic Phosphorylation.

Momeni, H.R. (2011). Role of calpain in apoptosis. Cell J. *13*, 65–72.

Naert, T., and Vleminckx, K. (2018). CRISPR/Cas9 disease models in zebrafish and Xenopus: The genetic renaissance of fish and frogs. Drug Discov. Today Technol. *28*, 41–52.

Naganawa, Y., and Hirata, H. (2011a). Developmental transition of touch response from slow muscle-mediated coilings to fast muscle-mediated burst swimming in zebrafish. Dev. Biol. *355*, 194–204.

Naganawa, Y., and Hirata, H. (2011b). Developmental transition of touch response from slow muscle-mediated coilings to fast muscle-mediated burst swimming in zebrafish. Dev. Biol. *355*, 194–204.

Nair, S., and Pelegri, F.J. (2011). Practical Approaches for Implementing Forward Genetic Strategies in Zebrafish. (Humana Press, Totowa, NJ), pp. 185–209.

Nasevicius, A., and Ekker, S.C. (2000). Effective targeted gene 'knockdown' in zebrafish. Nat. Genet. *26*, 216–220.

Nasiadka, A., and Clark, M.D. (2012). Zebrafish Breeding in the Laboratory Environment. ILAR J. *53*, 161–168.

Nguyen, C.T., Lu, Q., Wang, Y., and Chen, J.-N. (2008). Zebrafish as a model for cardiovascular development and disease. Drug Discov. Today Dis. Model. *5*, 135–140.

Nguyen, N.X., Armache, J.-P., Lee, C., Yang, Y., Zeng, W., Mootha, V.K., Cheng, Y., Bai, X., and Jiang, Y. (2018). Cryo-EM structure of a fungal mitochondrial calcium uniporter. Nature *559*, 570–574.

Nicholls, D.G. (2009). Mitochondrial calcium function and dysfunction in the central nervous system. Biochim. Biophys. Acta - Bioenerg. *1787*, 1416–1424.

Nita, I.I., Hershfinkel, M., Kantor, C., Rutter, G.A., Lewis, E.C., and Sekler, I. (2014). Pancreatic β-cell Na+ channels control global Ca2+ signaling and oxidative metabolism by inducing Na+ and Ca2+ responses that are propagated into mitochondria. FASEB J. *28*, 3301–3312.

Nita, I.I., Hershfinkel, M., Lewis, E.C., and Sekler, I. (2015). A crosstalk between Na^+ channels, Na^+/K^+ pump and mitochondrial Na^+ transporters controls glucose-dependent cytosolic and mitochondrial Na^+ signals. Cell Calcium *57*, 69–75.

Nowikovsky, K., Pozzan, T., Rizzuto, R., Scorrano, L., and Bernardi, P. (2012). The Pathophysiology of LETM1. J. Gen. Physiol. *139*, 445–454.

Nunnari, J., and Suomalainen, A. (2012). Mitochondria: in sickness and in health. Cell *148*, 1145–1159.

Ochi, H., and Westerfield, M. (2007). Signaling networks that regulate muscle development: Lessons from zebrafish. Dev. Growth Differ. *49*, 1–11.

van der Oost, J., Westra, E.R., Jackson, R.N., and Wiedenheft, B. (2014). Unravelling the structural and mechanistic basis of CRISPR–Cas systems. Nat. Rev. Microbiol. *12*, 479–492.

Ota, S., Hisano, Y., Ikawa, Y., and Kawahara, A. (2014). Multiple genome modifications by the CRISPR/Cas9 system in zebrafish. Genes to Cells *19*, 555–564.

Pagliarini, D.J., Calvo, S.E., Chang, B., Sheth, S.A., Vafai, S.B., Ong, S.-E., Walford, G.A., Sugiana, C., Boneh, A., Chen, W.K., et al. (2008). A mitochondrial protein compendium elucidates complex I disease biology. Cell *134*, 112–123.

Palty, R., Silverman, W.F., Hershfinkel, M., Caporale, T., Sensi, S.L., Parnis, J., Nolte, C., Fishman, D., Shoshan-Barmatz, V., Herrmann, S., et al. (2010). NCLX is an essential component of mitochondrial Na+/Ca2+ exchange. Proc. Natl. Acad. Sci. U. S. A. *107*, 436–441.

Pan, X., Liu, J., Nguyen, T., Liu, C., Sun, J., Teng, Y., Fergusson, M.M., Rovira, I.I., Allen, M., Springer, D.A., et al. (2013). The physiological role of mitochondrial calcium revealed by mice lacking the mitochondrial calcium uniporter. Nat. Cell Biol. *15*, 1464–1472.

Parnis, J., Montana, V., Delgado-Martinez, I., Matyash, V., Parpura, V., Kettenmann, H., Sekler, I., and Nolte, C. (2013). Mitochondrial exchanger NCLX plays a major role in the intracellular Ca2+ signaling, gliotransmission, and proliferation of astrocytes. J. Neurosci. *33*, 7206–7219.

Parsons, M.J., Pollard, S.M., Saúde, L., Feldman, B., Coutinho, P., Hirst, E.M.A., and Stemple, D.L. (2002). Zebrafish mutants identify an essential role for laminins in notochord formation. Development *129*, 3137–3146.

Patron, M., Checchetto, V., Raffaello, A., Teardo, E., Vecellio Reane, D., Mantoan, M., Granatiero, V., Szabò, I., De Stefani, D., and Rizzuto, R. (2014). MICU1 and MICU2 finely tune the mitochondrial Ca2+ uniporter by exerting opposite effects on MCU activity. Mol. Cell *53*, 726–737.

Patron, M., Granatiero, V., Espino, J., Rizzuto, R., and De Stefani, D. (2018). MICU3 is a tissue-specific enhancer of mitochondrial calcium uptake. Cell Death Differ.

Paupe, V., Prudent, J., Dassa, E.P., Rendon, O.Z., and Shoubridge, E.A. (2015). CCDC90A (MCUR1) is a cytochrome c oxidase assembly factor and not a regulator of the mitochondrial calcium uniporter. Cell Metab. *21*, 109–116.

Pendin, D., Greotti, E., and Pozzan, T. (2014). The elusive importance of being a mitochondrial Ca2+ uniporter. Cell Calcium *55*, 139–145.

Perocchi, F., Gohil, V.M., Girgis, H.S., Bao, X.R., McCombs, J.E., Palmer, A.E., and Mootha, V.K. (2010). MICU1 encodes a mitochondrial EF hand protein required for Ca2+ uptake. Nature *467*, 291–296.

Pinton, P., Ferrari, D., Magalhães, P., Schulze-Osthoff, K., Di Virgilio, F., Pozzan, T., and Rizzuto, R. (2000). Reduced loading of intracellular Ca(2+) stores and downregulation of capacitative

Ca(2+) influx in Bcl-2-overexpressing cells. J. Cell Biol. *148*, 857–862.

Pinton, P., Ferrari, D., Rapizzi, E., Di Virgilio, F., Pozzan, T., and Rizzuto, R. (2001). The Ca2+ concentration of the endoplasmic reticulum is a key determinant of ceramide-induced apoptosis: significance for the molecular mechanism of Bcl-2 action. EMBO J. *20*, 2690–2701.

Pivovarova, N.B., and Andrews, S.B. (2010). Calcium-dependent mitochondrial function and dysfunction in neurons. FEBS J. *277*, 3622–3636.

Plovanich, M., Bogorad, R.L., Sancak, Y., Kamer, K.J., Strittmatter, L., Li, A.A., Girgis, H.S., Kuchimanchi, S., De Groot, J., Speciner, L., et al. (2013). MICU2, a Paralog of MICU1, Resides within the Mitochondrial Uniporter Complex to Regulate Calcium Handling. PLoS One *8*, e55785.

Postlethwait, J., Amores, A., Cresko, W., Singer, A., and Yan, Y.-L. (2004). Subfunction partitioning, the teleost radiation and the annotation of the human genome. Trends Genet. *20*, 481–490.

Postlethwait, J.H., Woods, I.G., Ngo-Hazelett, P., Yan, Y.L., Kelly, P.D., Chu, F., Huang, H., Hill-Force, A., and Talbot, W.S. (2000). Zebrafish comparative genomics and the origins of vertebrate chromosomes. Genome Res. *10*, 1890–1902.

Prudent, J., Popgeorgiev, N., Bonneau, B., Thibaut, J., Gadet, R., Lopez, J., Gonzalo, P., Rimokh, R., Manon, S., Houart, C., et al. (2013). Bcl-wav and the mitochondrial calcium uniporter drive gastrula morphogenesis in zebrafish. Nat. Commun. *4*, 2330.

Qiu, J., Tan, Y.-W., Hagenston, A.M., Martel, M.-A., Kneisel, N., Skehel, P.A., Wyllie, D.J.A., Bading, H., and Hardingham, G.E. (2013). Mitochondrial calcium uniporter Mcu controls excitotoxicity and is transcriptionally repressed by neuroprotective nuclear calcium signals. Nat. Commun. *4*, 2034.

Quinlivan, V.H., and Farber, S.A. (2017). Lipid Uptake, Metabolism, and Transport in the Larval Zebrafish. Front. Endocrinol. (Lausanne). *8*, 319.

Raffaello, A., De Stefani, D., Sabbadin, D., Teardo, E., Merli, G., Picard, A., Checchetto, V., Moro, S., Szabò, I., and Rizzuto, R. (2013). The mitochondrial calcium uniporter is a multimer that can include a dominant-negative pore-forming subunit. EMBO J. *32*, 2362–2376.

Raffaello, A., Mammucari, C., Gherardi, G., and Rizzuto, R. (2016). Calcium at the Center of Cell Signaling: Interplay between Endoplasmic Reticulum, Mitochondria, and Lysosomes. Trends Biochem. Sci. *41*, 1035–1049.

Ran, F.A., Hsu, P.D., Wright, J., Agarwala, V., Scott, D.A., and Zhang, F. (2013). Genome engineering using the CRISPR-Cas9 system. Nat. Protoc. *8*, 2281–2308.

Rasola, A., and Bernardi, P. (2011). Mitochondrial permeability transition in Ca(2+)-dependent apoptosis and necrosis. Cell Calcium *50*, 222–233.

Rikin, A., Rosenfeld, G.E., McCartin, K., and Evans, T. (2010). A reverse genetic approach to test functional redundancy during embryogenesis. J. Vis. Exp.

Rizzuto, R., and Pozzan, T. (2006). Microdomains of intracellular Ca2+: molecular determinants and functional consequences. Physiol. Rev. *86*, 369–408.

Rizzuto, R., Simpson, A.W., Brini, M., and Pozzan, T. (1992). Rapid changes of mitochondrial Ca2+ revealed by specifically targeted recombinant aequorin. Nature *358*, 325–327.

Rizzuto, R., Brini, M., Murgia, M., and Pozzan, T. (1993). Microdomains with high Ca2+ close to IP3-sensitive channels that are sensed by neighboring mitochondria. Science *262*, 744–747.

Rizzuto, R., Pinton, P., Carrington, W., Fay, F.S., Fogarty, K.E., Lifshitz, L.M., Tuft, R. a, and Pozzan, T. (1998). Close contacts with the endoplasmic reticulum as determinants of mitochondrial Ca2+ responses. Science *280*, 1763–1766.

Robu, M.E., Larson, J.D., Nasevicius, A., Beiraghi, S., Brenner, C., Farber, S.A., and Ekker, S.C. (2007). p53 Activation by Knockdown Technologies. PLoS Genet. *3*, e78.

Rosen, J.N., Sweeney, M.F., and Mably, J.D. (2009). Microinjection of Zebrafish Embryos to Analyze Gene Function. J. Vis. Exp.

Rossi, A.E., and Dirksen, R.T. (2006). Sarcoplasmic reticulum: The dynamic calcium governor of muscle. Muscle Nerve *33*, 715–731.

Rossi, A., Kontarakis, Z., Gerri, C., Nolte, H., Hölper, S., Krüger, M., and Stainier, D.Y.R. (2015). Genetic compensation induced by deleterious mutations but not gene knockdowns. Nature *524*, 230–233.

Rutter, G.A., and Denton, R.M. (1988). Regulation of NAD+-linked isocitrate dehydrogenase and 2-oxoglutarate dehydrogenase by Ca2+ ions within toluene-permeabilized rat heart mitochondria. Interactions with regulation by adenine nucleotides and NADH/NAD+ ratios. Biochem. J. *252*, 181–189.

Ryu, S.-Y., Beutner, G., Kinnally, K.W., Dirksen, R.T., and Sheu, S.-S. (2011). Single channel characterization of the mitochondrial ryanodine receptor in heart mitoplasts. J. Biol. Chem. *286*, 21324–21329.

Saint-Amant, L., and Drapeau, P. (1998). Time course of the development of motor behaviors in the zebrafish embryo. J. Neurobiol. *37*, 622–632.

Sakai, C., Ijaz, S., and Hoffman, E.J. (2018). Zebrafish Models of Neurodevelopmental Disorders: Past, Present, and Future. Front. Mol. Neurosci. *11*, 294.

Sancak, Y., Markhard, A.L., Kitami, T., Kovács-Bogdán, E., Kamer, K.J., Udeshi, N.D., Carr, S.A., Chaudhuri, D., Clapham, D.E., Li, A.A., et al. (2013). EMRE is an essential component of the mitochondrial calcium uniporter complex. Science *342*, 1379–1382.

Schiaffino, S., and Reggiani, C. (2011). Fiber Types in Mammalian Skeletal Muscles. Physiol. Rev. *91*, 1447–1531.

Scorrano, L., Ashiya, M., Buttle, K., Weiler, S., Oakes, S.A., Mannella, C.A., and Korsmeyer, S.J. (2002). A Distinct Pathway Remodels Mitochondrial Cristae and Mobilizes Cytochrome c during Apoptosis. Dev. Cell *2*, 55–67.

Scorrano, L., Oakes, S.A., Opferman, J.T., Cheng, E.H., Sorcinelli, M.D., Pozzan, T., and Korsmeyer, S.J. (2003). BAX and BAK regulation of endoplasmic reticulum Ca2+: a control point for apoptosis. Science *300*, 135–139.

Semova, I., Carten, J.D., Stombaugh, J., Mackey, L.C., Knight, R., Farber, S.A., and Rawls, J.F.

(2012). Microbiota Regulate Intestinal Absorption and Metabolism of Fatty Acids in the Zebrafish. Cell Host Microbe *12*, 277–288.

Shah, A.N., Davey, C.F., Whitebirch, A.C., Miller, A.C., and Moens, C.B. (2015). Rapid reverse genetic screening using CRISPR in zebrafish. Nat. Methods *12*, 535–540.

Shah, A.N., Moens, C.B., and Miller, A.C. (2016). Targeted candidate gene screens using CRISPR/Cas9 technology. Methods Cell Biol. *135*, 89–106.

Sheng, Y., Ren, H., Limbu, S.M., Sun, Y., Qiao, F., Zhai, W., Du, Z.-Y., and Zhang, M. (2018). The Presence or Absence of Intestinal Microbiota Affects Lipid Deposition and Related Genes Expression in Zebrafish (Danio rerio). Front. Microbiol. *9*, 1124.

Shigeta, M., Sakane, Y., Iida, M., Suzuki, M., Kashiwagi, K., Kashiwagi, A., Fujii, S., Yamamoto, T., and Suzuki, K.T. (2016). Rapid and efficient analysis of gene function using CRISPR-Cas9 in *Xenopus tropicalis* founders. Genes to Cells *21*, 755–771.

Shimizu, H., Schredelseker, J., Huang, J., Lu, K., Naghdi, S., Lu, F., Franklin, S., Fiji, H.D., Wang, K., Zhu, H., et al. (2015). Mitochondrial Ca2+ uptake by the voltage-dependent anion channel 2 regulates cardiac rhythmicity. Elife *4*.

Shinya, M., Kobayashi, K., Masuda, A., Tokumoto, M., Ozaki, Y., Saito, K., Kawasaki, T., Sado, Y., and Sakai, N. (2013). Properties of gene knockdown system by vector-based siRNA in zebrafish. Dev. Growth Differ. *55*, 755–765.

Skromne, I., and Prince, V.E. (2008). Current perspectives in zebrafish reverse genetics: Moving forward. Dev. Dyn. *237*, 861–882.

Smith, L.L., Beggs, A.H., and Gupta, V.A. (2013). Analysis of skeletal muscle defects in larval zebrafish by birefringence and touch-evoke escape response assays. J. Vis. Exp. e50925.

Soman, S., Keatinge, M., Moein, M., Da Costa, M., Mortiboys, H., Skupin, A., Sugunan, S., Bazala, M., Kuznicki, J., and Bandmann, O. (2017). Inhibition of the mitochondrial calcium uniporter rescues dopaminergic neurons in *pink1* $^{-/-}$ zebrafish. Eur. J. Neurosci. *45*, 528–535.

Stackley, K.D., Beeson, C.C., Rahn, J.J., and Chan, S.S.L. (2011). Bioenergetic Profiling of Zebrafish Embryonic Development. PLoS One *6*, e25652.

Stainier, D.Y.R., Raz, E., Lawson, N.D., Ekker, S.C., Burdine, R.D., Eisen, J.S., Ingham, P.W., Schulte-Merker, S., Yelon, D., Weinstein, B.M., et al. (2017). Guidelines for morpholino use in zebrafish. PLOS Genet. *13*, e1007000.

De Stefani, D., Raffaello, A., Teardo, E., Szabò, I., and Rizzuto, R. (2011a). A forty-kilodalton protein of the inner membrane is the mitochondrial calcium uniporter. Nature *476*, 336–340.

De Stefani, D., Raffaello, A., Teardo, E., Szabò, I., and Rizzuto, R. (2011b). A forty-kilodalton protein of the inner membrane is the mitochondrial calcium uniporter. Nature *476*, 336–340.

De Stefani, D., Rizzuto, R., and Pozzan, T. (2016). Enjoy the Trip: Calcium in Mitochondria Back and Forth. Annu. Rev. Biochem. *85*, 161–192.

Summerton, J.E. (2007). Morpholino, siRNA, and S-DNA compared: impact of structure and mechanism of action on off-target effects and sequence specificity. Curr. Top. Med. Chem. *7*, 651–660.

Summerton, J.E. (2017). Invention and Early History of Morpholinos: From Pipe Dream to Practical Products. In Methods in Molecular Biology (Clifton, N.J.), pp. 1–15.

Szalai, G., Csordás, G., Hantash, B.M., Thomas, A.P., and Hajnóczky, G. (2000). Calcium signal transmission between ryanodine receptors and mitochondria. J. Biol. Chem. *275*, 15305–15313.

Takeuchi, A., Kim, B., and Matsuoka, S. (2013). The mitochondrial Na+-Ca2+ exchanger, NCLX, regulates automaticity of HL-1 cardiomyocytes. Sci. Rep. *3*, 2766.

Tannahill, D., Britto, J.M., Vermeren, M.M., Ohta, K., Cook, G.M., and Keynes, R.J. (2000). Orienting axon growth: spinal nerve segmentation and surround-repulsion. Int. J. Dev. Biol. *44*, 119–127.

Tarasov, A.I., Semplici, F., Ravier, M.A., Bellomo, E.A., Pullen, T.J., Gilon, P., Sekler, I., Rizzuto, R., and Rutter, G.A. (2012a). The mitochondrial Ca2+ uniporter MCU is essential for glucose-induced ATP increases in pancreatic β-cells. PLoS One *7*, e39722.

Tarasov, A.I., Griffiths, E.J., and Rutter, G.A. (2012b). Regulation of ATP production by mitochondrial Ca(2+). Cell Calcium *52*, 28–35.

Taylor, J.S., Braasch, I., Frickey, T., Meyer, A., and Van de Peer, Y. (2003). Genome duplication, a trait shared by 22000 species of ray-finned fish. Genome Res. *13*, 382–390.

Tosatto, A., Sommaggio, R., Kummerow, C., Bentham, R.B., Blacker, T.S., Berecz, T., Duchen, M.R., Rosato, A., Bogeski, I., Szabadkai, G., et al. (2016). The mitochondrial calcium uniporter regulates breast cancer progression via HIF-1α. EMBO Mol. Med. *8*, 569–585.

Tranchant, C., and Anheim, M. (2016). Movement disorders in mitochondrial diseases. Rev. Neurol. (Paris). *172*, 524–529.

Trenker, M., Malli, R., Fertschai, I., Levak-Frank, S., and Graier, W.F. (2007). Uncoupling proteins 2 and 3 are fundamental for mitochondrial Ca2+ uniport. Nat. Cell Biol. *9*, 445–452.

Trinh, L.A., Hochgreb, T., Graham, M., Wu, D., Ruf-Zamojski, F., Jayasena, C.S., Saxena, A., Hawk, R., Gonzalez-Serricchio, A., Dixson, A., et al. (2011). A versatile gene trap to visualize and interrogate the function of the vertebrate proteome. Genes Dev. *25*, 2306–2320.

Tsai, M.-F., Jiang, D., Zhao, L., Clapham, D., and Miller, C. (2014). Functional reconstitution of the mitochondrial Ca2+/H+ antiporter Letm1. J. Gen. Physiol. *143*, 67–73.

Tsai, M.-F., Phillips, C.B., Ranaghan, M., Tsai, C.-W., Wu, Y., Willliams, C., Miller, C., Abacioglu, Y., Fouts, T., Laman, J., et al. (2016). Dual functions of a small regulatory subunit in the mitochondrial calcium uniporter complex. Elife *5*, 371–381.

Tucker, B., and Lardelli, M. (2007). A Rapid Apoptosis Assay Measuring Relative Acridine Orange Fluorescence in Zebrafish Embryos. Zebrafish *4*, 113–116.

Umeda, K., and Shoji, W. (2017). From neuron to behavior: Sensory-motor coordination of zebrafish turning behavior. Dev. Growth Differ. *59*, 107–114.

Vacaru, A.M., Unlu, G., Spitzner, M., Mione, M., Knapik, E.W., and Sadler, K.C. (2014). In vivo cell biology in zebrafish - providing insights into vertebrate development and disease. J. Cell Sci. *127*, 485–495.

Vais, H., Mallilankaraman, K., Mak, D.-O.D., Hoff, H., Payne, R., Tanis, J.E., Foskett, J.K., Boyman, L., Chikando, A.C., Williams, G.S., et al. (2016). EMRE Is a Matrix Ca(2+) Sensor that Governs Gatekeeping of the Mitochondrial Ca(2+) Uniporter. Cell Rep. *14*, 403–410.

Vargas, R. (2018). Childhood obesity and the zebrafish as a model for the study of diet-induced obesity and its impact in cardiovascular system in adulthood - An overview. Trends Med. *18*.

Varshney, G.K., Sood, R., and Burgess, S.M. (2015). Understanding and Editing the Zebrafish Genome. Adv. Genet. *92*, 1–52.

VASINGTON, F.D., and MURPHY, J. V (1962). Ca ion uptake by rat kidney mitochondria and its dependence on respiration and phosphorylation. J. Biol. Chem. *237*, 2670–2677.

Webb, S.E., and Miller, A.L. (2011). Visualization of Ca^{2}+ signaling during embryonic skeletal muscle formation in vertebrates. Cold Spring Harb. Perspect. Biol. *3*.

Williams, G.S.B., Boyman, L., and Lederer, W.J. (2015). Mitochondrial calcium and the regulation of metabolism in the heart. J. Mol. Cell. Cardiol. *78*, 35–45.

Wolff, C., Roy, S., and Ingham, P.W. (2003). Multiple Muscle Cell Identities Induced by Distinct Levels and Timing of Hedgehog Activity in the Zebrafish Embryo. Curr. Biol. *13*, 1169–1181.

Wu, Y., Rasmussen, T.P., Koval, O.M., Joiner, M.-L.A., Hall, D.D., Chen, B., Luczak, E.D., Wang, Q., Rokita, A.G., Wehrens, X.H.T., et al. (2015). The mitochondrial uniporter controls fight or flight heart rate increases. Nat. Commun. *6*, 6081.

Xi, Y., Ryan, J., Noble, S., Yu, M., Yilbas, A.E., and Ekker, M. (2010). Impaired dopaminergic neuron development and locomotor function in zebrafish with loss of *pink1* function. Eur. J. Neurosci. *31*, 623–633.

Xu, S., and Chisholm, A.D. (2014). C. elegans epidermal wounding induces a mitochondrial ROS burst that promotes wound repair. Dev. Cell *31*, 48–60.

Yam, P.T., and Charron, F. (2013). Signaling mechanisms of non-conventional axon guidance cues: the Shh, BMP and Wnt morphogens. Curr. Opin. Neurobiol. *23*, 965–973.

Yam, P.T., Langlois, S.D., Morin, S., and Charron, F. (2009). Sonic Hedgehog Guides Axons through a Noncanonical, Src-Family-Kinase-Dependent Signaling Pathway. Neuron *62*, 349–362.

Zang, L., Maddison, L.A., and Chen, W. (2018). Zebrafish as a Model for Obesity and Diabetes. Front. Cell Dev. Biol. *6*, 91.

Zelenchuk, T.A., and Brusés, J.L. (2011). In vivo labeling of zebrafish motor neurons using an mnx1 enhancer and Gal4/UAS. Genesis *49*, 546–554.

Zeller, J., and Granato, M. (1999). The zebrafish diwanka gene controls an early step of motor growth cone migration. Development *126*, 3461–3472.

Zeller, J., Schneider, V., Malayaman, S., Higashijima, S., Okamoto, H., Gui, J., Lin, S., and Granato, M. (2002a). Migration of Zebrafish Spinal Motor Nerves into the Periphery Requires Multiple Myotome-Derived Cues. Dev. Biol. *252*, 241–256.

Zeller, J., Schneider, V., Malayaman, S., Higashijima, S., Okamoto, H., Gui, J., Lin, S., and Granato,

M. (2002b). Migration of zebrafish spinal motor nerves into the periphery requires multiple myotome-derived cues. Dev. Biol. *252*, 241–256.

Zhang, J., and Granato, M. (2000). The zebrafish unplugged gene controls motor axon pathway selection. Development *127*, 2099–2111.

Zhang, M., Sun, T., Jian, C., Lei, L., Han, P., Lv, Q., Yang, R., Zhou, X., Xu, J., Hu, Y., et al. (2015). Remodeling of Mitochondrial Flashes in Muscular Development and Dystrophy in Zebrafish. PLoS One *10*, e0132567.

6. ACKNOWLEDGEMENTS

A Million Thank You's Would Never Be Enough

To my parents,
Without them I won't be there and gone so far

To my brother and sister,
I always know they are there, ohana means family

To the amazing man that is always beside me,
No matter how much time I get to spend with you
It will never be enough

To my best (blonde) friend forever
Once again life shows us what really matters

To my amazing friends for all the D&D thursdays
Boardgames and Beer Saturdays
And Pandemic Sundays

To my boss and The Sofy,
Science and life are different with you Pessetts

To all the guys that shared with me
The Wonder and Madness of a (wet) Lab Life:

In these years I learnt so much,
not only about Science.